UNIVERSIDADE ESTADUAL DE CAMPINAS
FACULDADE DE ENGENHARIA QUÍMICA

ALIANDRA DUARTE BARBUTTI

PIV OPTIMIZATION IN THE INVESTIGATION OF TURBULENT FLOW IN A STIRRED TANK

OTIMIZAÇÃO PIV NA INVESTIGAÇÃO DO ESCOAMENTO TURBULENTO EM UM TANQUE DE MISTURA

CAMPINAS – SP

2022

ALIANDRA DUARTE BARBUTTI

PIV OPTIMIZATION IN THE INVESTIGATION OF TURBULENT FLOW IN A STIRRED TANK

OTIMIZAÇÃO PIV NA INVESTIGAÇÃO DO ESCOAMENTO TURBULENTO EM UM TANQUE DE MISTURA

Dissertation presented to the School of Chemical Engineering of the University of Campinas in partial fulfillment of the requirements for the degree of Master in Chemical Engineering.

Dissertação apresentada à Faculdade de Engenharia Química da Universidade Estadual de Campinas como parte dos requisitos exigidos para a obtenção do título de Mestra em Engenharia Química.

Adviser: Prof. Dr. Guilherme Jose de Castilho

Co-Adviser: Dr. Rodrigo de Lima Amaral

ESTE EXEMPLAR CORRESPONDE À VERSÃO FINAL DA DISSERTAÇÃO DEFENDIDA PELA ALUNA ALIANDRA DUARTE BARBUTTI, ORIENTADA PELO PROF. DR. GUILHERME JOSÉ DE CASTILHO E CO-ORIENTADA PELO DR. RODRIGO DE LIMA AMARAL.

CAMPINAS – SP

2022

Ficha catalográfica
Universidade Estadual de Campinas
Biblioteca da Área de Engenharia e Arquitetura
Rose Meire da Silva - CRB 8/5974

B234p

Barbutti, Aliandra Duarte, 1992-
PIV optimization in the investigation of turbulent flow in a stirred tank / Aliandra Duarte Barbutti. – Campinas, SP : [s.n.], 2021.

Orientador: Guilherme José de Castilho.
Coorientador: Rodrigo de Lima Amaral.
Dissertação (mestrado) – Universidade Estadual de Campinas, Faculdade de Engenharia Química.

1. Tanques. 2. Dinâmica dos fluidos - Medição. 3. Escoamento turbulento. 4. Informação mútua. 5. Campo de velocidade. 6. Pesquisa experimental. I. Castilho, Guilherme José de, 1983-. II. Amaral, Rodrigo de Lima, 1988-. III. Universidade Estadual de Campinas. Faculdade de Engenharia Química. IV. Título.

Informações para Biblioteca Digital

Título em outro idioma: Otimização PIV na investigação do escoamento turbulento em um tanque de mistura
Palavras-chave em inglês:
Tanks
Fluid dynamic measurements
Turbulent flow
Mutual information
Velocity field
Experiential research
Área de concentração: Engenharia Química
Titulação: Mestra em Engenharia Química
Banca examinadora:
Guilherme José de Castilho [Orientador]
João Lameu da Silva Júnior
Rogério Gonçalves dos Santos
Data de defesa: 15-12-2021
Programa de Pós-Graduação: Engenharia Química

Identificação e informações acadêmicas do(a) aluno(a)
- ORCID do autor: https://orcid.org/0000-0002-1061-1046
- Currículo Lattes do autor: http://lattes.cnpq.br/6634259870017684

Folha de Aprovação da Defesa de Dissertação de Mestrado defendida por **ALIANDRA DUARTE BARBUTTI** - e aprovada em 15 de dezembro de 2021 pela Comissão Examinadora constituída pelos doutores:

Prof. Dr. Guilherme José de Castilho - Presidente e Orientador

FEQ/ UNICAMP

Videoconferência

Prof. Dr. Rogerio Gonçalves dos Santos

FEM/ UNICAMP

Videoconferência

Dr. João Lameu da Silva Júnior

Universidade Federal do ABC

Videoconferência

A ATA da Defesa, assinada pelos membros da Comissão Examinadora, consta no SIGA / Sistema de Fluxo de Dissertação / Tese e na Secretaria do Programa da Unidade.

To God for the faith and gratitude that moves me every day and never lets me give up.

ACKNOWLEDGMENTS

All the way through this project it was necessary to have the help and encouragement of many people and institutions. I am extremely grateful for everyone and express my gratitude in no specific order.

To my advisor, Prof. Dr. Guilherme Jose de Castilho, for having accompanied me since my undergraduation. Thank you for the opportunity to continue working with you, for your guidance and friendship during these years. Also, thank you for always believing in my potential and pushing me to go even further.

To my co-advisor Dr. Rodrigo de Lima Amaral for all his support, guidance and development of new ideas that were essential for this work.

To Unicamp and the Faculty of Chemical Engineering for being part of my history, for the structure and opportunity provided.

To my undergraduate and master's colleagues/friends, especially Paula Trindade da Silva and Lucas Freitas, for working together during this period, rooting for each other's success.

I thank my family that is what motivates me every day to be better. I thank my parents, Cilene Orrú Duarte Barbutti and Sergio Aliandro Barbutti, for supporting all my dreams and encouraging the pursuit of education. My sister, Heloisa Duarte Barbutti, and my boyfriend and best friend Rodrigo Allegretti Artioli, for everything. My grandparents, Yvette Beraldo and Aparecida Duarte, for always taking care of me and our family.

To my lifelong friends, Ana Paula, Yuna Anjos, Raíssa Gomes, Eduardo Bertoni, Gustavo Moreira, Luís Felipe, Guilherme Mendes, Filipo Daltoê, Pedro Ferreira, Nikolai Lantaler (*in memoriam*) for the laughter, fellowship, advices, emotional support, and eternal bonds we create together.

To my co-workers at DEPro (Department of Process Engineering), for the support provided during the experiments. Especially to Prof. Dr. José Roberto Nunhez and Dr. Helder Moura for all the help during these years of work and dedication to the project.

To all my colleagues and friends from the companies where I had the great opportunity to work: DuPont, Rhodia/Solvay and Suzano. I am grateful for the teachings that formed me as a professional and person.

This study was financed in part by the Coordenação de Aperfeiçoamento de Pessoal de Nível Superior - Brasil (CAPES) - Finance Code 001.

This work was partially supported by Conselho Nacional de Desenvolvimento Científico e Tecnológico – CNPq (Grant No. 2018/168390-3).

Finally, I would like to express my gratitude to Petrobras S/A –Brazil (Grant No. 2017/00376-1) for the financial support they provided.

ABSTRACT

Stirred tanks are widely used in industries for the most diverse types of applications. The efficiency of the mixing process is directly related to the tank-impeller configuration, to the ability to characterize the flow pattern, to understand the effects of turbulent flow and, consequently, its turbulent parameters and mixing index. A widely experimental approach used in fluid dynamics applied to stirred tanks is the particle image velocimetry (PIV). The combination of high-resolution cameras and lasers makes this method capable of recording the velocity field in turbulent regime. In this technique, immersed tracer particles following the flow and their displacement is calculated by the cross-correlation of two consecutive images. Besides the intrinsic three-dimensionality of the flow, some of the difficulties that can be found by applying this technique are related to the tank curvature, different refractive index between tank material and fluid, light reflections from the wall or impeller and dominant noisy sources. Furthermore, the quality of PIV measurements can be affected by noise sources as: out-of-plane motion, high displacement gradients, image distortions, background lighting and low tracer concentration. All those factors can make measurements difficult and need to be solved to ensure reliable results from PIV recordings. The noisy sources deteriorate the velocity fields and compromise the PIV measurements, mainly in the estimation of the turbulent parameters. In those cases, strategies are applied to eliminate or reduce these effects in the turbulent kinetic energy (TKE) fields. These noises can be compensated and minimized through techniques in the physical space (but it is often expensive or unfeasible) or in the image space. This work aims to define strategies in the image space to optimize the processing of PIV measures in the investigation of a stirred tank, through different approaches of pre-processing, processing, and post-processing of PIV images. The PIV optimization methods in stirred tanks proposed in this work are: use of a multicalibration method for image distortion compensation of PIV measurements in a stirred tank without a wedge around it; proposal of a new method of field correction based on mutual information (MI) and analyses of its performance on velocity and turbulent kinetic fields measurements.

Keywords: *PIV, Stirred Tank, Image Distortion Compensation, Multicalibration, Field Correction, Mutual Information, TKE.*

RESUMO

Tanques agitados são amplamente utilizados em indústrias para os mais diversos tipos de aplicações. A eficiência do processo de mistura está diretamente relacionada à configuração tanque-impelidor, à capacidade de caracterizar o padrão de escoamento, de compreender os efeitos do escoamento turbulento e, consequentemente, seus parâmetros turbulentos e índice de mistura. Uma abordagem experimental amplamente utilizada em dinâmica de fluidos aplicada à tanques agitados é a Velocimetria de Imagem de Partículas (PIV). A combinação de câmeras de alta resolução e lasers torna este método capaz de registrar o campo de velocidade em regimes turbulentos. Nesta técnica, partículas traçadoras imersas seguem o fluxo e o seus deslocamentos são calculados por correlação cruzada de duas imagens consecutivas. Além da tridimensionalidade intrínseca do fluxo, algumas das dificuldades que podem ser encontradas ao aplicar esta técnica estão relacionadas à curvatura do tanque, diferentes índices de refração entre o material de construção e o fluido do tanque, reflexos de luz na parede ou no impelidor e fontes ruidosas dominantes. Além disso, a qualidade das medidas PIV pode ser afetada por fontes de ruído como: movimento para fora do plano, elevados gradientes de deslocamento, distorções de imagem, iluminação de fundo e baixa concentração do traçador. Todos esses fatores podem dificultar as medições e precisam ser resolvidos para garantir resultados confiáveis dos dados PIV. As fontes ruidosas deterioram os campos de velocidade e comprometem as medidas de PIV, principalmente na quantificação dos parâmetros turbulentos. Nesses casos, estratégias são aplicadas para eliminar ou reduzir esses efeitos nos campos de energia cinética turbulenta (TKE). Esses ruídos podem ser compensados e minimizados por meio de técnicas aplicadas no espaço físico (mas muitas vezes é caro ou inviável) ou no espaço da imagem. Este trabalho visa definir estratégias aplicadas no espaço de imagens para otimizar o processamento de medidas PIV na investigação de um tanque agitado, através de diferentes abordagens de pré-processamento, processamento e pós-processamento de imagens. Os métodos de otimização de PIV em tanques agitados propostos neste trabalho são: uso da multicalibração para compensação de distorção de imagem em medições PIV de um tanque agitado sem uso de uma caixa de correção (cunha); proposta de um novo método de correção de campo baseado em informação mútua (MI) e análise de seu desempenho em medições de velocidade e de campos cinéticos turbulentos.

Palavras chaves: *PIV, Tanque Agitado, Compensação de Distorção de Imagem, Multicalibração, Correção de Campo, Informação Mútua, TKE.*

LIST OF ILLUSTRATIONS

CHAPTER 2

CHAPTER 3

CHAPTER 4

LIST OF TABLES

LIST OF SYMBOLS

Latin Letters

B	Baffle width $[m]$
C	Distance from the impeller to the straight bottom of the tank $[m]$
C_{max}	Primary peak height $[px]$
C_2	Height of the second highest peak $[px]$
C_{rms}	Root mean square of the correlation plane$[px]$
d_i	Distance from the effective center of the lens to the image plane
d_o	Distance from the effective center of the lens to the object plane
$\mathrm{d_p}$	Tracer particle diameter [µm]
D	Impeller diameter $[m]$
D_I	Interrogation window length $[px]$
F_I	Loss of correlation due to in-plane movement
F_O	Loss of correlation due to movement outside the plane
F_Δ	Displacement gradients
F_σ	Image noise
H	Height of the liquid in the tank $[m]$
k	turbulent kinetic energy $[m^2 s^{-2}]$
M_0	Magnification of image
N	Impeller speed $[s^{-1}]$
N_I	Number of particle images
N_p	Número de Potência
N_{ppp}	Number of particles per pixel
px	Pixel
r/R	Dimensional radial distance [-]
Re	Reynolds Number
t	Time $[s]$
T	Tank diameter $[m]$
T_f	Torque $[Nm]$

u	Fluid velocity vector[$m\ s^{-1}$]
u	Axial velocity component [$m\ s^{-1}$]
$\tilde{u}^2$	RMS velocity to the axial component
$\bar{u}_i$	Periodic fluctuation
u_i'	Turbulent fluctuation
U	Two-dimensional average velocity based on components u, v [$m\ s^{-1}$]
U_i	Instantaneous velocity [$m\ s^{-1}$]
$\bar{U}_i$	Average velocity [$m\ s^{-1}$]
$\lvert\bar{U}\rvert$	Average velocity module 2D x-y [m s^{-1}]
U_{tip}	Velocity at the tip of the impeller [$m\ s^{-1}$]
v	Radial velocity component [$m\ s^{-1}$]
$\tilde{v}^2$	RMS velocity to the radial component
Y_k, Y_ω	Dissipation terms for k and ω [kg m^{-1} s^{-2}]
w	Tangential velocity component [$m\ s^{-1}$]
W	Size of the correlation plane [px]
z/H	Dimensionless height in the tank [-]

Greek Letters

Δt	Time interframes
ϵ	Turbulent kinetic energy dissipation rate[$m^2 s^{-3}$]
η	Kolmogorov scale [mm]
λ	Laser wavelength [nm]
λ_T	Taylor microscale
μ	Fluid viscosity[$Pa\ s^{-1}$]
ρ	Density [$kg\ m^{-1}$]
Ω	Angular velocity of the fluid [$rad\ s^{-1}$]
ν	Kinematic viscosity [$m^2\ s^{-1}$]
ω	Specific rate of turbulent kinetic energy dissipation [s^{-1}]

Superscript

R	Reynolds

ACRONYMS AND ABBREVIATIONS

AR	Angle resolved
AZ	Azimuthal plane
CAPES	Coordenação de Aperfeiçoamento Pessoal De Nível Superior
CCD	Charge-Coupled Devices
CFD	Computacional Fluid Dynamics
CMC	Carboxymethyl cellulose
EDR	Eddy Dissipation Rate
FBT	Flat Blade Turbine
IA	Interrogation Area
IW	Interrogation Window
LDV	Laser Doppler Velocimetry
MI	Mutual Information
Nd: YAG	Neodymium-doped yttrium aluminium garnet
NMT	Normalized Mean Threshold
PBT	Pitched Blade Turbine
PCE	Peak Correlation Energy
PIV	Particle Image Velocimetry
PMT	Prochem Maxflo T
POD	Proper Orthogonal Decomposition
PPP	Particle Per Pixel
PPR	Primary Peak Ratio
PRMSR	Peak Root Mean Square Ratio
RANS	Reynolds Average Navier-Stokes
RMS	Root Mean Square
RPM	Rotation Per Minute
SCC	Standard Cross-Correlation
SNR	Signal-to-Noise Ratio
SPIV	Stereo-PIV
TKE	Turbulent Kinetic Energy
VDP	Valid Detection Probability

CONTENTS

CHAPTER 1

INTRODUCTION

This chapter presents an introduction in which the contextualization for choosing the theme of this Master Dissertation is exposed. Moreover, the general and specific objectives of this dissertation are defined. Finally, the outline of this dissertation is presented.

1.1. INTRODUCTION

In the industrial scenario, stirred tanks by the action of impellers are used in the homogenization of mixtures, gas dispersion in liquids, mixtures with suspension of solids and in chemical reactors. Impellers are the moving part of a stirring system, responsible for defining the flow pattern and increase its velocity inside a tank. These devices directly influence the quality of the mixture and the homogenization of the medium. The use of impellers can cause the formation of vortices and swirling flows, which decrease the efficiency of the agitation system. This problem is solved by using deflectors, which are long plates fixed to the inner walls of the tank. Deflectors or baffles prevent fluid turbulence and create the disordered flow needed to improve the mixing process. For each type of application there is a specific tank configuration, impeller geometry, type and number of deflectors that ensure maximum process performance. Since inside stirred tanks the flows are complex, it is necessary to investigate turbulent flows to obtain more reliable and efficient mixing processes and equipment designs (Uhl & Gray, 1966; Guida, et al., 2010).

In the investigation and characterization of flows, it is important to determine its velocity field, which is directly related to the configuration of the equipment and the rheological characteristics of the fluid. In addition to the velocity profile, other turbulent flow parameters must also be analyzed. Turbulent kinetic energy, turbulence dissipation rate, Reynolds shear stresses, recirculation, and swirl zones are examples of parameters

that directly influence the quality of the mixture and can be related to the process parameters (RPM, power , impeller type and geometry) (Baldi & Yianneskis, 2004).

PIV is a technique that has been used to characterize flow patterns in mixtures with one or more phases. The combination of high-resolution cameras and lasers with a high repetition rate makes this method capable of fully recording and characterizing the velocity field in turbulent regimes. Thus, depending on the configuration of the PIV measurement system, it is possible to measure up to three velocity components, C, in up to three dimensions, D (Wang, et al., 2006; Wieneke, 2017). The PIV method is non-intrusive and quantitative, making it possible to obtain the distribution of velocity vectors in the research area. In addition to the velocity field, these measurements allow to calculate vorticity, Reynolds tensors and turbulent flow parameters. PIV measurements are used both for identifying flow patterns and for validating CFD studies (Westerweel, 1993).

The use of the PIV technique is subject to interference caused by noise sources that generate measurement uncertainties, directly affecting the representativeness and quality of the data. These noises can be caused by image distortions, lack of focus, laser light reflection, vibration, tracer particle diameter, size of interrogation window, correlation peak adjustment, different refractive index, background noise, displacement gradients (interframe time limitation) and movement out of the light plane (Dabiri, 2006). The performance and feasibility of the PIV application is related to the entire experimental system. Thus, many aspects must be investigated to understand the limitations in the context of the experiment (Willert & Gharib, 1991; Prasad, 2000; Raffel, et al., 2018).

To minimize the effects of noise on the quality of PIV measurements, they must be compensated in physical space or image space. Reducing laser light reflection sources, using high-performance filters, adjusting the focus of cameras, reducing out-of-plane movement, minimizing refractive effects by using a correction box are all means that can be employed to reduce noise in physical space before starting image recordings (Willert & Gharib, 1991; Raffel, et al., 2018). Compensating for noise in the physical space is often not a viable technique due to the high cost and spatial limitations of the experimental apparatus.

Noise effects that cannot be minimized in the physical space must be addressed in the image space in the processing steps. However, these are more difficult to be compensated due to their complexity. During the pre-processing it is possible to reduce the background noise from images, from laser light reflection from the tank wall and from the impeller. In the post-processing step, it is possible to identify, remove and replace spurious vectors that deteriorate the quality of the PIV measurement (Escudié & Liné, 2003; Aubin, et al., 2004). Despite the growing number of research studies that propose to investigate PIV performance in other scenarios, such as Wieneke (2005) and Sciacchitano (2013), there are few studies on noise sources and optimization of PIV image processing in stirred tanks. The lack of research in this field and the importance of reliably characterizing the flow velocity fields in a tank by the PIV technique highlight the need to make efforts to expand the knowledge in this area.

1.2. OBJECTIVES

1.2.1. GENERAL OBJECTIVE

This work aims to propose different PIV optimization strategies in the image space of measurements of turbulent flow in a stirred tank using pre-processing, processing and post-processing approaches. The performance on the identification and elimination of noisy values of the proposed methods was also investigated.

1.2.2. SPECIFIC OBJECTIVES

The specific objectives of this work are:

- Definition of experimental PIV setup.
- To propose a robust strategy for image distortion compensation in PIV measurements in a stirred tank without the use of a correction box.
- To propose a robust strategy for outlier correction in a vector field based on mutual information (MI).
- Evaluate the effect of the proposed strategies on high spatial resolution measurements.

- To evaluate the effect of the proposed strategies on the distribution of turbulent kinetic energy (TKE).

1.3. OUTLINE OF THIS DISSERTATION

This Master's Dissertation has five chapters in addition to the annexes**. Chapter 1** presents the introduction and the objectives of this Dissertation, and the remaining chapters are summarized as follows:

- **Chapter 2** provides a comprehensive review of the literature on the importance and challenges of PIV applications in stirred tanks. Therefore, it shows the technique and the PIV system fundamentals, addressing its main noisy sources and quality indicators. Moreover, the chapter discusses about the PIV optimization strategies.
- **Chapters 3 and 4** present the results and discussion of the optimization approaches by presenting a published and a submitted research articles.
    - **Chapter 3** presents an article which is going to be submitted to the Journal of the Brazilian Society of Mechanical Sciences and Engineering. This work evaluates and compares the performance of the standard calibration technique and a new proposal of a strategy (multicalibration) to compensate the image distortion of PIV measurements in a stirred tank. This new strategy is based on two calibration steps. The results were analyzed for images obtained at two different angles from the normal plane of light. Both techniques have good results for reducing image distortion, but the multicalibration strategy showed a better adjustment for regions close to the tank wall.
    - **Chapter 4** presents an article already published in an international journal intitled “Measurement”, by Elsevier. This study proposes a new post-processing filter based on mutual information (MI) for correction of velocity fields of PIV measurements in stirred tanks. The MI technique, which is already used to quantify the uncertainty of PIV measurements, was applied to identify outliers and to correct the fields, comparing its performance with other

standard strategies. The new proposed method presented better results in the elimination of false vectors for high spatial resolutions, preserving the information of the mean velocity and turbulent kinetic energy fields.

- **Chapter 5** presents the final considerations and recommendations for future works.

CHAPTER 2

THEORETICAL FOUNDATION

To contextualize the theme of this Dissertation, this chapter presents the main key concepts of this work and how they are related to each other. Additionally, the application of particle image velocimetry (PIV) techniques in stirred tanks is discussed, as well as their challenges and the noise sources that deteriorate the velocity fields. Quality indicators of PIV measurements are also assessed. Finally, different strategies to optimize the processing of PIV images are presented.

2.1. FLOW IN STIRRED TANKS

Stirred tanks are widely used in different types of industries, such as chemical, pharmaceutical, food, metallurgical and oil industries. The main advantages of this equipment are the ability to operate in different conditions, good mixing performance, and have several designs and configurations available. These characteristics allow stirred tanks to have different types of applications for heat, mass and moment transfer (Alonzo-Garcia, et al., 2019).

Most stirred tanks are cylindrical and with pressures close to atmospheric. They are applied for biphasic mixtures (gas-liquid, liquid-liquid, solid-liquid) or even triphasic systems, with high or low viscosity. The global trend in process optimization involves developing more efficient agitation systems providing products with more quality and with less energy demand (Kumaresan & Joshi, 2006; Kotek, et al., 2017).

The main function of agitation is to promote the mixing of components in order to process the desired product: obtaining solutions, emulsions and suspensions, potentiating the mass transfer between phases and chemical reactions (Tatterson, 1994). The quality of the mixture homogenization can be influenced by several factors related to the design of the agitation system, such as: the geometry of the impeller, the diameter and position of the impeller in the tank, type of flow (upward or downward), the number of impellers used, the use of deflectors, and the shape of the tank. (Kumaresan & Joshi, 2006; Alonzo-Garcia, et al., 2019). Figure 2.1Figure 2.1. Geometry of stirred tank shows the conventional configuration of a tank agitated by a central impeller.

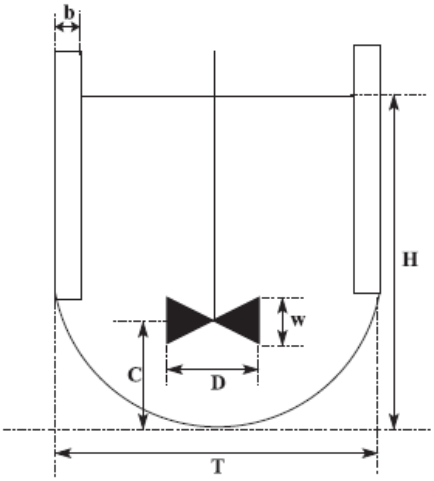

Figure 2.1. Geometry of stirred tank *(Delafosse, et al., 2011)*

In standard configurations of a stirred tank with a single impeller, the liquid has a height (H) equal to the inner diameter of the tank (T). The diameter of the impeller is D = T/3 and the length of its blades has a ratio close to w = D/5. The height of the impeller in relation to the bottom of the tank corresponds to approximately C = T/3. Usually, the tank is equipped with four equally spaced baffles with a width of b = T/10 (Perrard, et al., 2000; Delafosse, et al., 2011).

In most applications, the flow regime is turbulent, being responsible for promoting the increase in heat and mass transfer rates (Wilcox, 1998). The flow inside the tank must be composed of recognizable patterns of turbulent circulation that are influenced by the characteristics of the mixing system (Alonzo-Garcia, et al., 2019). For optimal system design, it must be able to distribute turbulent shear and dissipated energy throughout the tank. Also, for the mixing process to be efficient in the shortest time, several vortices and eddies must be present and provide an efficient mass exchange between the axial and radial flows (Zhang, et al., 2018).

For the mechanisms of the mixing process in stirred tanks to be fully understood, it is necessary to detail its hydrodynamics. For example, the size and periodicity of eddies and vortices influence the mixing models and parameters, especially the turbulent kinetic energy and its dissipation rate (Kresta & Wood, 1991). Therefore, studying and understanding the flow pattern, the associated energy consumption and the mixing characteristic is highly important for the development of industrial applications and optimization (Kumaresan, et al., 2005).

2.1.1. IMPELLERS

Impellers are mobile mixers connected to an axis and driven by a motor that controls the rotation speed. These can be in different positions inside the tank and define the flow pattern of the fluid, directly influencing the quality of the mixture and the homogenization. The flow generated by impellers is characterized by the existence of strong axial, radial and tangential velocity components which have periodic and turbulent parameters (Kumaresan, et al., 2005).

The use of impellers can cause the formation of vortices and swirling flows, which decrease the performance of the agitation system. This problem is solved using deflectors or

baffles, which are long plates fixed to the inner walls of the tank. Deflectors prevent fluid swirling and create the disordered flow needed to improve mixing (Uhl & Gray, 1966).

Impellers can be classified according to the operating regime: laminar or turbulent or in relation to their type of movement: radial, axial, or mixed as presented in Figure 2.2. In laminar flow, the impeller diameter is large and may even approach the size of the tank depending on the type of application and in these cases, baffles are not used. In turbulent flow the transfer of the amount of movement is efficient and thus the diameter of the impeller is much smaller than in laminar flow, and hardly reaches half the tank diameter. In turbulent flow impellers are classified as axial flow and radial flow impellers (Sophia, 2010; Zhang, et al., 2018).

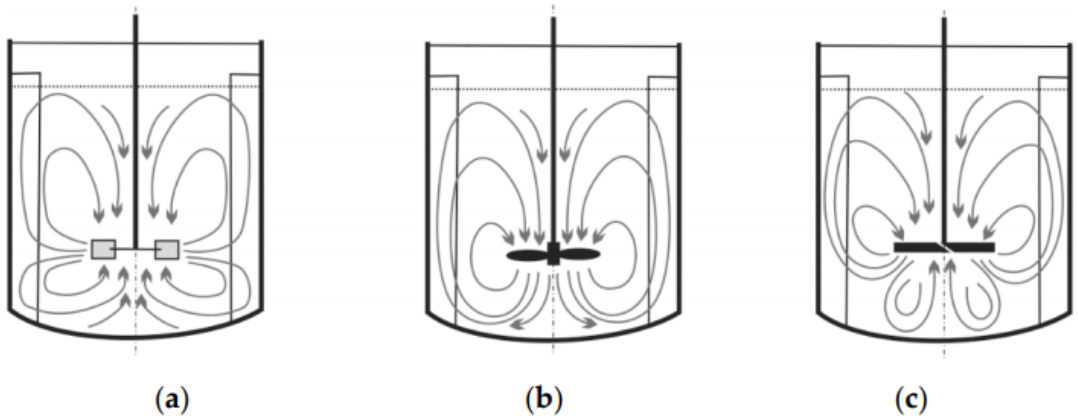

Figure 2.2. Flow motion generated by different impellers types: (a) radial; (b) axial; (c) mixed *(Jaszczur & Młynarczykowska, 2020)*.

Axial impellers are usually used in downward flows and offer great advantages over radial impellers. Also, since the 1980s, upward flows have been used as a more efficient alternative, especially for gas-liquid applications. Much of the investigation of this type of agitation is based on the characteristics of energy and mixing time (Aubin, et al., 2004).

There are numerous configurations of impellers, but the main types used in turbulent regimes are: the naval, flat blade turbine (FBT), pitched blade turbine (PBT), anchor and the Rushton turbine type. FBT and Rushton impellers develop radial flow and are used for high shear stresses and turbulence. PBT impellers produce a mixed flow (radial and axial), being used for both laminar and turbulent regimes, and for suspending solids. The anchor type produces a tangential flow and is used for laminar regimes with high viscosity fluids, while the

naval impeller produces a high speed and low shear stress for axial flow and low and medium viscosity fluids (Uhl & Gray, 1966; Vergel, 2013).

The non-homogeneous regions of turbulence occurring near the impeller blades have been studied by several authors, suggesting that the flow consists in formation of vortex structures that are successively removed. Velocity measurements show a strong periodic component with overlapping fluctuations. The mean velocity field at the discharge of the impeller has a similarity profile that is established only a short distance away (Yianneskis, et al., 1987; Kresta & Wood, 1991).

For each type of application there is a specific configuration of the tank, design of impeller, type and number of deflectors that guarantee the maximum efficiency of the process. Since the flows are complex inside the stirred tanks, it is necessary to investigate the turbulent flows to obtain more reliable and efficient mixing processes and equipment designs. Choosing the type and dimensions of the impeller is important to ensure the optimum mixing point. Thus, knowing and understanding the flow profile and characteristics are necessary to optimize the stirred tank design and evaluate its applications (Uhl & Gray, 1966; Guida, et al., 2010; Story, et al., 2018).

2.1.2. FLOW CHARACTERIZATION

The flow in a stirred tank is influenced not only by the type and shape of the impeller, but also due to the rheological parameters of the fluid. Many studies are aimed at evaluating the flow of Newtonian fluids, however, in practice, most industrial fluids are non-Newtonian (polymers, oils, paints, among others). Non-Newtonian fluids are more complex due to their viscosity and elasticity, which are functions of the shear rate. The increase in the shear rate increases the elastic properties of the fluids. This situation occurs close to the region of the impeller and the walls of the tank, where high velocity gradients are present (Ferguson & Kemblowski, 1991; Story, et al., 2018).

The level of complexity of an agitated system increases according to its characteristics, such as: presence of multiple phases; use of non-Newtonian fluids; the flow regime is located in a transition band (between laminar and turbulent); flow is chaotic and random in turbulent

regimes; and the existence of complex initial conditions such as a process containing solids suspension (Sophia, 2010).

The flow in a stirred tank is three-dimensional and characterized by continuous fluctuations of all velocity components, in space and time (Story, et al., 2018). In most applications in stirred tanks, the flow regime is turbulent and has periodic fluctuations. Turbulence is responsible for promoting increased rates of heat and mass transfer between phases, intensifying reactions, and obtaining suspensions (Tatterson, 1994; Wilcox, 1998).

Countless investigations study the characterization of flows in the regions close to the impeller, however it is also important to know the flow characteristics in the region of the tank walls (Yianneskis, et al., 1987; Zhou & Kresta, 1996). Patwardhan & Joshi (1999) developed a CFD model to determine the mixing pattern and thus demonstrated that the turbulence generated by many impellers is excessive for its applications. According to the studies conducted by them, there is a possibility to reduce the diffusion of the eddies to 20% of the real value and still achieve the same order of mixing efficiency. This reduction represents a substantial saving in operating energy costs.

The flow parameters analyzed in a stirred tank are the instantaneous and average velocities, the periodically induced stress, mixing efficiency, mass transfer and the Reynolds stress. These parameters assist in the identification and quantification of the transfer of kinetic energy between the flow, and the periodic and turbulent fluctuations. The rate of dissipation of turbulent kinetic energy is also estimated using these parameters. Understanding how these phenomena relate to geometry and configuration is essential for optimizing processes, scale-up and engineering projects (Escudié & Liné, 2003; de Lamotte, et al., 2017).

The determination of turbulent flow parameters requires instantaneous information of the velocity field in axial, radial and tangential directions (Khan, et al., 2006). For this, different experimental and numerical techniques can be applied. Velocity components and turbulent parameters, for example, can be obtained through the techniques of Particle Image Velocimetry (PIV) or Laser Doppler Velocimetry (LDV). Furthermore, the PIV technique is effective for detecting and quantifying the eddy scales and for evaluating mixing processes (de Lamotte, et al., 2017; Alonzo-Garcia, et al., 2019).

2.2. PIV PRINCIPLE

The operating principle of PIV technique consists of a laser that illuminates the region of interest of the flow interacting with the particles suspended in the fluid (tracer particles) and it is synchronized with high resolution cameras. The tracer particles reflect the laser light, allowing images to be captured every two consecutive instants of time (double-frame) by CCD sensors (Charge-Coupled Devices) of the recording cameras that are usually positioned at 90º from the laser light sheet. Subsequently, in the processing stage, the images are processed and divided into small areas known as interrogation windows (IW). Then, the PIV analysis correlates the pairs of images of the particle population in these windows, determining the velocity vector. These allow to obtain the velocity field by cross-correlation analysis between the two frames. The number of particle images, common between two consecutive frames, are the basis of the cross-correlation that produces the velocity measurement in the PIV. The PIV technique can be classified according to the number of dimensions of the measures (D) and the components (C) of the velocity distribution: PIV 2D-2C (PIV Classic 2D), PIV 2D-3C (Stereo-PIV) and PIV 3D -3C (Tomographic-PIV) (Liu, et al., 2007; Adrian & Westerweel, 2011; Raffel, et al., 2018).

The classic PIV technique uses a single camera to measure fluid displacement over a period, providing two velocity components in a two-dimensional domain (2C-2D system). The approach consists of three main steps: calibration, image acquisition (recording) and image processing, the latter being divided into pre-processing, processing, and post-processing. Using a second camera or placing a set of mirrors in front of the recording lens, it is possible to record the same region of interest in different projections. The visualization of different angles of the same region of interest and the apparent displacement of the particle image outside the plane allow the reconstruction of the third velocity component - also called 3C reconstruction. This technique is known as Stereo-PIV (SPIV) and can reduce measurement uncertainty for the other two velocity components due to the perspective error (Willert, 1997; Adrian & Westerweel, 2011). Figure 2.3 presents the principle of operation and the steps of the PIV and SPIV techniques.

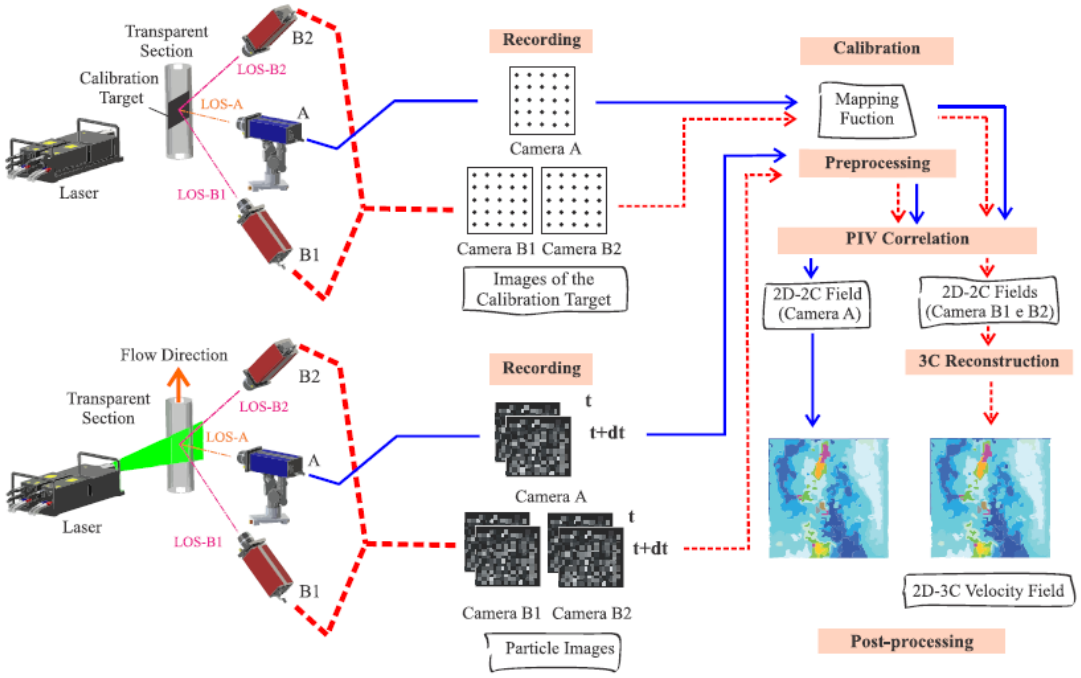

Figure 2.3. Operation principle of PIV (blue line) and SPIV (red line) *(Amaral, 2017)*.

The choice of the tracer particle is extremely important for calculating the velocity based on its instantaneous position. To guarantee the characterization of the entire control volume, the particles must faithfully follow the flow, be homogeneously distributed, and be present in sufficient quantity to represent the entire flow. This parameter is also known as seeding density (Amaral, 2017).

The PIV approach provides raw data, which requires post-processing to detect, correct or remove spurious vectors (outliers) using temporal and spatial filters based on neighborhood connectivity. In addition, after applying these filters, it is necessary to fill in the empty spaces left after removing the outliers (Foucaut, et al., 2000; Adrian & Westerweel, 2011). The problem is that these filters can fail in the presence of groups of false vectors, also known as clusters of outliers. PIV quality and performance are subject to interference caused by different noise sources that generate uncertainties in the measurements, directly affecting the representativeness of the data. In a field without noise, the velocity vectors in the interrogation window vary smoothly in relation to their neighborhood. However, despite studies to minimize noise sources in the physical and image spaces, it is difficult to avoid the presence of false vectors altogether (Dabiri, 2006; Adrian & Westerweel, 2011; Sciacchitano & Scarano, 2014).

2.2.1. CALIBRATION

Calibration is an important step in the PIV technique, which provides the correlation between the physical space and the image space. Calibration can be affected by optical distortions, imperfections in the lens, different refractive index of the optical windows, fluid interfaces and other optical elements. In the 2D-3C PIV, the vector fields of each camera are reconstructed to obtain the third velocity component and the quality of this information depends on the accuracy of the calibration (Prasad, 2000; Adrian & Westerweel, 2011).

The procedure is performed by mapping a standard calibration plate. The mapping function obtained will associate the actual size of the object with the pixel size of the image and thus determine an image/object scale factor compensating for the distortion of the physical space. According to Adrian and Westerweel (2011), linear or polynomial mapping functions are used before PIV correlation to compensate for image distortion. Also, peak locking effects can occur if the particle image diameter is less than 3 pixels.

This step can be performed before or after the acquisition of the experimental images. However, once the equipment has been adjusted and aligned, it must be maintained throughout the recording. While for conventional PIV calibration is an optional step, for SPIV this is mandatory. In this case, the calibration will provide the geometric parameters necessary to obtain the third velocity component (Adrian & Westerweel, 2011; Raffel, et al., 2018).

2.2.2. PRE-PROCESSING

PIV pre-processing aims to increase image quality, reducing noise before proceeding with the cross-correlation step between frames. Using different specific techniques and temporal or spatial filters, it is possible to minimize background noise, normalize the distribution of light intensity and improve the particle image. However, it is necessary to be careful in choosing the approaches that will be used, as the treatment of the image with these filters can have the opposite effect and damage the information of the recorded images (Adrian & Westerweel, 2011; Raffel, et al., 2018).

Figure 2.4 illustrates the configuration of a conventional stirred tank and presents an image recorded by Driss et al. (2014) of the mixing system. From the recorded image, it is

possible to see that the laser light is reflected in the impeller blades, deflectors and the tank walls, the latter occurs due to its curvature. Shadows are noticed due to the deflectors and the impeller. These characteristics are dependent on the angle between the laser plane and the recording plane. The reflection of the laser light and the shadows are noise sources that cause distortions and significantly compromise the quality of the PIV images, making the processing steps more difficult.

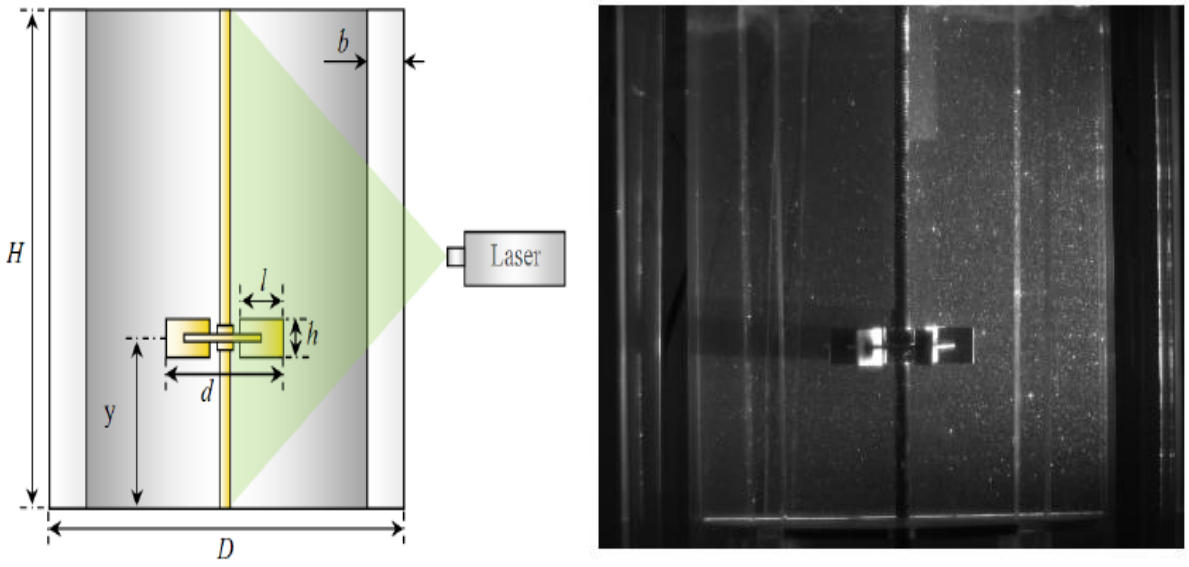

(a) (b)

Figure 2.4. (a) Conventional configuration of a stirred tank; (b) Grayscale recorded image of the mixing system *(Driss, et al., 2014)*.

2.2.3. PROCESSING

The recorded images are subjected to the PIV interrogation method, or correlation step. In this procedure, the images are subdivided into interrogation windows (IW) and each one has several images of particles. Then, the analysis relates the pairs of consecutive images and determines the moving average of small populations of these particles, providing a displacement vector per window as shown in Figure 2.5. The magnification of the image (M_0) is calculated from Equation 2.1 (Figure 2.5a), where d_i and d_o are the distance from the effective center of the lens to the image plane and to the object, respectively. The mapping function then relates the location of the particle in the three-dimensional physical flow field to the plane of the recorded image (Adrian & Westerweel, 2011; Raffel, et al., 2018).

The correlation produces a table of correlation values and the general displacement of the particles in the window is represented by a peak among these values. The errors related to this stage occur mainly due to insufficient data, the low seeding density of the particles or low image quality. These can be minimized with high spatial resolution, control of particle density and size of interrogation windows (Hart, 2000).

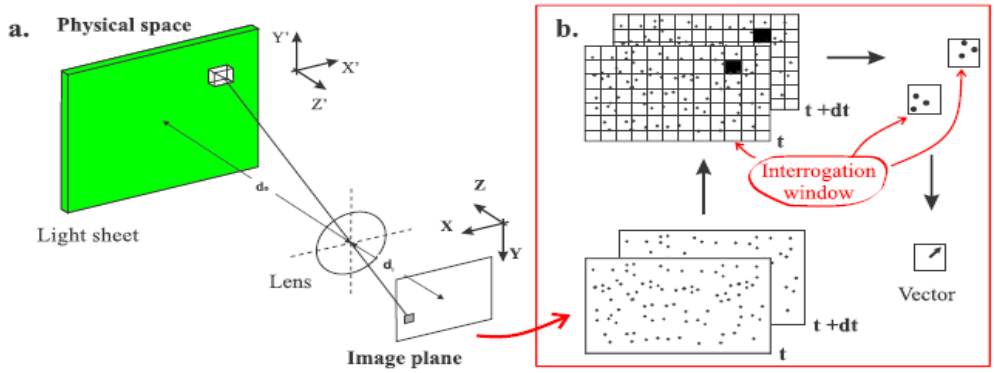

Figure 2.5. Representation of (a) geometric image and (b) PIV interrogation *(Amaral, 2017)*.

$$M_0 = \frac{d_i}{d_o}$$ Equation 2.1

The subsequent action of the iterative methods is to use the measurement information to adapt the system and obtain better fields. In systems with compensation of the deformation of the particle pattern, a third image is obtained from the deformation and displacement of the second image of the pair. This approach reduces relative distortion and increases the signal-to-noise ratio (SNR) (Nogueira, et al., 1997).

Large gradients of velocity, particle movements out of the investigation plane and limited spatial resolution can compromise the reliability of the displacement vectors obtained. One strategy that can be employed to reduce these noises and produce fewer false vectors is to vary the size and overlap of the interrogation window (Huang, et al., 1993; Adrian & Westerweel, 2011). The greater the overlap, the closer the grid of calculated velocity vectors. The size of the interrogation window and the overlap determine the spacing between two neighboring vectors in the field. In other words, for windows of 32 x 32 pixels without overlapping, the distance between the vectors will be 32 pixels. If these same windows have a

50% overlap, the spacing is reduced to 16 pixels, thus increasing the number of vectors (La Vision, 2017).

From the subdivision of the images in a regular grid of overlapping windows, a single velocity vector is found for each window using correlation algorithms. A more cohesive vector field can be obtained with the techniques of overlapping and decreasing the size of the interrogation windows. The increase in overlap also influences to represent the flow more effectively, increasing the spatial resolution and the precision of the PIV measurements (Howell, 2018). The ideal overlap between regions is dependent on the flow characteristics and seeding density. To improve the resolution space, many of the correlation algorithms use a 50% overlap in adjacent regions (Willert, 1997; Hart, 2000).

When interrogation windows are overlapped, the same particle images are used to obtain multiple vectors, so there is a potential for errors due to random correlation in space (Cressall & Smith, 2006). The overlay increases the density of the vector grid, keeping the windows large enough to contain the required number of particles to produce reliable vectors. As the size of the overlapping region decreases, there is a reduction in the level of correlation anomalies, due to the lower level of information shared between windows (Hart, 2000).

The overlapping of the interrogation windows can also influence the random error. Raffel et al. (2018) investigated the increase in random uncertainty in a laminar flow vortex from the increase in the overlap of the interrogation windows. A greater random error was obtained due to the decrease in grid spacing even with the unchanged uncertainty and the increasing overlap of the data.

Roth and Katz (2000) evaluated different methods to improve the quality and accuracy of PIV data. One of these is the overlapping of adjacent interrogation windows by not correlating the part of the new window that overlaps the old one (Figure 2.6). In theory, a 50% overlap of the windows, the processing speed can be 300% faster. In practice, the most efficient algorithm with 50% overlap doubles this speed. The practice of overlapping adjacent interrogation windows results in redundant calculations, regardless of the type of correlation employed. To eliminate wasted time, Roth and Katz (2000) developed a truncated parallel multiplication method, which stores the information from previous windows to reduce the time needed to calculate each vector.

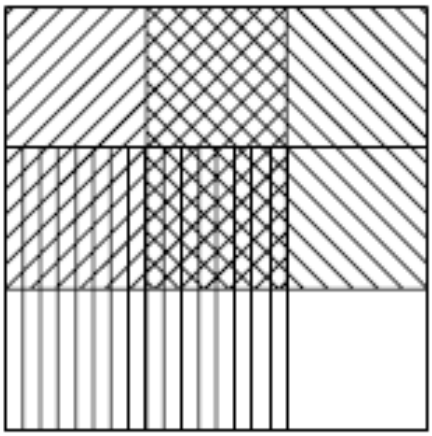

Figure 2.6. Four adjacent interrogation windows that overlap 50% in both directions: horizontal and vertical *(Roth & Katz, 2001)*.

Some of the parameters used in the correlation step can be considered as noise sources. The choices of these properties directly influence the increase or decrease in the noise of the PIV images. They are the size and shape of the interrogation window, correlation, the peak correlation estimator, the deformation and the displacement of the second frame window (offset) (Adrian & Westerweel, 2011; Raffel, et al., 2018).

Studies of these steps are essential to define image processing strategies that minimize noise sources in PIV analysis in a stirred tank. Figure 2.7 shows the possible noise sources, before and during the correlation step, that can affect the quality of PIV images in stirred tanks.

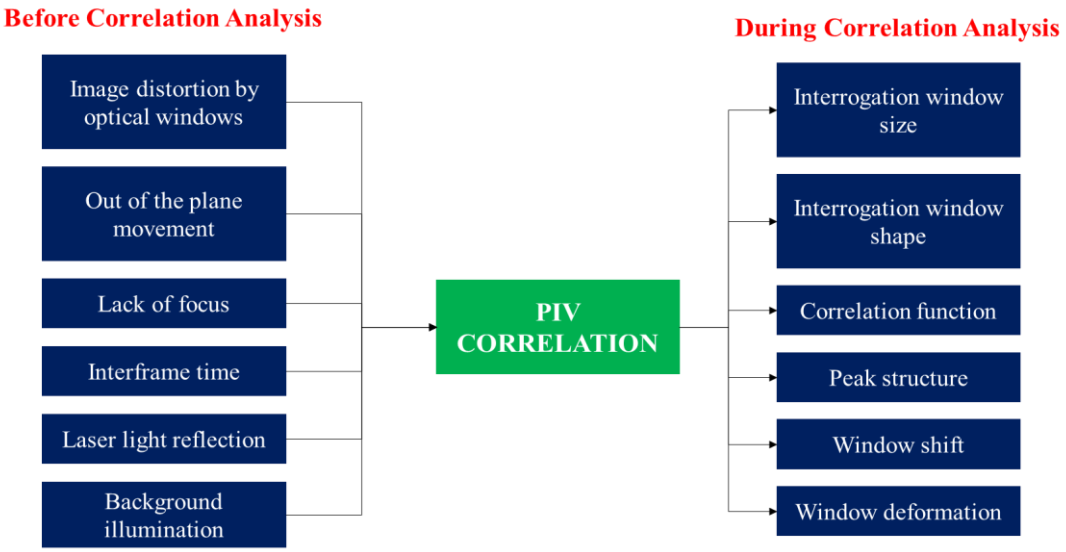

Figure 2.7. Noise sources scheme (before and during the correlation step).

2.2.4. POST-PROCESSING

After the correlation step and obtaining the velocity vectors, post-processing of the images is carried out to correct the fields. The presence of false vectors (outliers) introduces inconsistencies in the velocity distribution within the investigated plane. Thus, before proceeding with data analysis, it is necessary to identify the anomalous values, replace the incorrect values and smooth the data (Moura, 2017). Several types of methodology have been proposed to identify and remove spurious vectors in the velocity measurements of the PIV technique. Each method can be applied in a different stage of the PIV approach, some are used in the correlation stage and others after this, in the post-processing of the images. A technique that can be used to detect outliers and allow validation of the PIV analysis is the normalized median test proposed by Westerweel and Scarano (2005). The disadvantage of this conventional method is that the presence of a large peak makes it difficult to obtain an accurate assessment of the displacement, increasing the measurement uncertainty.

Westerweel (1994) investigated three procedures for detecting extreme values by comparing local statistics: the local average, the local median, and the global average. The three proposed methods were compared and the one with the highest efficiency was the local median. Foucaut et al. (2000) suggested an iterative method, based on a comparison between the velocity obtained at each point and the estimated velocity, using a median filter. It was necessary two steps: In the first, three highest peaks of the correlation plane are recorded, ordered with respect to the module of the difference between the velocity given by the peak and the estimator, afterwards the best of them is selected iteratively; In the second step, this module, given the best peak, is limited.

In the correlation plane, the quality of the PIV measures is directly associated with the calculation of the displacement of the highest peak. In addition, the Valid Detection Probability (VDP) is the probability that the highest correlation peak corresponds to the true mean displacement of the set of particle images. In valid measurements of a vector, the peak displacement is greater than the secondary peak. If the two correlation peaks have the same height, a spurious displacement vector can be calculated (Keane & Adrian, 1992).

2.2.4.1. VALID DETECTION PROBABILITY (VDP)

In the PIV technique, the velocity of a group of particles is estimated through the cross-correlation function of two interrogation windows containing the images of corresponding particles in two consecutive times (Raffel, et al., 2018). Under ideal experimental conditions, the flow of particles is predominantly uniform and homogeneous and there is a sufficiently large number of images of particles between two images. In addition, the particle size must be identical, and the illumination of the plane must be uniform to ensure that the size and brightness of the particle images are similar (Scharnowski, et al., 2019).

Keane and Adrian (1992) defined the valid detection probability (VDP) as the probability that the highest correlation peak corresponds to the true mean displacement of the set of particle images in the interrogation window. The research also corroborated that VDP is almost guaranteed when the number of images of particles within the interrogation window (N_I) is greater than or equal to 6. If this number is less than 6, the probability of a random peak being greater than the peak corresponding to the actual displacement of the particle image, strongly increases in the correlation function.

Keane and Adrian (1990) determined a parameter that relates the probability of reaching a valid measurement in the PIV with 95% valid detection, known as the effective number of particle images. Thus, this parameter, presented in Equation 2.2, is calculated as the product of the number of particle images (N_I), the loss of correlation due to movement in the plane (F_I), and the loss of correlation due to movement out the plane (F_O).

$$N_I F_I F_O \geq 6 \qquad \text{Equation 2.2}$$

According to Scharnowski et al. (2019), only meet this relationship does not guarantee an adequate VDP. In cases of optimization of interframe time to obtain low uncertainty and high spatial resolution, a large particle displacement in a thin beam of laser light will increase the probability of loss of particle images pairs due to movement in and out of the plane, reducing F_I and F_O.

Some parameters can interfere and deteriorate the quality of the VDP, such as: the loss of correlation due to the movement in the plane (F_I) and out the plane (F_O), displacement

gradients (F_Δ) and also the image noise (F_σ) . Therefore, correlation loss for PIV images can be compensated by increasing the number of particle images. By increasing the movement of particle images in the plane and out of the plane, it is possible to increase the loss of correlation between the image pairs (lower values of F_I and F_O) and consequently decrease the effective number of particle images (Keane & Adrian, 1992). Based on this, Scharnowski et al. (2019) adapted the Equation 2.2 to Equation 2.3.

$$N_I F_I F_O F_\Delta F_\sigma \geq 6 \qquad \text{Equation 2.3}$$

The number of particles images within a square interrogation window (N_I) is obtained by Equation 2.4, in which D_I is the length of the window and N_{ppp} is the average number of particles per pixel. D_I can be changed using different interrogation window sizes, while the last parameter is related to the density of particle images in the experiment and can be changed through the amount of tracer particles that is added to the flow (Scharnowski, et al., 2019).

$$N_I = N_{ppp} {D_I}^2 \qquad \text{Equation 2.4}$$

If the result of the cross-correlation between two images produces a secondary peak larger than the actual displacement peak, this is considered an outlier, that is, a vector that incorrectly represents the flow. Larger interrogation windows and smaller particles images increase the VDP. However, it is important to note that the authors recommend selecting a particle image diameter between 2 and 3 pixels to avoid polarization errors due to peak locking. The normalized correlation height of the displacement peaks and the secondary peak are also influenced by the presence of image noise (Scharnowski, et al., 2019).

One way to remove outliers is to compare these to the behavior of their neighborhood. Still, it is essential to use an interrogation window size that provides a 95% VDP to avoid clusters of incorrectly displaced vectors. One of the main reasons that can influence the presence of outliers is the low number of images of particles in the interrogation window associated with the loss of correlation due to the movement out of the investigation plane (Scharnowski, et al., 2019).

Scharnowski et al. (2019) evaluated that to reduce the number of spurious vectors, the search radius of the displacement peak can be reduced, but for this it is essential to have prior knowledge of the flow field. Through synthetic images, the authors studied how the different parameters presented influence the height of the correction peaks and consequently also in the VDP. As analyzed, the parameters that have the greatest influence on the VDP are F_O, N_{ppp} and N_I. In this way, a high VDP value is achieved based on the choice of the size of the interrogation window, which must be related to the density of particle images and the movement out of the plane.

Different alternatives can be used to improve the VDP, such as: increasing the size of the interrogation window, reducing the interframe time, increasing the particle density, reducing the size of the particle image, reducing the level of image noise and thickening the beam of laser light. Optimization techniques in the acquisition of PIV data and in the processing steps are important as these parameters influence spatial resolution and measurement uncertainty (Scharnowski, et al., 2019).

2.2.4.2. SIGNAL-TO-NOISE RATIO (SNR)

The signal-to-noise ratio (SNR) is defined as the ratio of the signal peak divided by the highest noise peak in the correlation domain. Differences in the propagation density between parts of the image disturb this indicator, due to differences in the average value over which the peaks arise. Regardless of the correlation method, a SNR metric can be applied to assess the quality of their results and quantify their uncertainty. Nogueira et al. (2001) suggest an alternative equation to allow a more uniform comparison across the image according to Equation 2.5

$$SNR = \frac{signal\ peak - mean\ value}{highest\ noise\ peak - mean\ value} \qquad \text{Equation 2.5}$$

The average value of Equation 2.5 is obtained in the correlation domain using all values smaller than the two peaks already defined. If the SNR <1 means that the noise peak is greater than the signal peak. This could only indicate a different value from what was the real displacement (Nogueira, et al., 2001).

Signal-to-noise ratios are measures that can be used to assess the quality of cross-correlation and measurement uncertainty to detect the presence of outliers. The work developed by Xue et al. (2014) demonstrated that the SNR metrics produce efficient estimators for the measurement of PIV uncertainty. A SNR metric is the primary peak ratio (PPR), which provides the relationship between the primary displacement correlation peak and the second highest peak. The PPR was used to detect true displacements and was considered valid measure if its value was higher than the threshold defined by the user (often 1,2) (Xue, et al., 2014).

Hain and Kahler (2007) used the PPR value close to 2 to avoid spurious vectors. In addition, the authors proposed a method for optimal selection of the cross-correlation at different time intervals. According to the authors, many factors can influence the correlation peak height and ratio. Thus, the threshold must be chosen and adapted to the image quality and the PIV system used. Charonko and Vlachos (2013) related the distribution of the velocity error magnitude and the value of the PPR to calculate the uncertainty of a measure without previous knowledge of the image quality or the local flow. For standard cross-correlation (SCC) techniques, the uncertainty determined by the PPR is not reliable due to the noise effects that do not receive the appropriate treatment.

The PPR is defined as the ratio between the height of the primary peak (C_{max}) and the height of the second highest peak (C_2), according to Equation 2.6 (Kumar & Hassebrook, 1990).

$$PPR = \frac{C_{max}}{C_2} \qquad \text{Equation 2.6}$$

Kumar and Hassebrook (1990), in addition to using the PPR, also quantified the SNR through the peak-to-root mean square ratio (PRMSR) and the peak-to-correlation energy (PCE). These last two, however, are parameters based on the theory of signal processing and previously were not considered as measures of quality in the correlation. Xue et al. (2014) developed models for estimating uncertainty using PPR, PRMSR, PCE and cross-correlation entropy. The authors also refined the considerations about invalid measurements and investigated the shape of the PIV measurement error distribution, eliminating the hypothesis that it follows a normal distribution.

The PRMSR is defined as the ratio between the magnitude of the cross-correlation plane (C_{max}) and the square of the root mean square of the correlation plane (C_{rms}), according to Equation 2.7 (Kumar & Hassebrook, 1990; Xue, et al., 2014).

$$PRMSR = \frac{|C_{max}|^2}{{C_{rms}}^2}$$ Equation 2.7

The magnitude of the cross-correlation plane is calculated as the square of the height of the primary peak and the noise is calculated using Equation 2.8, in which Ω indicates the group of points on the correlation plane where the correlation value is less than half of the primary peak height (Kumar & Hassebrook, 1990; Xue, et al., 2014).

$${C_{rms}}^2 = \left[\sqrt{\frac{1}{N_\Omega}\sum_{i\in\Omega}|C(i)|^2}\right]^2$$ Equation 2.8

PCE (Equation 2.9) is defined as the ratio between the magnitude of the cross-correlation plane and the correlation energy (Kumar & Hassebrook, 1990; Xue, et al., 2014).

$$PCE = \frac{|C_{max}|^2}{Ec}$$ Equation 2.9

The magnitude is calculated as in the PRMSR and the noise parameter, or correlation energy, is defined by Equation 2.10, W being the size of the correlation plane (Kumar & Hassebrook, 1990; Xue, et al., 2014).

$$Ec = \frac{1}{W}\left(\sum_{w}|C(x)|^2\right)$$ Equation 2.10

These SNR metrics test the detectability of the primary peak against other correlations. While the PPR is a metric created for this purpose, an analytical derivation of the PRMSR and PCE can be applied if the statistical properties of the signal are known. The graphs in Figure 2.8 are a representation of all three SNR metrics mentioned before.

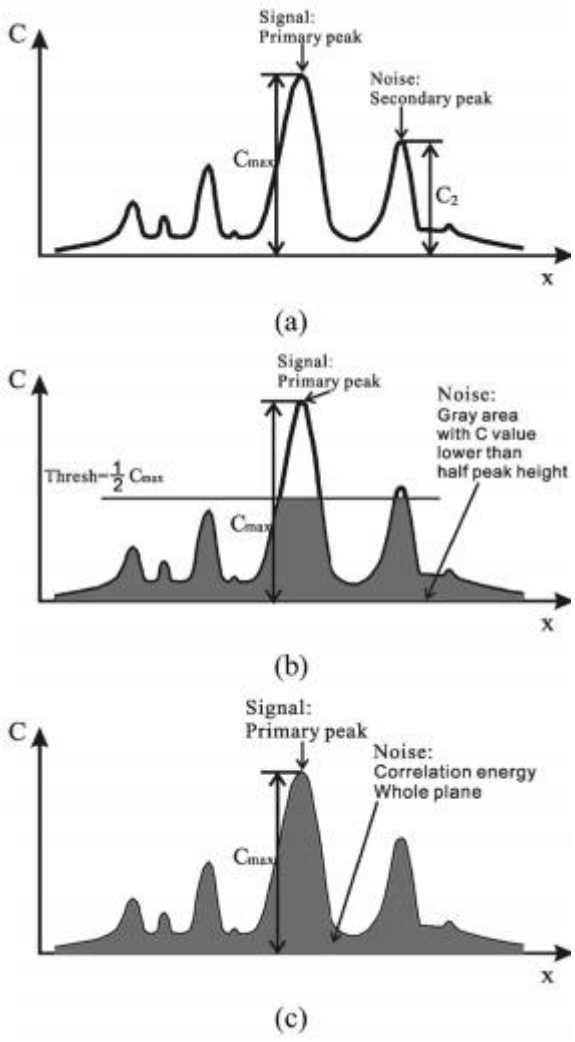

Figure 2.8. SNR correlation graphs: a. PPR; b. PRMSR, c. PCE *(Xue, et al., 2014)*

2.2.5. SPATIAL RESOLUTION

The PIV measures produce many instantaneous velocity vectors that allow the identification of the spatial structures and obtain quantitative spatial information even in unsteady flow fields. The performance of the PIV system and the quality of its measurements are defined by its spatial resolution, detection rate and accuracy. The spatial resolution for correlation analysis is limited by the size of the measurement volume, which is determined by the intersection of the laser beam with the density distribution in the interrogation window. Also, the spatial resolution should be small if compared to the flow field length scales (Keane, et al., 1995).

The spatial resolution required for PIV measurements depends on the amount of flow measured. The equipment-dependent limits are described by Adrian (1997), stating that the spatial velocity intervals depend on the size of the image and the resolution of the recording medium. To obtain accurate PIV measurements on a very fine spatial scale, it is recommended to improve the spatial resolution. This is essential to characterize turbulent flows, in which the resolution of the order of the Kolmogorov length scale allows the measurements of vorticity and the dissipation of turbulent kinetic energy to be accurately acquired (Keane, et al., 1995). The Kolmogorov length scale is the smallest scale in a turbulent flow and is defined by the relationship of turbulent viscosity to dissipation rate (Escudié & Liné, 2003).

According to Raffel et al. (2018), in the correlation analysis, the interrogation windows must be small enough that the velocity gradients within the investigation area do not have a significant influence on the results. Another factor that influences spatial resolution is the size of the camera sensor used to acquire images.

In conventional techniques, the interrogation windows are optimized globally, and non-ideal conditions are accepted in some regions, introducing false vectors and uncertainties. Iterative methods as multipass or multigrid techniques, can also be used to adapt the subdivision of the frame in the interrogation window and increase the quality of the measure (Nogueira, et al., 2001; Adrian & Westerweel, 2011). Using adapted techniques, it is possible to improve spatial resolution locally while maintaining the level of robustness and accuracy of the analysis (Theunissen, et al., 2006).

One of the simplest methods to improve spatial resolution is to enlarge the images, however this reduces the field of view. If the displacements of the tracer particles are determined by correlation analysis, the spatial resolution is defined by the size of the interrogation window, since the correlation algorithms determine the mean displacements of the region (Keane et al., 1995).

Improvements in spatial resolution through conventional PIV correlation methods have been studied by Huang et al. (1993). The authors used an iterative technique of cross-correlation analysis on single exposure image fields with successive image fields to remove the local effects of velocity gradients. Advanced iterative techniques first evaluate the image with larger interrogation windows to obtain the local mean displacement and then analyze the same image with smaller interrogation windows to increase spatial resolution (Raffel, et al., 2018).

2.3. PIV APPLICATION IN STIRRED TANKS

Since the PIV can record the velocity field for up to three components in three dimensions, it can be used in studies of complex flows, especially those caused using impellers in stirred tanks. The PIV technique was used by Bakker et al. (1996) to characterize laminar and turbulent flows in a tank agitated by a 45° inclined blade impeller and by Perrard et al. (2000) to study the average angle of the velocity fields around a Rushton impeller in a stirred tank. Chung et al. (2009) studied the effects of periodicity and turbulent parameters in flows using the PIV technique and angle-resolved in stirred tanks with different configurations. The agitation was provided by a PBT impeller with six blades inclined to 45° of upward flow. The results showed that the square tank showed a stronger radial-axial flow and shorter mixing time, so that it can be a good substitute for tanks with deflectors. More recently, Li et al. (2018) used the PIV method to explore the flow of suspended solids in stirred tanks with 45 ° inclined blade impeller. In addition, the results from the PIV technique have a good agreement with what already exists in the literature and with the results obtained by CFD (Wang, et al., 2006).

Turbulent kinetic energy (TKE) and turbulent dissipation rate are important parameters for stirred tank design and process performance. In relation to TKE, velocity fluctuations are related to turbulent dispersion and mixing. The geometry of the impeller, its position in the tank and the rotation speed influence the quality of the mixture, especially in the regions close to the tank wall and the impeller blades, where swirls are formed. The turbulent dissipation rate is related to heat transfer, chemical reaction and mixing at smaller scales (Alonzo-Garcia, et al., 2019).

Numerous authors aimed to study the turbulent flow parameters in stirred tanks. Guida et al. (2010) investigated the effects of the azimuth position of the measurement plane in a tank agitated by an inclined blade impeller using the 2D PIV technique (Figure 2.9a). Based on average velocity convergence analysis, the authors used 500 pairs of images to estimate the averages and turbulent parameters (Figure 2.9b). Seventeen planes located at 5 degree intervals between two adjacent deflectors under totally turbulent conditions were analyzed in order to obtain the average velocity (Figure 2.10a) and the turbulent kinetic energy fields (Figure 2.10b).

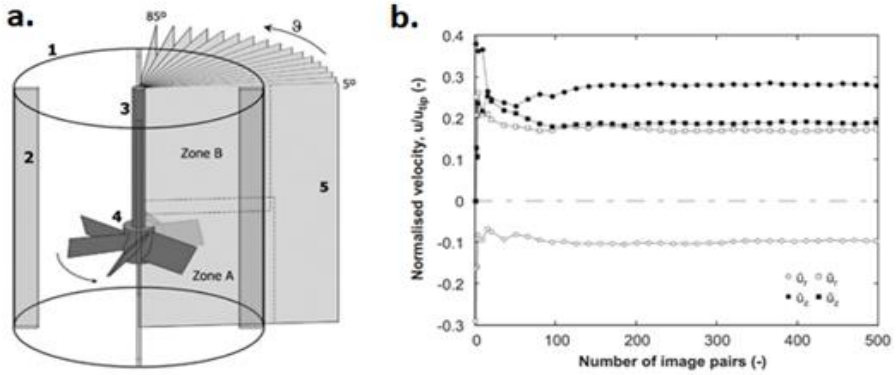

Figure 2.9. (a) PIV experimental setup and (b) effect of the image number at one point to analyze the effect of the azimuth position of the measurement plane *(Guida, et al., 2010)*.

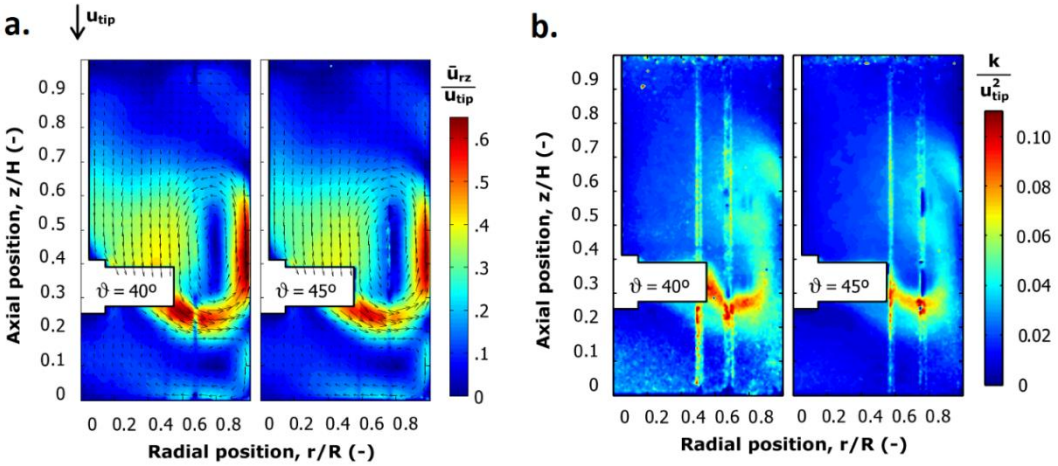

Figure 2.10. Effect of the azimuth position of the measurement plane on (a) the distribution of the average velocity and (b) the normalized turbulent kinetic energy *(Guida, et al., 2010)*

Although the authors do not address the subject, it is possible to observe some measures inconsistent with the phenomenon through the quality of the PIV images. In Figure 2.10a, spatial discontinuities are observed in the measurements, mainly close to the impeller in the plane at the 40º position. There is also a discontinuity in the downward flow in the tank wall for angles greater than 30º. These disconnected regions can be caused by the loss of information due to the position of the laser system or by noise sources, such as reflection and distortion. As the authors do not provide detailed information about this arrangement, the presence of the noise effect is difficult to be ruled out. In addition, in the Figure 2.10a the average flow velocity is provided as a function of the velocity at the tip of the impeller (U_{tip}). In this way, the highest velocity values found are just below the impeller blades and on the tank walls.

In Figure 2.10b, there are precise indications of noise in the images. Incoherent points are observed that do not correspond to its neighborhood, two vertical “lines” are observed to “move” horizontally as the angle varies, there are still light points at the top of the image. In these cases, the reflection of the laser light, caused mainly by the curvature of the tank, can be the dominant noise source. In addition to reflection, other sources of error may be present and compromise the results, such as image distortion error and sampling error (the number of images is insufficient to estimate the turbulent parameters).

Guida et al. (2010) evaluate the position of the angles and cameras without exposing the uncertainty of each plan. There is no evidence of quality for each investigated plane and they also do not present the raw images of each plane, the distortion effects, or the optical image analysis. As can be seen in Figure 2.4b, the raw image obtained with the PIV technique shows shadows due to the reflection of the laser light in the impeller, in the deflectors and in the walls of the tank and these points were not addressed in the study by Guida et al. (2010). Due to the inconsistencies observed in the images and the lack of information, the variation of the measurements with the azimuth position may be due to the PIV quality (presence of noisy sources) and not due to the flow phenomenon.

Liu et al. (2016) investigated the influence of spatial resolution on the estimation of the turbulent flow field using two different sized interrogation areas. The anisotropy of the turbulent flow is analyzed through the turbulent kinetic energy and the energy dissipation rate obtained from different measurement angles. The authors state that the resolution of the PIV is limited by the size of the interrogation area.

Kotek et al. (2017) used PIV measures to evaluate the flow profile in a stirred tank by a Rushton turbine for different degrees of spatial resolution and to demonstrate the influence of spatial resolution on the representation of the vortexes. The experiments conducted by Kotek et al. (2017) consisted of moving the camera of the laser light sheet (approaching or moving away) keeping the central pixel of the camera focused on the same location. The results showed that the average velocity field is characterized by a smooth flow of the impeller and has no vortex structures.

Story et al. (2018) studied the flow in a stirred tank by a PMT (Prochem Maxflo T) impeller with a rotation frequency inducing transition and turbulent regimes. The experiments were carried out with Newtonian (water) and non-Newtonian fluids (0.2 wt.% CMC -

Carboxymethyl cellulose). Through the PIV technique, the average velocity vector fields were obtained for planes with angular positions of 45° and 0° in relation to the deflectors.

Numerous studies seek to determine the global circulation of the tank, on a macro scale, such as the average radial velocity in the jet of the impeller. These studies also demonstrate that the ratio of the average velocity components normalized by impeller tip velocity (U_{tip}) are independent of the diameter and rotational speed of the impeller, as also the tank diameter. The different results can be attributed to the different configurations of the tank-impeller, such as deflectors, baffles, blade thicknesses, among others (Adrian & Westerweel, 2011; Raffel, et al., 2018).

Despite several studies on the macro-instabilities of a flow, there is a predominance of smaller turbulence structures that have a greater impact on the determination of turbulent kinetic energy (TKE). The resolution of the PIV method depends on the optical components used, especially the optical magnification system, the measuring distance of the camera, the size of the camera chip, and also on the processing methods (Kotek, et al., 2017).

The synchronization of the data acquisition with the angle-resolved PIV measurements can be used to separate the periodic and turbulent fluctuations. This technique also allows to obtain the organized movement velocity to a specific position in relation to the measurement plane. Turbulent kinetic energy is a parameter that can be obtained by applying the technique of angle-resolved measurements and is usually normalized by the square of the velocity at the tip in the impeller (Escudié & Liné, 2003).

2.4. TURBULENT KINETIC ENERGY FROM PIV MEASUREMENTS

Over the years, the PIV technique has influenced countless advances in the study and understanding of complex and turbulent flows. However, despite increasing progress in examining single-phase systems, there is still a large gap in the study of the turbulent properties of multiphase flows. Some of the main parameters evaluated are the turbulent kinetic energy (TKE) and the energy dissipation rate (Escudié & Liné, 2003; Raffel, et al., 2018).

To determine the TKE, it is necessary to obtain the three velocity components, which can be measured using Stereo PIV or even Volumetric PIV. However, to investigate optimizations in mixing processes, the 2D PIV method can be used, in which the third velocity

component comes from the other two components measured. The resolution depends on the optical components used and on the processing methods, especially the determination and overlapping of the investigation areas (Kotek, et al., 2017).

Three different scales can be used to characterize the turbulent regime: Kolmogorov scale, Taylor microscale and macro length scale. The Kolmogorov scale (η), calculated by Equation 2.11, are the smallest turbulent structures and the turbulent kinetic energy is dissipated through molecular viscosity. The Taylor microscale (λ_T), Equation 2.12, has its size characterized by the smallest energetic structures and the macro length scale corresponds locally to the size of the most energetic turbulent structure. The latter is dependent on the radial and axial locations in the tank (Escudié & Liné, 2003).

$$\eta = \left(\frac{\nu^3}{\epsilon}\right)^{1/4} \qquad \text{Equation 2.11}$$

$$\lambda_T = \sqrt{\frac{10\ \nu k}{\epsilon}} \qquad \text{Equation 2.12}$$

Where ϵ is the dissipation rate of the turbulent kinetic energy, ν is the kinematic viscosity and k is the turbulent kinetic energy.

Despite the importance of determining the local dissipation rate of turbulent kinetic energy for characterizing flows, its measurement is difficult, since it is necessary to capture precisely the smallest turbulent structures (Escudié & Liné, 2003). Some authors have devoted themselves to developing methods to estimate this parameter, through the balance of kinetic energy in a control volume (Cutter, 1966) or dimensional analysis (Zhou and Kresta, 1996).

Escudié and Liné (2003) studied the flow in a stirred tank with a Rushton turbine. The dissipation rate of TKE cannot be estimated directly due to the high spatial resolution. To calculate this parameter, the authors used a TKE balance equation, analyzing different types of kinetic energy and the interaction between turbulence and vortexes. The types of kinetic energy are related to the different types of movements generated in the tank: average flow, periodic fluctuations, and turbulent fluctuations.

According to the results of the experiments by Escudié and Liné (2003), the order of magnitude of the Taylor microscale corresponds to the spatial resolution of the experiments. To

optimize the processing, the calculations were performed for 1000 instantaneous velocity fields. The authors also verified the convergences for the mean velocity, Reynolds stress components and third-order velocity fluctuations.

In the multi-phase experiments carried out by Liu et al. (2016), the vortex area in the impeller region showed the highest increase in turbulent kinetic energy (TKE) according to the increase in the volumetric fraction of the aqueous phase. This still shows some fluctuations; however, the region of the tank circulation shows a tendency to increase the TKE with an increase in the dispersed fraction. Generally, in single phase mixtures, the fluctuations in TKE and velocities parameters are inhibited with higher densities and viscosities of the fluids.

Delafosse et al. (2011) point out that turbulent flow properties such as TKE and EDR (Eddy Dissipation Rate), when obtained through the PIV technique, are influenced by spatial resolution. In addition, the spatial resolution must be of the same magnitude as the Kolmogorov scale to provide a more accurate estimate of the EDR. In the work developed by Liu et at. (2016), the effect of spatial resolution in obtaining the TKE is investigated using interrogation windows of 32 x 32 pixels² and 16 x 16 pixels² to obtain the turbulent fields of the systems. Despite the similarities, the TKE results obtained experimentally are higher according to the higher resolution (16 x 16 pixels²), as shown in Figure 2.11. In addition, the TKE increases first near the axis of the impeller and at the top edge of the tank and then expands from the top to the center.

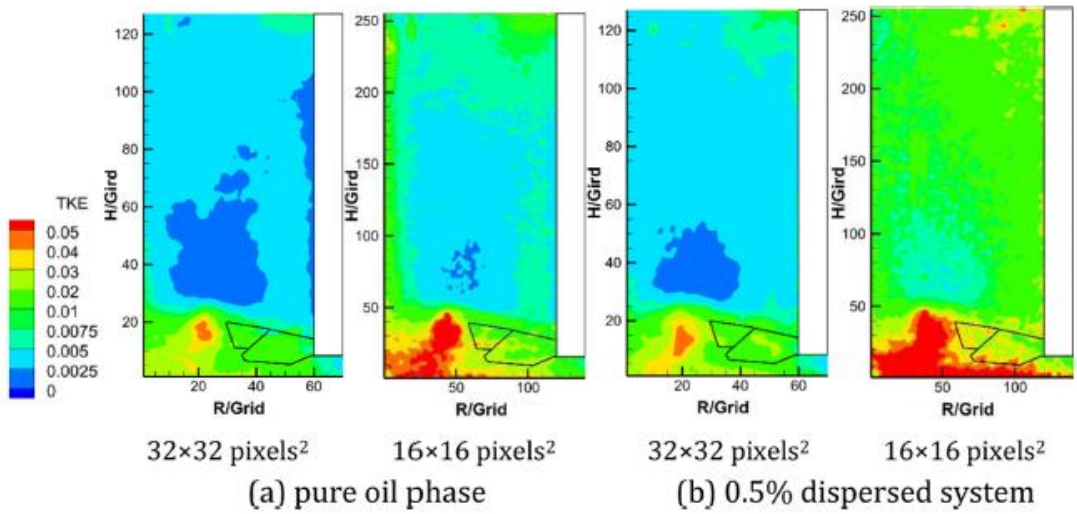

Figure 2.11. Comparison of the average TKE distribution between different spatial resolutions: (a) pure oil phase and (b) 0.5% dispersed system *(Liu, et al., 2016)*.

Large interrogation areas can be responsible for omitting turbulent fluctuations while small areas have higher local velocities. Increasing the number of velocity vectors is more likely to improve TKE and this parameter tends to increase as the fraction dispersed in the biphasic system increases and the spatial resolution improves. In the circulation region, deviations can be caused by periodic fluctuations in the rotation of the impeller and are high due to the limits of the tank walls. Due to the limitation of spatial resolution and experimental conditions for the acquisition of PIV images, the dissipation rate of turbulent kinetic energy cannot be calculated directly, since it could filter the Kolmogorov turbulence scale (Liu, et al., 2016).

Despite the countless studies aimed at the study and characterization of flows in stirred tanks, some aspects are still not well defined and need to be further investigated. The flow velocity in a stirred tank can be divided into three types of movements: the global circulation or mean flow, the vortices induced by the rotation of the impeller, which cause periodic fluctuations, and the turbulences that dissipate the kinetic energy. These properties can be estimated through the triple decomposition of the velocity presented in the Equation 2.13 (Escudié & Liné, 2003).

$$U_i = \overline{U}_i + \widetilde{u}_i + u_i' \qquad \text{Equation 2.13}$$

U_i is the instantaneous velocity, $\overline{U}_i$ is the average velocity, $\widetilde{u}_i$ and u_i' are the periodic and turbulent fluctuations, respectively.

For reconstruction and reproducibility of measurements, the experiments can be performed in three perpendicular planes. In this way, it is possible to determine the three velocity components and the six stress tensors terms required for the calculation. Angle-resolved measurements are also performed on each plane to determine all components (Escudié & Liné, 2003).

Reynolds and Hussain (1972) carried out the triple decomposition of the velocity to calculate the turbulence in the flow with periodic movement and to establish the dynamic equations for the three movements. Through Navier-Stokes, they obtained the flow field continuity and momentum equations. Using the balance equations obtained experimentally, the authors estimated the terms of diffusion involving fluctuations in pressure and the dissipation rate of turbulent kinetic energy.

Escudié and Liné (2003) performed the triple decomposition by synchronizing the data acquisition and the position of the impeller blades to capture the decomposed flow phenomena. The number of planes depends on the geometry of the impeller, in this case a Rushton turbine with six blades equally spaced was used. In these conditions, the flow reconstruction was performed using measurements of 1° angle-resolved, recording a total of 60 different planes.

According to the experiments performed by Escudié and Liné (2003), the radial profile of TKE increases and then decreases. In addition to determining the exchange of kinetic energy between the different flows, this radial behavior was evaluated through the balance of the different types of kinetic energy (mean, periodic and turbulent). The impeller does not promote a symmetrical radial jet, but the flow is smoothly directed upwards, since the top of the tank is a free surface and the bottom has a wall. Additionally, the impeller is not symmetrically located at the height of the tank (Escudié and Liné, 2003). According to Yanneskis (2000) there is a difficulty in comparing different sets of data to validate measurements. The standardization of velocity measurements with respect to the tip speed and height of the impeller is only valid for comparing data if the geometries of the stirred tank are the same.

Through a Reynolds decomposition in the tank it is possible to measure the total fluctuation of the kinetic energy, as shown in Equation 2.14. However, this cannot be analyzed close to the impeller blades since it is not possible to separate this fluctuation of random and periodic fluctuations generated by the movement of the blades (Escudié and Liné, 2003).

$$k_{total} = \bar{k}_{periodic} + k_{turbulent} \qquad \text{Equation 2.14}$$

Studies conducted by Escudié and Liné (2003) showed that in the center of the tank, the periodic kinetic energy represents more than 80% of the total kinetic energy. Near the impeller blades, the vortices have higher tangential velocities and significant periodic energy. The total kinetic energy presents higher values in the jet and in the regions close to the impeller. Its value falls with greater velocity after the point where the radial location (r/R) is 1.5. For regions close to the impeller, the values of the turbulence quantities are measured in a stirred tank according to the rotation speed of the impeller. This requires high spatial and temporal resolution, with low speed accuracy in the impeller area with high speed of rotation. Their influence on PIV measurements can be assessed through turbulent kinetic energy (Saarenrinne, et al., 2001).

The vortices disappear as the distance from the impeller blades increases, and in this case, there is also a greater radial variation in the TKE. This increase may be linked to the decrease in periodic kinetic energy in the same region, keeping the total kinetic energy constant. Thus, the exchange of kinetic energy can exist between the turbulent and periodic components (Escudié & Liné, 2003).

2.5.PIV OPTIMIZATION AND CHALLENGES

PIV is a set of methods for evaluating the particle displacement using statistical cross-correlation in consecutive images (Adrian & Westerweel, 2011). However, PIV methods are becoming more sophisticated and exceeded the ability to quantify its measurement uncertainty. This situation is intensified by the fact that measurements involving instruments and algorithms coupled with uncertainty sources, making it more complex to determine the quality of the PIV measurements (Xue, et al., 2014). Thus, it is important to develop methodologies that allow quantifying the PIV uncertainty, increasing the reliability of its results.

Timmins et al. (2012) employed a "uncertainty surface" methodology that is constructed by mapping the effects of primary error sources, such as local shear, displacement, and particle density. The method is like the standard calibration procedure, whose surface of uncertainty provides the means to associate the distribution of errors from any source. However, all possible parameters combinations must be tested to quantify the uncertainty, which can make the use of this method unfeasible due to the computational cost.

Sciacchitano et al. (2013) developed a method based on the correspondence of particle images, which calculates the displacement uncertainty from a set of disparity vectors between pairs of particles in the interrogation windows. This method is effective for errors from random and systematic sources, but peak-locking errors cannot be detected. Another limitation of this method is that it fails to explain the effects of particle loss outside the plane.

Xiu et al (2014) investigated the quantification of PIV measurement uncertainty through information contained in the cross-correlation plane. This plane represents the distribution of probabilities for all possible detachments of the particle image pattern between consecutive frames, combined with the other characteristics of the particles and the effects of error sources.

The developed methodology proposes to quantify the quality of the cross-correlation through the signal-to-noise ratio (SNR).

PIV velocity measurements are influenced by parameters such as the seed concentration, the size of the measurement area, the interframe time and the spatial resolution. These can be optimized for more reliable results. The investigation area must be as large as possible while the spatial resolution must be small enough to identify and measure any significant turbulent structures. To find the best configuration, different sizes of measurement domain can be tested, however these are restricted to the region near the tip of the impeller, where the exchange of kinetic energy are the most significant (Escudié & Liné, 2003).

2.5.1. NOISE SOURCES, ERROR AND PIV STRATEGIES

The curvature of the tank causes the image recording plane to be tilted in relation to the plane of the object, causing the recorded image to blur. The presence of metallic structures in the tank, such as baffles and even the impeller blades are a source of noise due to the reflection of laser light in these parts. The imperfection of the lenses, the different indexes of refraction and the misalignment of the recording plane in relation to the object plane also influence the distortion of the images. Image magnification and blur introduce systematic bias errors in the measurements (Soloff, et al., 1997).

To reduce the effects of refractive index on measurements by minimizing laser light distortion, Chung et al. (2009), Delafosse, et al. (2011) and Alonzo-Garcia et al. (2019) inserted the cylindrical experiment tank into a cubic correction box filling both with the same type and level of fluid. Yet Chung et al. (2009) and Delafosse, et al. (2011) painted the non-transparent parts in matte black to minimize the reflection of the laser light.

Unadkat et al. (2011) applied the Stereo PIV technique to study the characteristics of turbulent flow in stirred tanks. The authors determined the three displacement components, the local dissipation rates and discussed the effects of spurious vectors on PIV measurements. The experiments were carried out in a cylindrical tank that was placed inside a larger pentagonal tank, filled with the same fluid to eliminate the dispersion fraction in the curvature of the tank. Also, the deflectors are painted in matte black to minimize reflections.

Li et al. (2013) studied the mean velocity and the TKE in stirred tanks by Rushton impellers using Stereo PIV. The authors also used the stirred cylindrical tank inside a correction box to minimize the refraction of the light beam and used a water prism to keep the lens axis of the two cameras perpendicular to the corresponding air-water interfaces.

One of the main challenges for the application of PIV in stirred tanks is the effects of optical distortion caused mainly by the curvature of the tank and the illuminated particles when they are observed through an optically inhomogeneous medium. Soloff et al. (1997) formulated a PIV calibration procedure to compensate the distortion of PIV and Stereo PIV images, however this method is applicable only for fixed optical windows.

Elsinga et al. (2005a) observed in the field of aerospace engineering that the images of the velocity field in non-homogeneous media can present deformations and blurs. In addition, it is possible to identify errors in the position and velocity of the particle. These last two are associated with the systematic error of the velocity measurement, by the geometric deformation of the image, and are originated by the gradient of the refractive index. These blurs alter the particle sizes, directly influencing the accuracy of their tracking by cross-correlation analysis. These errors become more significant in large-scale PIV applications.

In recent years, researchers have been developing methods to estimate the uncertainty limits and provide solutions to minimize specific noises. It is important to note that all uncertainty quantification methods have strengths and limitations. Sciacchitano and Scarano (2014) studied the use of a high-pass temporal filter to remove unstable background reflections. This method is based on frequency domain signal decomposition. In this way it is possible to separate the contribution of particle images (high frequency) from reflections (low frequency signal), removing the latter.

Figure 2.12 represents the correlation plane of the image pairs captured at two different time points. This plane is obtained through a PIV correlation algorithm and shows the probability distribution of all possible displacements of the particle image between consecutive frames. In quality PIV measurements, the highest peak must correspond to the actual displacement of the particle. In addition, a combination of noise effects that affect the accuracy of the actual image shift is also shown in the correlation plane (Amaral, 2017).

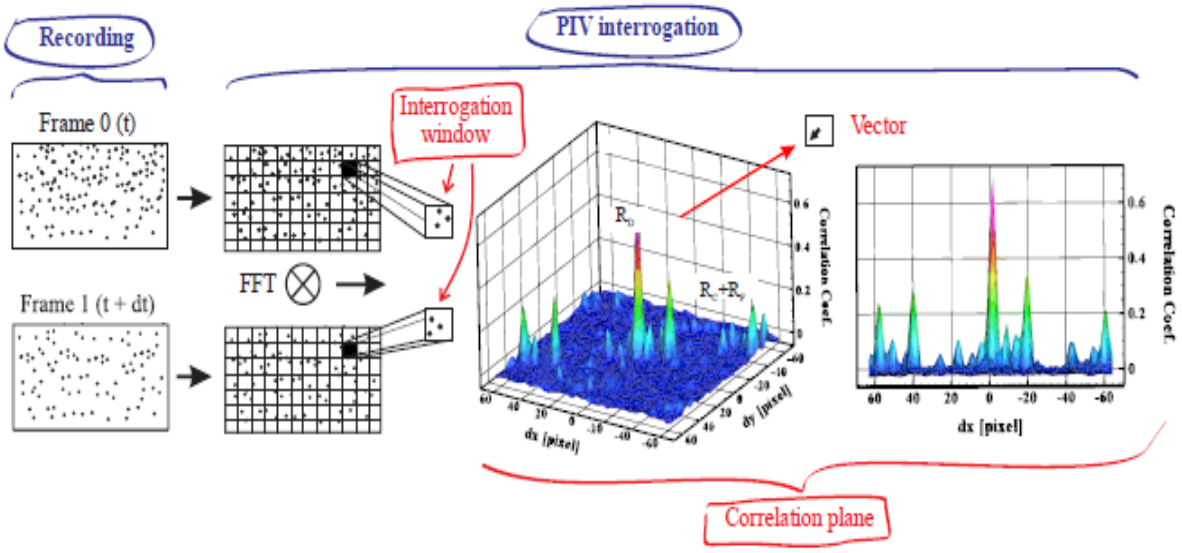

Figure 2.12. Correlation peaks of the displacement of particle images (Rd) and noise sources (Rc and Rf) in the correlation plane for a 128 pixel interrogation window *(Amaral, 2017)*

In a noiseless field, the velocity value in the interrogation window varies slightly in the neighborhood. However, it is difficult to avoid the presence of false vectors in the field. After the cross-correlation, the post-processing of the images is performed through temporal and spatial filters to improve the quality of the PIV measurement. The problem is that these filters can fail in the presence of outliers (Adrian & Westerweel, 2011; Masullo & Theunissen, 2016; Raffel, et al., 2018). Figure 2.13 shows the effect of PIV post-processing in fields with outliers, that is, false vectors that are easy to detect. It is observed that in the field without post-processing, that is, with a greater presence of outliers, some regions present values with high discrepancy in their neighborhood.

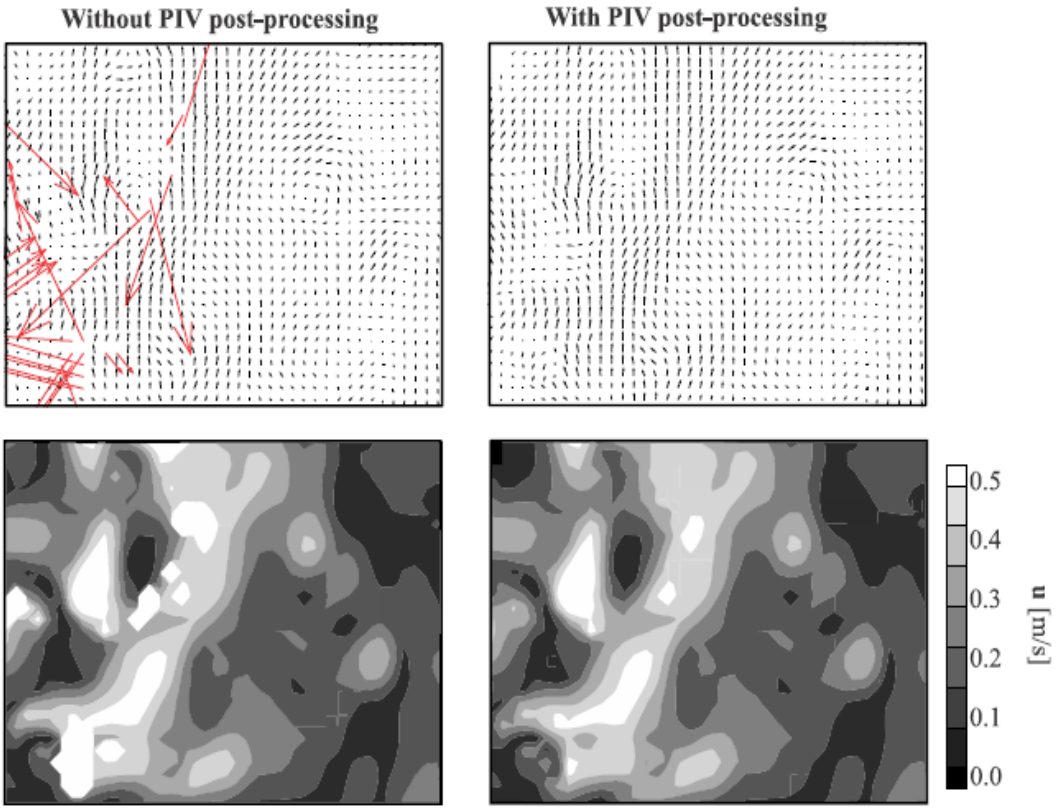

Figure 2.13. Effect of PIV post-processing in fields with outliers *(Amaral, 2017)*

Reflection of laser light against solid surfaces is one of the parameters that affect the quality of PIV measurements. A high correlation peak can be generated in cases where the reflections have high intensity. If the peak of the noise source is greater than the peak corresponding to the actual displacement of the particle images, a spurious vector is generated. Therefore, the reflections affect the accuracy of the method in determining the flow velocity, especially in the regions close to these surfaces (Adatrao & Sciacchitano, 2019).

Some practices can be adopted to avoid or reduce the reflections of the laser light in the acquisition of experimental data. Matt black paint can be used to cover solid surfaces, especially metallic components (impeller, deflectors, screws, and others) so that most of the laser light is absorbed rather than reflected. Fluorescent paint can also be applied to surfaces. In this case, instead of avoiding reflection, it changes the wavelength of the reflected light from green to red so that the green light is only from the tracer particles. And a bandpass filter can be attached to the camera lens to reject red light from the surface (Gui, et al., 2001; Depardon, et al., 2005; Adatrao & Sciacchitano, 2019).

Despite the benefits in relation to the reflection of light, painting solid surfaces can change the roughness, thickness and other characteristics of the experimental system that can influence the results. As a result, some authors have investigated the use of other materials and the influence of the image angle on the quality of the measurements. Kähler et al. (2006) used the lighting of the tangential model to reduce the effects of unwanted reflections on flat surfaces. Kähler (2009) studied the reflection of light in different materials and concluded that the use of highly polished aluminum presents better results.

In situations where it is not possible to minimize the reflections of the laser light in the physical space, these must be performed in the pre-processing stage of the images. With image restoration it is possible to remove background noise from the image, keeping only the particle image signal. This can be done by subtracting recorded images. The investigation area is recorded without the presence of the tracer particles and this is subtracted from the image with the particles, removing background noise (Adatrao & Sciacchitano, 2019). Honkanen and Nobach (2005) performed a background removal method for double-frame PIV images. According to the authors, in regions of low velocities or with high seeding, the removal of images of recorded particles may occur. In addition to this double recording, background images can also be generated by statistics in relation to the light intensity of each pixel. This technique, however, only brings satisfactory results for stationary problems (Adrian & Westerweel, 2011).

Many authors suggest that while background reflections have a large extension, particle images have smaller scales, between 1 and 5 pixels. In this way, high-pass spatial filters can be applied to filter the contribution of the background image. However, some filters may perform poorly in some regions, such as isotropic in regions with sharp reflections. Despite studies to develop different methods of eliminating unwanted reflexes in PIV measurements, there is still a lack of knowledge. It is necessary to develop an effective methodology without the use of image statistics for applications where the reflection of light is unstable (Adatrao & Sciacchitano, 2019).

Adatrao and Sciacchitano (2019) developed a new approach that proved to be effective in removing unstable background reflections that would not be possible with statistical analysis. The presented method uses anisotropic diffusion, in which the intensity of the image is diffused only along the edges and not through them, maintaining sharp reflections in the background image. This last image is subtracted from the original one, producing a pre-processed image

with only the images of particles and absent of reflections. This method also does not cause distortions in the regions that are not affected by the reflection.

There is an increasing number of studies that propose to investigate the measurement noise of the PIV technique, these are mostly related to theoretical modeling of the processing algorithm and mostly by Monte Carlo simulations. However, it is known that the latter underestimate the errors that occur in PIV experiments, since the flow conditions are very idealized (Stanislas, et al., 2005; Sciacchitano, et al., 2015). In addition, most authors focus their studies on creating alternatives for a specific noise source. Thus, there is still a knowledge gap for optimizing the uncertainties of PIV measurements.

2.5.2. SPACIAL RESOLUTION AND INTERROGATION WINDOWS

Non-intrusive techniques, such as PIV, offer numerous advantages when measuring turbulent flows. However, it is important to highlight that these techniques need to be validated to estimate the limitations of spatial resolution. Although the PIV methodology has been presenting numerous advances, there are questions about the influence and capacity of the method's spatial resolution to accurately measure turbulent parameters (Lavoie, et al., 2007).

To analyze complex flows with PIV, some domain locations require a high spatial resolution. While in conventional techniques, interrogation windows are optimized globally, with adapted techniques it is possible to locally improve the spatial resolution. In the standard method, as non-ideal conditions are accepted in some regions, there is a greater number of false vectors, increasing the uncertainty of the method. In the locally adapted technique, the SNR in these regions is kept almost constant (Theunissen, et al., 2006).

The size of the interrogation window is an important parameter for the quality of PIV measurements and should be selected based on the spatial resolution and quality of data required. It is still essential to know the size of the detection domain and the smallest relevant flow scale. Scales smaller than the measurement volume can introduce significant errors in the results of velocity measurements. The number of outliers increases as the size of the interrogation window decreases, as there is a reduction in the number of particle images in each window, and movement out of the window increases (Lavoie, et al., 2007).

Lavoie et al. (2007) evaluated the use of the PIV technique to solve scales in a turbulent flow comparing it with theoretical predictions. The authors also analyzed the statistical convergence and the spatial resolution of PIV. They developed a method to quantify and correct the effect of finite spatial resolution on PIV measurements that compensates for the reduction in velocity fluctuations. The turbulent kinetic energy parameters are significantly underestimated due to the low spatial resolution.

The PIV interrogation volume is defined by the size of the interrogation window and the thickness of the laser light beam. Multigrid iterative techniques increase spatial resolution by adjusting the size and shape of the interrogation window, which is an important feature, since most flows are not uniform. From a progressive refinement the parameters such as size and overlap factor can be adjusted at each step (Theunissen, et al., 2006; Lavoie, et al., 2007).

Theunissen et al. (2007) propose to use locally adapted windows based on their location and size to improve spatial resolution. Furthermore, the spatial variation of the velocity field was the parameter used to define the spacing between windows. Delafosse, et al. (2011) studied the application of the PIV technique to estimate the kinetic energy dissipation rate in a stirred tank with a downward-pumping axial impeller used for animal-cell cultures. The authors used an adaptive correlation windowing strategy with a final IW of 16 x 16 px with 50% overlap and tested four spatial resolutions for each rotation speed.

In standard PIV processing, the size of the interrogation window can be kept constant, for example 32x32 or 64x64 pixels. It is essential that each window present enough image particles for correlation. In flows, the number of particles varies randomly and are smaller in regions of low seeding or with greater movements out of the plane. In these cases, advanced adaptive algorithms can be used. These adapt to flow and velocity gradients, especially in regions with vortices and high shear rates (Wieneke & Pfeiffer, 2010).

The spatial resolution influences the reproduction of turbulent structures such as vortices and eddies regions. Thus, this phenomenon also interferes with the mean profile and maximum velocity of the flow. When compared with high spatial resolutions, regions with low spatial resolution (larger interrogation areas) have higher flow velocity in the entire field. As turbulent structures are not accurately evaluated at low spatial resolution, they do not significantly integrate the statistical calculation of the flow velocity profiles. Another important point is that the standard deviation is higher in measurements with high spatial resolution due to a clearer

interpretation of the vortex structures that decrease the average flow velocities (Kotek, et al., 2017).

2.5.3. PIV IMAGE CORRELATION

Recorded particle images using PIV are subject to distortion, warping, and focus issues. Optical windows with complex geometries and fluids with different refractive indices can cause image distortion. The distribution of the refractive index in the environment produces two types of systematic errors: position error and velocity error. The different refractive indices, in addition to the fluids, are also caused by the material of construction of the experimental system (e.g. glass or acrylic) and its curvature (Adrian & Westerweel, 2011; Amaral, 2017).

The mapping function obtained in the calibration step is used to correct the distortion caused by the optical window through image reconstruction. Otherwise, blur compensation of a single-particle image is more difficult. In addition to the focus problem, the particle image can also deviate from its current position due to refraction (Amaral, 2017).

Elsinga et al. (2005b, 2005c) explained that the main effects of particle image blur are the reduction of image contrast and signal-to-noise ratio (SNR), which can also lead to increased correlation peaks and decreased measurement accuracy of PIV. Figure 2.14 presents the correlation plane for the distortion and undistorted particle images. It is possible to observe that the elongation of the peak depends on the displacement of the tracer particles between the image frames.

As shown in Figure 2.15, when a tracer particle moves from an undistorted region to a distorted one, the cross correlation peak will be elongated, resulting in a subpixel order error. In regions with heterogeneous refractive indices, the duplication of particle images can also occur. These situations generate false velocity vectors that compromise the quality of PIV measurements. The duplication of individual images of particles causes displacements that do not represent the actual movement of the particles in the flow, and with this there is a reduction in the signal-to-noise ratio (Elsinga, et al., 2005c).

Medium heterogeneity and distortion effects can produce blurry particle images. If these are blurred in the same amount between consecutive frames, the correlation plane is symmetric and will not show polarization errors, making it possible to obtain the real velocity vector.

Figure 2.16 shows the four types of particle images that can be found in a heterogeneous medium, caused by differences in refractive indices. According to simulations conducted by Elsinga et al. (2005b), particle images can be undistorted (ideal situation), stretched or blurred, duplicated, and duplicated with blur.

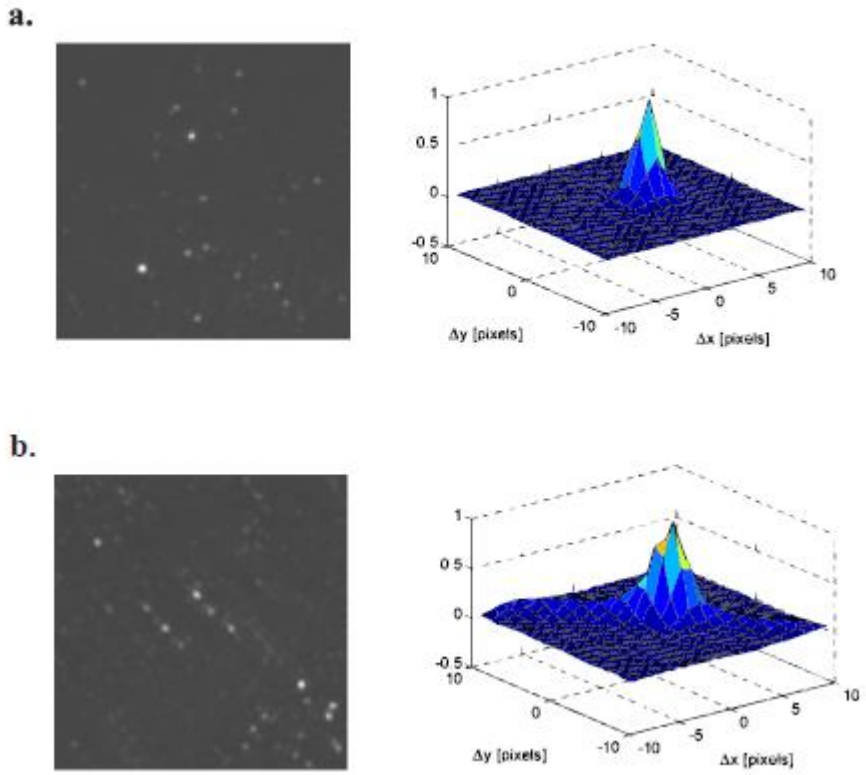

Figure 2.14. Correlation plane for the image (a) without and (b) with distortion effect *(Elsinga, et al., 2005b)*

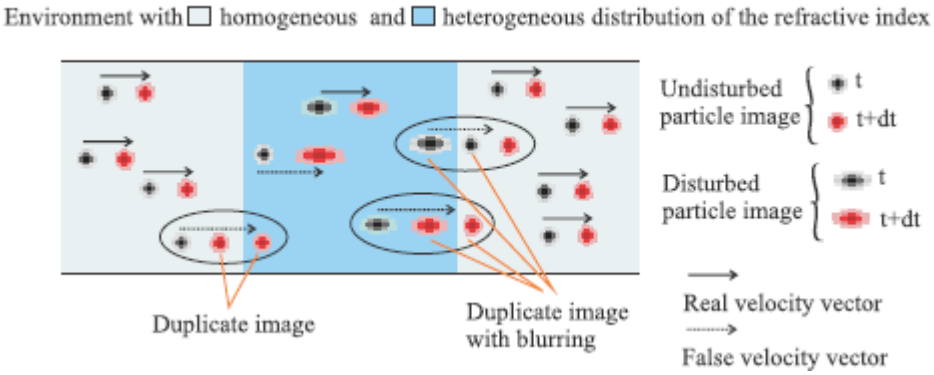

Figure 2.15. Differences between distorted and undistorted medium *(Elsinga, et al., 2005c)*

Figure 2.16. Four types of particle images in an environment with heterogeneous refractive index distribution: (a) undistorted, (b) blurred (stretched), (c) duplicated, and (d) duplicated with blur *(Elsinga, et al., 2005b)*

Since different refractive index can cause disparities in obtaining correlation peaks, it is necessary to evaluate how their behavior can compromise the quality of PIV measurements. Furthermore, it is important to investigate ways to compensate for image distortion in physical and image space.

2.6. POST-PROCESSING FILTERS – USE AND LIMITATIONS

According to Raffel et al. (2018), some important steps in post-processing are the verification of the original data and the replacement of incorrect data. False vectors or outliers are data generated in the processing step that have characteristics different from their surroundings. Eliminating this inconsistent data is crucial for the quality of the results, and this can be done by a highly reliable algorithm.

Many authors have dedicated themselves to the development of post-processing filters to detect outliers. A simple standard approach is based on neighborhood comparison. In the temporal and/or spatial dimensions, spurious vectors that are incompatible with neighboring vectors are removed. However, the intermediate detection of these vectors in iterative image processing sequences may only be subject to spatial information (Masullo & Theunissen, 2016).

Westerweel (1994) applied a data validation algorithm through median filtering, making it possible to remove noise and treat spurious velocity vectors. The author classified the neighboring velocity vectors linearly in relation to the magnitude of the velocity vector. The central value in this order is the median value. Later, Westerweel and Scarano (2005) improved this algorithm, developing a robust detection filter based on the normalized mean threshold (NMT). In this method, the difference between a correct vector (which represents the real

displacement of the particle) and its estimator is based on the median of the neighborhood. However, Duncan et al. (2010) highlighted that this filter is not suitable for application to unstructured data and must include a weight inversely proportional to the distance between the vectors.

In the experiments conducted by Kotek et al. (2017), two validation methods were used to eliminate outliers. In the first step, the authors employed the interval validation, in which all vectors with a size greater than 3 m/s were eliminated. Then they chose a validation method based on the moving average filter. All vectors that did not correspond to its neighborhood were eliminated and replaced by the mean value.

Outlier detection filters can have underdetection and overdetection failures in image post-processing. The main challenge in data validation is to develop algorithms that are balanced and avoid these types of failures. Underdetection occurs due to the presence of spurious vector clusters that are erroneously considered to be correct. In this case, the vector agrees with its neighborhood, but the entire region is incorrectly representing the flow. This situation is due to the increased level of fluctuation which makes the normalized limit at the same level as the correct vectors. The presence of areas with low density of tracer particles or with strong light reflections directly influence these cases. On the other hand, overdetection occurs by identifying correct vectors as erroneous due to the presence of large velocity gradients (Masullo & Theunissen, 2016; Raffel, et al., 2018).

Nogueira et al. (1997) developed a method to minimize outlier detection failures. These false vectors are iteratively discriminated based on the interpolation of the eight closest vectors evaluated as coherent. This is quantified as the ratio between the residual mean and the mean magnitude of the vectors. However, this method does not show good results in the presence of clusters of outliers, since it can consider correct a set of vectors that are incoherent. Coherence should only be used as a parameter to predict the number of neighbors that should be used to estimate the real velocity of the local flow and should not be used to identify outliers. For a vector to be considered coherent, it must agree with a second-order surface fitted to the eight closest neighbors (Masullo & Theunissen, 2016).

Later, Shinneeb et al. (2004) applied a local median filter to identify potential outliers and replace them with a value based on the weighted average of the Gaussian. The authors emphasize that in most experiments the selection of the threshold is not clear. For example, very small threshold can reject numerous valid vectors. However, in this method, the limit is

adjusted with an average variation between the evaluated vector and its eight neighbors. After this step, the residual between the measured vector and the forecast is evaluated. This approach has produced promising results for reducing over and underdetection.

Masullo and Theunissen (2016) developed a new adaptive vector validation approach that can detect outlier clusters. This method can reduce the degree of overdetection, without presenting high computational complexity and increasing processing costs. In the first step, the number of neighboring vectors used in the comparison is adjusted based on the coherence of the local flow. Next, the average weighted median is performed to reduce excess detections, restricting the importance to closer data. Finally, spurious vectors are classified as local anomalies in the direction and magnitude of the vector. In this algorithm, each vector must be considered valid from the start and the coherence must only dictate the extent of proximity to be considered.

The quality of PIV measurements is subject to interference due to experimental apparatus and its conditions, and processing methods. Noise sources cause image distortion, which can lead to incorrect data and outliers. To ensure the quality and accuracy of PIV measurements and to be able to obtain reliable turbulent flow data in stirred tanks, it is important to develop robust filters and methods for field correction in the PIV processing steps.

CHAPTER 3

COMPENSATION OF IMAGE DISTORTION ON PIV MEASUREMENTS OF A STIRRED TANK

In this chapter, the results and discussions are presented in an article format. This first article is going to be submitted to the Journal of the Brazilian Society of Mechanical Sciences and Engineering.

COMPENSATION OF IMAGE DISTORTION ON PIV MEASUREMENTS OF A STIRRED TANK

Aliandra Duarte Barbutti[1], Aline G. De Mitri[1], Jenniffer S. Ayala1, Rodrigo de L. Amaral[2], Helder L. de Moura[1], José R. Nunhez[1], Guilherme J. de Castilho[1].

[1]University of Campinas, School of Chemical Engineering, Process Engineering Department.

[2]POLI, University of São Paulo, POLI, Department of Mechanical Engineering, NDF.

Manuscript under review for journal submission

ABSTRACT - Particle image velocimetry (PIV) measurements are increasingly common in investigating turbulent flow parameters for the optimization of stirred tanks. Generally, PIV applications are performed by positioning the camera perpendicularly to the light plane. In some cases, the use of tilted images is the most suitable when there is a limitation of the optical access. In the case of measurements in a tank, the curvature changes the relationship between the physical space and the image plane, causing distortions, which can be compensated in the physical space using a correction box around the tank, for example. However, this can often become expensive or unfeasible in the experimental arrangement. Another way to correct the distortion effect is by applying a third-order polynomial function from a calibration procedure. Nonetheless, this global function could fail in regions with high distortions. In this context, this work aims to investigate the performance of the image distortion compensation on PIV measurements of a stirred tank by applying a polynomial function from a calibration procedure in one and two steps (calibration and multicalibration, respectively). Two cameras at different positions were used simultaneously to record a calibration target, without using a box filled with the work fluid around the tank. This approach showed promising results mainly for the camera positioned with the smallest angular displacement in relation to the object plane. We also determined the turbulent kinetic energy (TKE) distribution of the tank flow by applying

the best camera position setting. It was verified that the calibration and the multicalibration procedures did not present significant differences in the TKE results.

Keywords: Image Distortion Compensation, Calibration, Stirred Tank, PIV

1. INTRODUCTION

Stirred tanks are widely used for various industrial applications involving heat, moment, and mass transfer operations. The equipment geometry, number of baffles, model and arrangement of the impeller are characteristics that influence the turbulent flow pattern inside the vessel (Alonzo-Garcia, et al., 2019). Pharmaceutical industries, for example, have used mechanically agitated high-throughput experimentation (HTE) reactors to develop catalysts for polymerization reactions. These reactors are small-scale and if associated with low Reynolds numbers, can have low mixing efficiency and limited mass transfer rate. A more detailed understanding of the hydrodynamics and the mixing pattern inside these reactors is essential to optimize their operation and thus maximize the efficiency of the formulations (Chung, et al., 2007). Moreover, in the petrochemical industry, stirred tanks are used to store crude oil and fuels such as gasoline and diesel to guarantee the homogenization of the liquid mixture. In these situations, the mixing parameters are often determined in a heuristic manner as there are few studies involving their evaluations, even on a laboratory scale. (Gómez, et al., 2010; Fang, et al., 2011). In order to fully comprehend these mixing mechanisms in stirred tanks, it is necessary to detail their hydrodynamics. For instance, the size and periodicity of eddies and vortices formed by agitation influence the mixing models and parameters, especially the turbulent kinetic energy and energy dissipation rate (Kresta & Wood, 1991).

Flow parameters usually analyzed in stirred tanks are the instantaneous and average velocities, the periodically induced stress, the mixing efficiency, the mass transfer and its interactions, and the Reynolds stress. These parameters support the identification and quantification of the kinetic energy transfer between the mean flow, periodic, and turbulent fluctuations (Escudié & Liné, 2003; de Lamotte, et al., 2017). They also allow the estimation of the turbulent kinetic energy (TKE) and the energy dissipation rate, which are essential characteristics for stirred tank designs. Regarding TKE, the velocity fluctuations are related to turbulent dispersion and mixing, impeller geometry, position in the tank, and

the rotation speed. The TKE influences the mixture quality and its effect is clearly observed in regions close to the tank's wall and close to the impeller blades where eddies are formed.

The identification of turbulent flow parameters requires instantaneous velocity field information in axial, radial and tangential directions (Khan, et al., 2006). Different experimental techniques can be applied, such as the particle image velocimetry (PIV), which allows quantifying the characteristic eddies scales and evaluating the mixing processes (de Lamotte, et al., 2017; Alonzo-Garcia, et al., 2019). PIV is a quantitative and non-intrusive technique capable of determining velocity fields by analyzing tracer particle images. The measurement principle consists of a laser system that illuminates the region of interest in the flow and interacts with the particles immersed in the fluid to allow the acquisition of images every two consecutive times (double-frame) by cameras usually positioned at 90º to the light sheet. The determination of the speed field is carried out through the analysis of cross-correlation between the particle images in small areas known as interrogation windows. Hence, this method reconciles the use of high-resolution cameras and powerful lasers that can register all points of a velocity field in flow, even in turbulent regimes (Adrian & Westerweel, 2011; Wieneke, 2017; Raffel, et al., 2018).

The quality of PIV measurements is directly related to the precision in which the displacements of the particle images can be measured and thus represent the average displacement of the particle population in an interrogation window. Image distortion is an effect that can deteriorate the quality of these measurements, as it creates a non-linear relationship between the positions of the tracking particles in physical space and their corresponding image. The distortion occurs when any source promotes variation in the magnification as a function of the position of the particle in the plane. Magnification is the ratio between the distance of the image and the object to the center of the lens and its leading causes are imperfections in the lens design, misalignment of the image recording plane with the object plane and refraction. The distortion associated with the heterogeneity of refraction is evidenced by the curvature of the investigation system, which can be a tank, a bubble column or a pipe, for example, as well as with differences in the refractive index of the fluid and the equipment material. The curvature can act as an optical lens and blur the recorded image and these variations cause systematic errors concerning the velocity and the position of the vector in the image plane. However, this effect can be repaired from experimental calibration or distortion compensation algorithms (Soloff, et al., 1997; Elsinga, et al., 2005a; Raffel, et al., 2018).

In order to compensate image distortions, two different approaches can be applied. The first is to reduce the interference in the physical space by changing the physical structure of the experimental system. A “correction box”, which is a transparent component either solid or hollow and filled with a transparent liquid, can be employed to minimize the effects of the curvature of the tank and ensure an orthogonal position of the line of sight of the cameras. For better performance of the correction boxes, they must have thin walls, be produced with the same transparent material as the structure of the experiment (glass or acrylic, for example), and be filled with the same liquid of the main flow (Prasad & Jensen, 1995). Sharp & Adrian (2001) applied a rectangular box to assess the turbulent structures in a cylindrical tank agitated by Rushton impellers. Micheletti et al. (2004) encased the tank with a square correction box to carry out Laser Doppler Anemometry (LDA) and PIV measurements to identify the energy dissipation rate of flows induced also by a Rushton impeller. The obtained values were compared with estimations from numerical methods showing good agreement. Chung et al. (2007; 2009) inserted the experimental cylindrical tank into a cubic box and performed PIV experiments to evaluate different arrangements: with deflectors, without deflectors and with the impeller in an eccentric position. These studies were able to characterize the flow periodicities and to estimate the turbulent parameters without the influence of refractive distortions.

Li et al. (2011) employed a rectangular box around the experimental tank with the same objective of minimizing optical refraction. The authors studied the influence of the diameter of the Rushton impeller on the turbulent flow of a stirred tank using PIV measurements at a resolved angle and Large Eddy Simulations (LES) and obtained satisfactory results for both methods. Stelmach et al. (2019) evaluated the distribution of turbulent kinetic energy in a tank agitated by a self-aspirating disk impeller. The study was carried out with a PIV system in which a rectangular box around the cylindrical tank was applied, similarly to Li et al. (2011). Alonzo-Garcia et al. (2019) used PIV data measured in a tank placed inside a cubic tank filled with water to validate different turbulence simulation models. Despite all these applications, the use of “correction box” has as main problem: the complexity of the box construction, which makes its application often unfeasible, as well as the high cost of installation and use, especially if the study fluid is not water. Furthermore, when it is important to perform measurements at different azimuthal positions to eliminate the periodic component on the turbulent parameters, the use of the box can be unpractical.

When methods based on changes in the physical space are not sufficient to eliminate optical distortions, a second approach can be applied. It refers to perform the image reconstruction using a mapping function. This function relates the location of the tracking particles in the physical space with the image recording plane and determine an image/object scale factor compensating for the distortion of the physical space. The procedure is carried out by mapping a standard calibration target, before or after the acquisition of the experimental images. Most PIV correlation methods use a uniform grid fixed in the pixel matrix of the image acquisition camera to determine the velocity vectors, which it would be difficult if the grid was non-uniform or distorted. However, by using the mapping function, vectors can be interpolated in any grid within the function domain. The latter methods can be applied if the distortions are not so severe as to make the image of the calibration target unacceptably inaccurate (Soloff, et al., 1997; Adrian & Westerweel, 2011; Raffel, et al., 2018).

The mapping function is obtained from a calibration procedure using a calibration target. According to Soloff et al. (1997), this target must be elaborated based on the characteristics of the system under study and it is a fundamental step for a successful calibration. The calibration target must have characteristic marks, usually dots, placed under an equally spaced Cartesian grid. The image of the mark pattern is responsible for defining how the positions in the object plane are mapped in relation to the positions in the image plane. Thus, the number of marks and the space between them are chosen based on the acquisition area and the distortion in the experiment. The size and geometry of the target are defined and limited by the measurement medium, but they must be large enough to occupy the entire field of view of the camera. Before starting the calibration procedure, it is necessary to define the origin of the coordinate system, while the other points are measured concerning this origin mark.

Based on the mapping function, it is possible to calculate the displacements of particles anywhere in the studied area. Many numerical methods can be used to obtain the mapping function; however, it is common to use a multidimensional polynomial due to its simplicity. The relative error of the function is associated with the domain size of the mapping function in the investigated direction. It indicates the deviation among flow displacements regarding the size of the mapped region. The calibration procedure proposed by Soloff et al. (1997) establishes the magnification matrix of a distorted image system, in which it is possible to obtain a mapping function that provides an accurate way to correct distortions and to calculate velocity field displacements. This method has been applied in

many studies to allow the recombination of stereoscopic images in building three-dimensional velocity fields (Kilander & Rasmuson, 2005; Khan, et al., 2006; Alberini, et al., 2017).

Rottier et al. (2010) applied a similar calibration approach to compensated distortion effects of endoscopic PIV images in high-temperature furnaces. In these procedures, a calibration target was used, consisting of a grid pattern of regular crosses, each one separated by 10 mm from the other crosses. Due to the experimental characteristics and high distortion of the images (mainly in the radial direction), the method using polynomial function did not prove to be accurate to reconstruct the entire image in this case. Thus, the authors developed a method based on a square grid pattern in which regions are successively corrected and the correlation analysis was performed with a direct algorithm. Besides, Zhang et al. (2014) used a related calibration strategy to correct image distortions of measurements on the spray mixing process. It was used a calibration target in the two optical channels, but the correction parameters were based in the pinhole camera model proposed by Tsai (1987). The strategy of image distortion compensation proposed in this work has been only applied in different processes and there is a lack of studies on its application in stirred tanks. Only recently, Barbutti et al. (2011) applied a 2D calibration based on the Soloff et al. (1997) method and used a third-order polynomial function to compensate for image distortion caused by the curvature of the stirred tank.

The present work aims to investigate the performance of the approach developed by Soloff et al. (1997) to compensate the image distortions of PIV measurements in a stirred tank without the use of correction boxes. The proposed method uses two cameras positioned at different angles from the normal light plane to evaluate the results of the angular displacement in relation to the object plane. The calibration procedure is carried out using a calibration target to obtain the mapping function. Besides the usual single calibration method, this work proposes a new strategy, called multicalibration, in which the dewarped images underwent a second calibration. The distortion compensation is then assessed through qualitative and quantitative analysis of the adjustment of the mapping function to the images of a calibration target. Moreover, the influence of the approach on the distribution of the turbulent kinetic energy from the flow is verified.

2. EXPERIMENTAL

2.1. Experimental apparatus and data acquisition

A pilot unit of a stirred vessel (Figure 3.1a) was used in the experiments. The acrylic cylindrical tank has an inner diameter T = 380 mm and a standard torispherical base ASME of 10%. The liquid was agitated by a 45° pitched blade turbine (PBT) with a diameter D = 2T/5 and clearance C = T/3. The tank was equipped with four equally spaced baffles of width B = T/10 (Figure 3.1b) and filled with water (density ρ = 997 kg/m³ and viscosity μ = 1,002.10-3 Pa.s) to a height of H = T.

In order to assess the positioning of the camera in distortion compensation, the recording was made simultaneously by two cameras FlowSense EO 8M-21 model (3312 x 2488 pixels, 5 Hz) in different angular positions (Figure 3.1c): camera 1 at $\sigma + \beta = 40^o$ and camera 2 at $\sigma = 10^o$ to the normal of the light sheet (object plane). Despite the unusual configuration, the Scheimpflug principle was respected, that is, the collinearity between the planes of the object, the lens, and the image was ensured to guarantee the focus on the object plane (Prasad, 2000). Figure 3.2d provides a more detailed view of the arrangement between cameras, laser and stirred tank. The calibration target was a 210 mm x 750 mm plate made of ABS polymer, printed in a dot pattern with a diameter of 0.5 mm equally spaced at a center-to-center distance of 1.5 mm. The aperture of the lens was manually adjusted to make sure the complete image was in focus. The image acquisition was performed using the Dynamic Studio software (Dantec Dynamics).

Figure 3.2 shows the raw images of the calibration target obtained by Cameras 1 (Cam 1) and 2 (Cam 2). To better visualize the distortion of the images, two regions were selected and zoomed in: Region 1 (R1), close to the shaft, and Region 2 (R2), close to the tank wall. Concerning Camera 1, positioned closer to the calibration target plane, both regions showed negative slopes in the dot pattern. These slopes were - 15.29º ± 0.50º for R1 and -20.34° ± 1.40º for R2. However, for Camera 2, positioned closer to the normal axis of the calibration target, the dots in R1 were practically straight, with a slight inclination of 0.84º ± 0.32º. At the same time, the dot pattern in R2 presented a significant positive inclination of 17.20º ± 0.55°. Although both cameras present distortions in the images, for Camera 1 the whole image follows a similar pattern of variation whereas, for Camera 2, the regions exhibited very different inclinations. In the latter case, the correction by the calibration procedure using a global mapping function becomes more challenging.

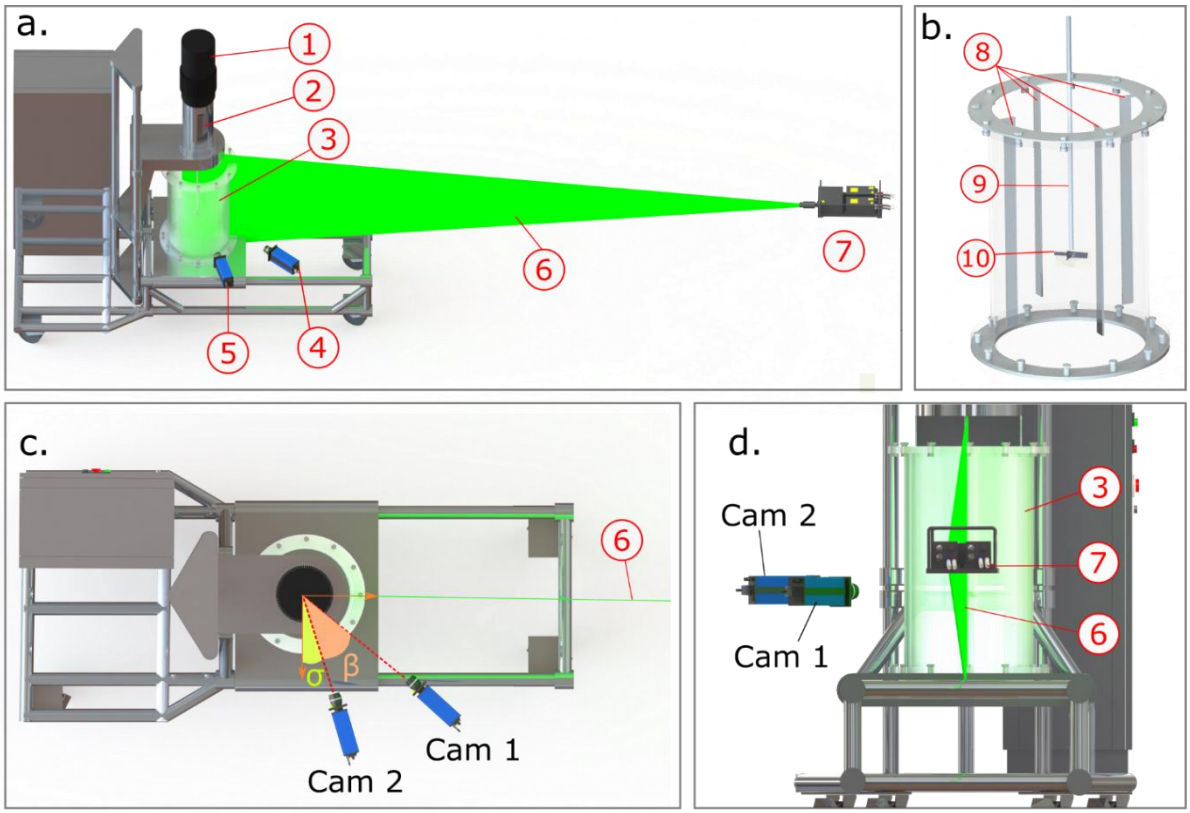

Figure 3.1. Experimental apparatus (a), stirred vessel (b), lateral (c) and vertical (d) field of view of the position of the cameras and the light sheet. Legend: 1. Engine, 2. Torque meter, 3. Stirred tank, 4. Camera 1, 5. Camera 2, 6. Light sheet, 7. Laser, 8. Baffles, 9. Shaft, 10. Impeller.

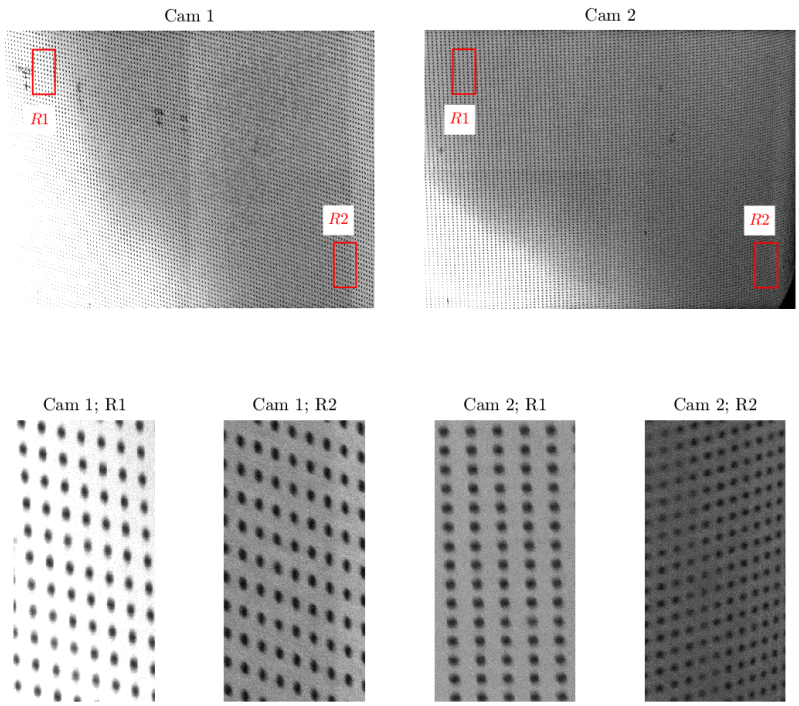

Figure 3.2. Raw images of the calibration target for the cameras 1 (Cam 1) and 2 (Cam 2) highlighting two regions: close to the shaft (R1) and close to the wall (R2).

2.2. Calibration of Soloff et al. (1997)

In the calibration procedure, the relationship between the physical coordinates (*X'*, *Y'*) and the image coordinates (*x*, *y*) was described by a mapping function, according to the strategy proposed by Soloff et al. (1997). The function was obtained by adjusting the points identified on the target to a third-order polynomial (Equation 3.1). This model was considered to be more suitable for situations with high error from a global or local perspective (Wieneke, 2005).

$$\begin{pmatrix} x_i \\ y_i \end{pmatrix} = \begin{bmatrix} X' + \partial X(X', Y') \\ Y' + \partial Y(X', Y') \end{bmatrix} \quad \text{Equation 3.1}$$

where $\partial X'$ and $\partial Y'$ are defined by Equation *3.2*:

$$\begin{pmatrix} \partial X' \\ \partial Y' \end{pmatrix} = \begin{bmatrix} a_0 + a_1 s + a_2 s^2 + a_3 s^3 + a_4 t + a_5 t^2 + a_6 t^3 + a_7 st + a_8 s^2 + a_9 s^2 \\ b_0 + b_1 s + b_2 s^2 + b_3 s^3 + b_4 t + b_5 t^2 + b_6 t^3 + b_7 st + b_8 s^2 + b_9 s^2 \end{bmatrix}$$

Equation 3.2

The displacements $\partial X'$ and $\partial Y'$ are determined by normalized coordinates *s* (Equation 3.3) and t (Equation 3.4)

$$s = 2 \cdot \left(X'_i - X'_i / n_x \right) \quad \text{Equation 3.3}$$

$$t = 2 \cdot \left(Y'_i - Y'_i / n_y \right) \quad \text{Equation 3.4}$$

where n_x and n_y are the size of images in pixel in different image coordinates (x, y). Thus, the determination of the mapping function is done by recognizing the dots in the calibration target (*X´* and *Y´* values of physical coordinates) and estimating the a_i and b_i coefficients of Equation *3.2* by the method of least-squares. This procedure was performed using *Davis 8.4* software (LaVision).

The reference dots X'_0 and Y'_0 identified in the target image were defined in the center of the plate's raw image. A search pattern was used considering a second and a third

dots spaced 1.5 mm above and to the right of the reference dot (Figure 3.3a). In the next step, the other marks in the calibration image are located respecting the previously defined origin dots (Figure 3.3b). After the identification, the mapping function coefficients were estimated. According to Soloff et al. (1997), the adjustment of the mapping function is ideal when the adjustment error is less than 1 pixel. In this work, the quality of the adjustment was analyzed by overlaying a grid with the same spacing as the calibration target with a center in X_0' and Y_0' (Figure 3.3c). The resulting mapping function was considered adequate as the grid overlapped the dots in the plate image. In the reconstruction, the image was dewarped using the mapping function and a cubic interpolation.

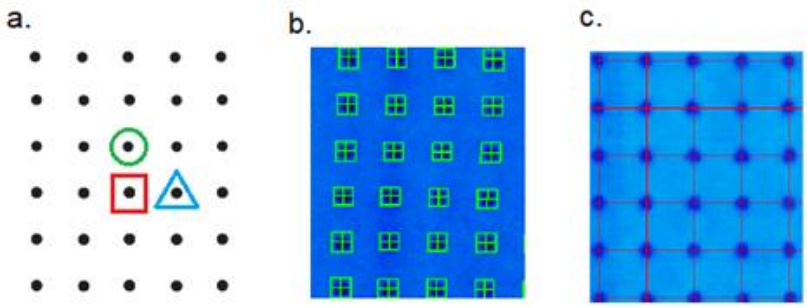

Figure 3.3. Basics steps of the calibration proposed by Soloff et al. (1997).

2.3. Data acquisition

The PIV technique was applied in the stirred tank as described in Figure 3.1. The impeller speed (660 rpm) was chosen to achieve a turbulent regime of the flow ($Re = \rho N D^2/\mu \cong 170.000$). Images for the flow analysis were obtained using a 2D-2C PIV system (two dimensions and two components) developed by Dantec Dynamics. The total area investigated was 0.39 m x 0.19 m and, as previously mentioned, Camera 1, positioned at 40º from the normal plane of the light sheet (Figure 3.1c), was used to acquire the images. An Nd:YAG laser (532 nm, 200 mJ) supplied a light sheet with 2 mm thickness was used. As tracer particles, silver-coated hollow glass spheres with an average diameter of 10 µm and density of 1100 kg / m³ were used. Since the tracking particles density was close to the fluid density, we can guarantee the faithful following of the flow (Raffel, et al., 2018). A set of 1000 pairs of images were recorded with an interframe time of 100 µs.

With the purpose of analyzing the velocity fluctuations in different position the turbulent flow, images at six angles resolved (AR 0 º, 15º, 30º, 45º, 60º and 75º), that is,

blade positions, were acquired. The images recorded at AR 0° had the light plane shifted about 0.5° from the baffled to minimize the effect of the structure light reflection. The methodology for carrying out AR measurements consists of the use of a microcontroller to synchronize the blade position with the data acquisition. The pulsation of the laser, the recording of the cameras and the rotation of the impeller were synchronized by a microcontroller. This device received the value of the rotation speed and sent a signal of the axis revolution time to the PIV system synchronizer, which, in turn, reconciled the activation of the laser with the camera, in order to obtain images of a pulse per revolution of the axis.

2.4. Data processing

After going through the calibration and multicalibration procedures, the dewarped images were preprocessed through the application of different filters: Gaussian (3x3 pixels kernel, 0.3 standard deviation); subtraction by local minimum (7x7 pixels kernel) and intensity capping. Subsequently, the subtraction by local average filter was applied three times (11x11 pixels kernel) and the Gaussian filter with a higher standard deviation (0.6) was used. In the PIV processing, standard cross correlation (SCC) optimized by an iterative multigrid interrogation window deformation strategy was applied for the adjustment of the spatial resolution (Scarano, 2001; Kim & Sung, 2006). In this strategy, the processing was made in 5 steps, in which the size of the interrogation window was progressively decreased from 48 x 48 pixels to 20 x 20 pixels, with a 25% reduction in each step and with a percentage of overlap between neighbor windows of 25% for the first four steps and 50% in the last step. The resulting final analysis area obtained had 10 x 10 pixels (0.37 x 0.37 mm).

After each step, simple postprocessing was applied to eliminate outliers based on the work of Westerweel and Scarano (2005). Finally, a complete postprocessing based on mutual information thresholding was also used. This strategy was proposed by our research group and more detailed information can be found in the work of Barbutti et al. (2021). It is important to notice that, based on the distortion analysis performed by Elsinga et al. (2005), that no changes were observed related to the correlation peaks or in the signal-to-ratio (SNR) metrics in the wall region (R3) for the interrogation windows used in this work.

3. RESULTS AND DISCUSSION

3.1. Analysis of the calibration of Sollof et al. (1997)

The dewarped images after calibration, acquired by Cameras 1 and 2 are shown in Figure 3.4 and Figure 3.5, respectively. Each one had approximately 9000 dots recognized in the entire image after applying the calibration method. Three regions were analyzed in detail: close to the impeller shaft (R1), close to the impeller tip (R2) and close to the tank wall (R3). The adjustment error of the global mapping function was 0.85 and 6.80 pixels for Camera 1 and 2, respectively. For Camera 1 (Figure 3.4), the grid overlapped the target of dot pattern in both R1 and R2. However, the overlap failed close to the tank wall (R3). The lack of adjustment in the region close to the wall can be explained mainly by the difficulty in identifying the dots pattern in this region. The curvature of the wall distorted the dots image, which appeared elongated and with variations in the center-to-center spacing. This effect is even more evident in R3 measured by Camera 2 (Figure 3.5). For this camera, besides the non-homogeneous distortion, as observed in Figure 3.2 and the high adjustment error of the mapping function (of 6.80 pixels), the failure in the calibration can be verified by the lack of overlapping of the grid with the calibration target for the three regions analyzed, as presented in Figure 3.5.

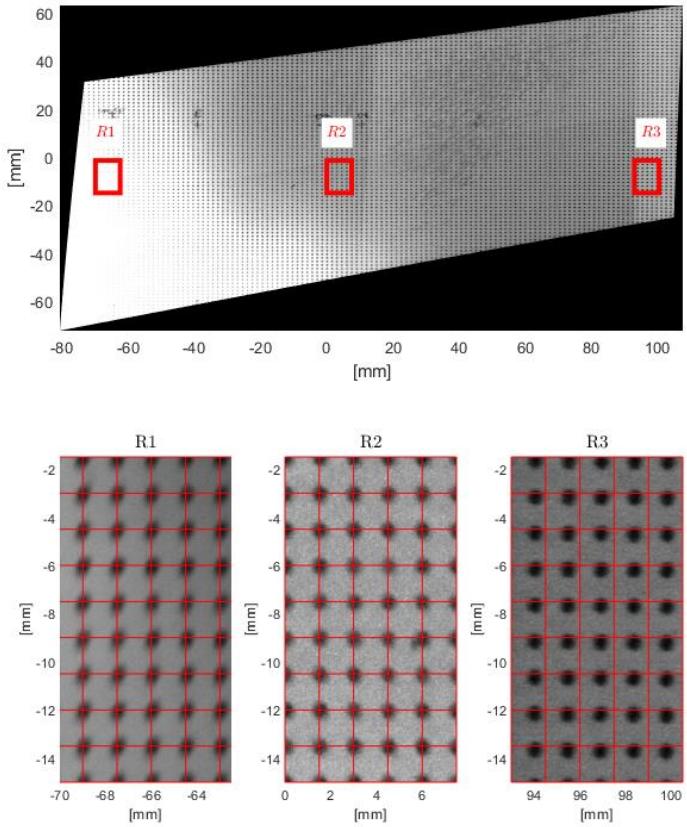

Figure 3.4. Dewarped image of the calibration target from Camera 1 after the calibration based on the method of Soloff et al. (1997). Comparison between the dewarped images and the mapping function adjustment close to the impeller shaft (R1), close to the impeller tip (R2) and close to the tank wall (R3).

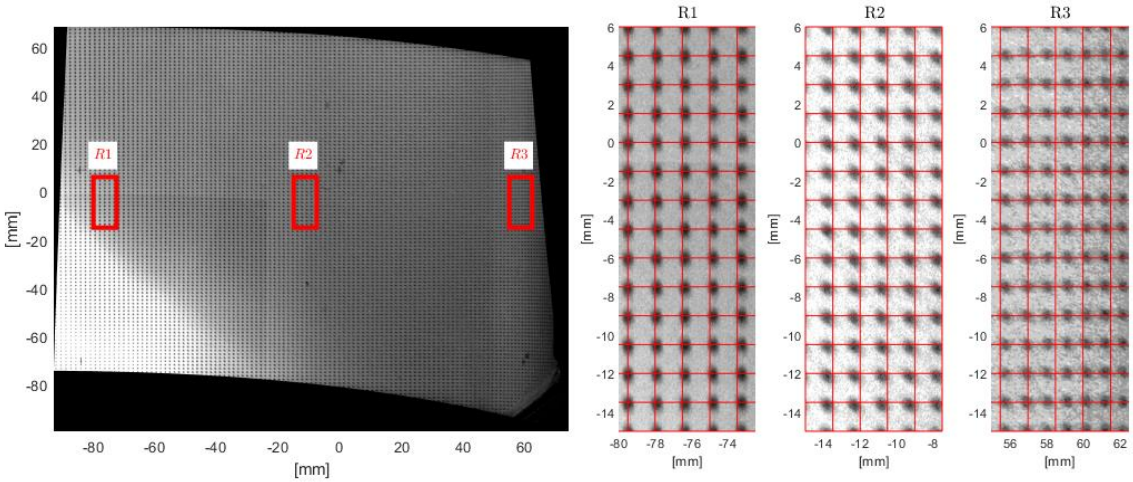

Figure 3.5. Dewarped image of the calibration target from Camera 2 after the calibration based on the method of Soloff et al. (1997). Comparison between the dewarped images and the mapping function adjustment close to the impeller shaft (R1), close to the impeller tip (R2) and close to the tank wall (R3).

After observing the poor adjustment of the global mapping function, especially close to the tank wall, it was proposed to perform a new calibration step. Figure 3.6 shows the multicalibration strategy proposed and implemented in this situation, which was also performed using the Davis 8.4 software (LaVision). In this new proposal, the dewarped images of the calibration target (Figure 3.4) underwent a second calibration, in which the reference dots $X'_{0,2}$ and $Y'_{0,2}$ were selected close tank wall region. In order to identify more dots in this region, the dot diameter was defined as 0.75 mm and the center-to-center distance was maintained as 1.5 mm. The procedure for obtaining the mapping function was repeated, resulting in a new reconstructed image.

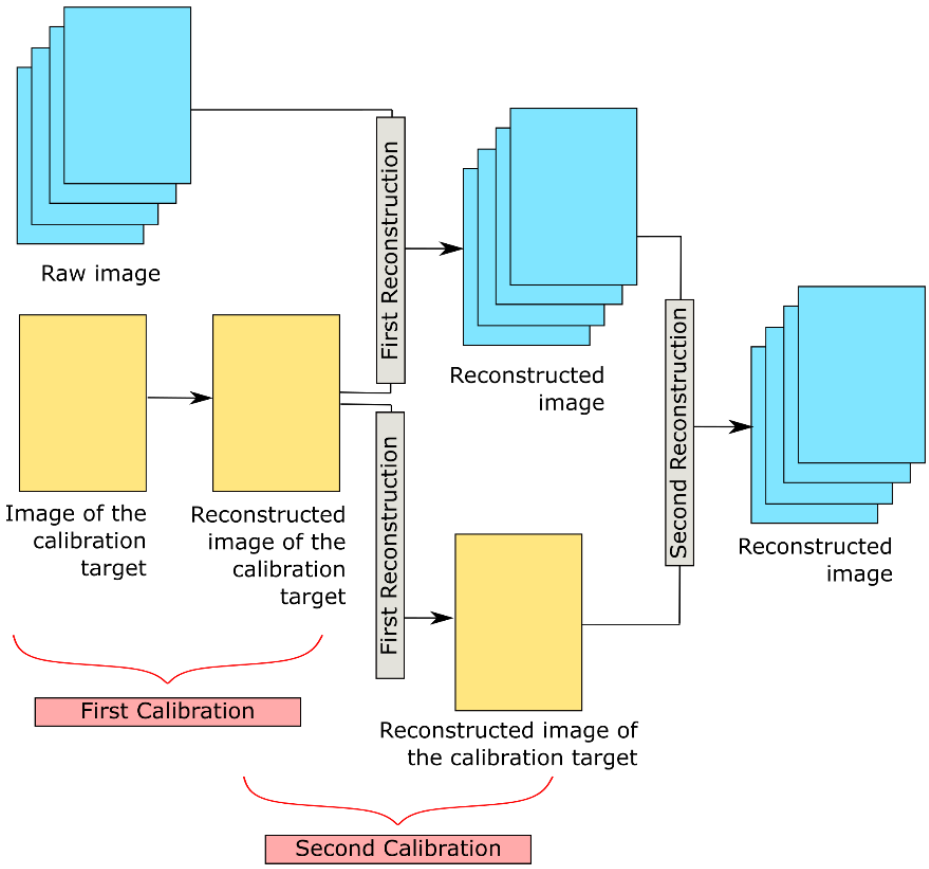

Figure 3.6. Multicalibration strategy.

A better adjustment of the mapping function in the region close to the wall was observed for Camera 1 (Figure 3.7). However, the dots in the impeller shaft region (R1) in the images obtained by both Cameras 1 and 2 were not identified. This could have happened probably due to the variation in the size of the dots. For Camera 2, the lack of adjustment observed in the first calibration was verified again in this new stage. In the

second calibration, the adjustment errors were 1.24 and 9.25 pixels for Cameras 1 and 2, respectively.

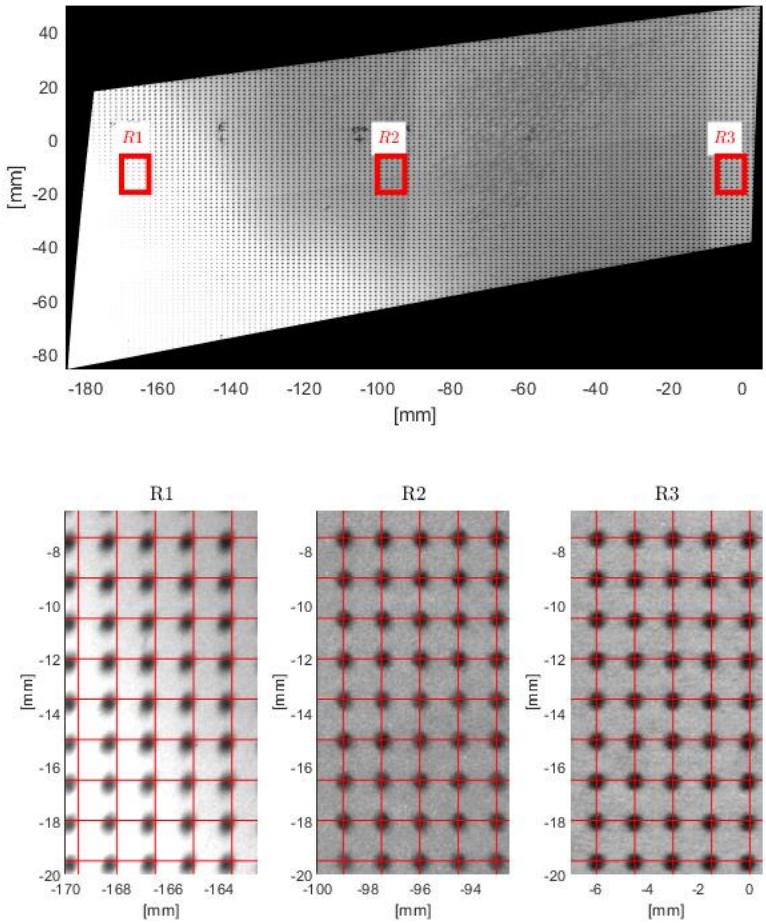

Figure 3.7. Dewarped image of the calibration target from Camera 1 after the multicalibration. Comparison between the dewarped images and the mapping function adjustment close to the impeller shaft (R1), close to the impeller tip (R2) and close to the tank wall (R3).

3.2. Effect of the distortion compensation on the turbulent kinetic energy distribution (TKE)

Based on the information analyzed and results concerning the cameras positioning, it was decided to analyze the performance of the calibration approaches in the stirred tank flow only with images acquired by Camera 1.

The turbulent kinetic energy (TKE) was estimated from Equation 3.5.

$$k = \frac{3}{4}\left(\overline{u'^2} + \overline{v'^2}\right) \qquad \text{Equation 3.5}$$

where $\overline{u'^2}$ and $\overline{v'^2}$ are the root mean square velocity in radial (*x*) e axial (*y*) directions, respectively. Equation 3.6 presents an example for calculating the root mean square velocity in the x direction. For the y direction, the same model can be applied.

$$\overline{u'^2} = \overline{(u - \bar{u})^2} \qquad \text{Equation 3.6}$$

Considering that in PIV 2D-2C measurements the third velocity component (in tangential direction) is unknown, the isotropic flow was assumed to calculate this velocity component. This assumption was evaluated by Khan et al. (2006) and Chung et al. (2007) and negligible deviations were found compared to PIV 2D-3C (two dimensions and three components).

Figure 3.8 shows the TKE distributions obtained by the three different image distortion compensation approaches and measured at six AR positions. The impeller axis was chosen as a reference for the coordinates. It was observed that there were no significant variations between the TKE distributions obtained with calibration and with multicalibration procedures. This result can be clearly seen when assessing the TKE profiles at y = 85 mm and x = 57 mm, as shown in Figure 3.9 and Figure 3.10, respectively. The profiles positions correspond to the dashed lines in Figure 3.8, that is, x = 57 mm and y = 85 mm. In addition, the distorted images that were not submitted to any calibration method, presented lower TKE values. For Camera 1, both calibration strategies are indicated if the mapping function is adjusted in the region of interest. In other words, this can be achieved if the reference grid is aligned with the dots on the plate. On the other hand, multicalibration is necessary if the region of interest is close to the wall.

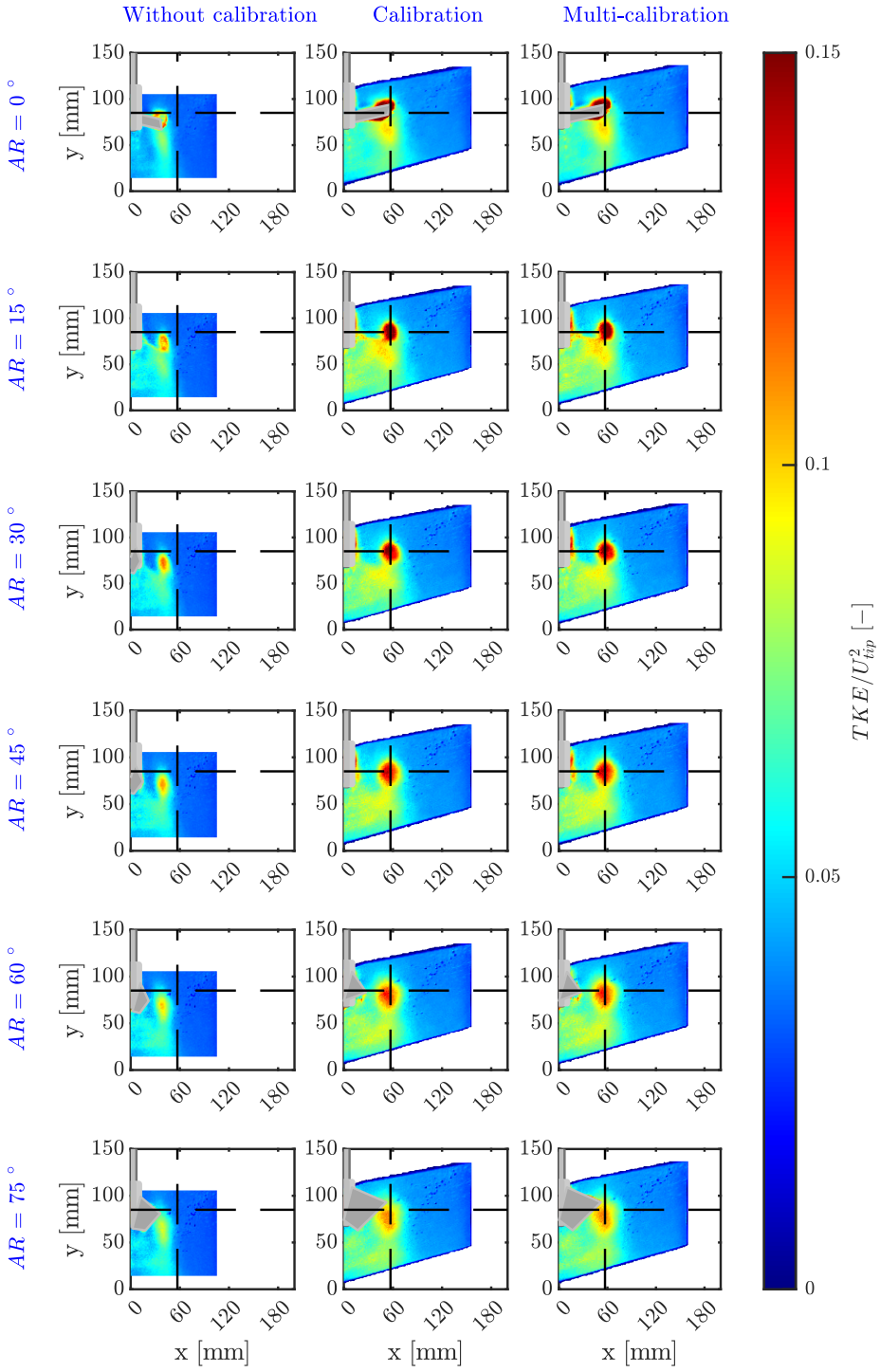

Figure 3.8. Normalized turbulent kinetic energy distributions for images without calibration, with calibration (Soloff et al., 1997) and with the proposed multicalibration.

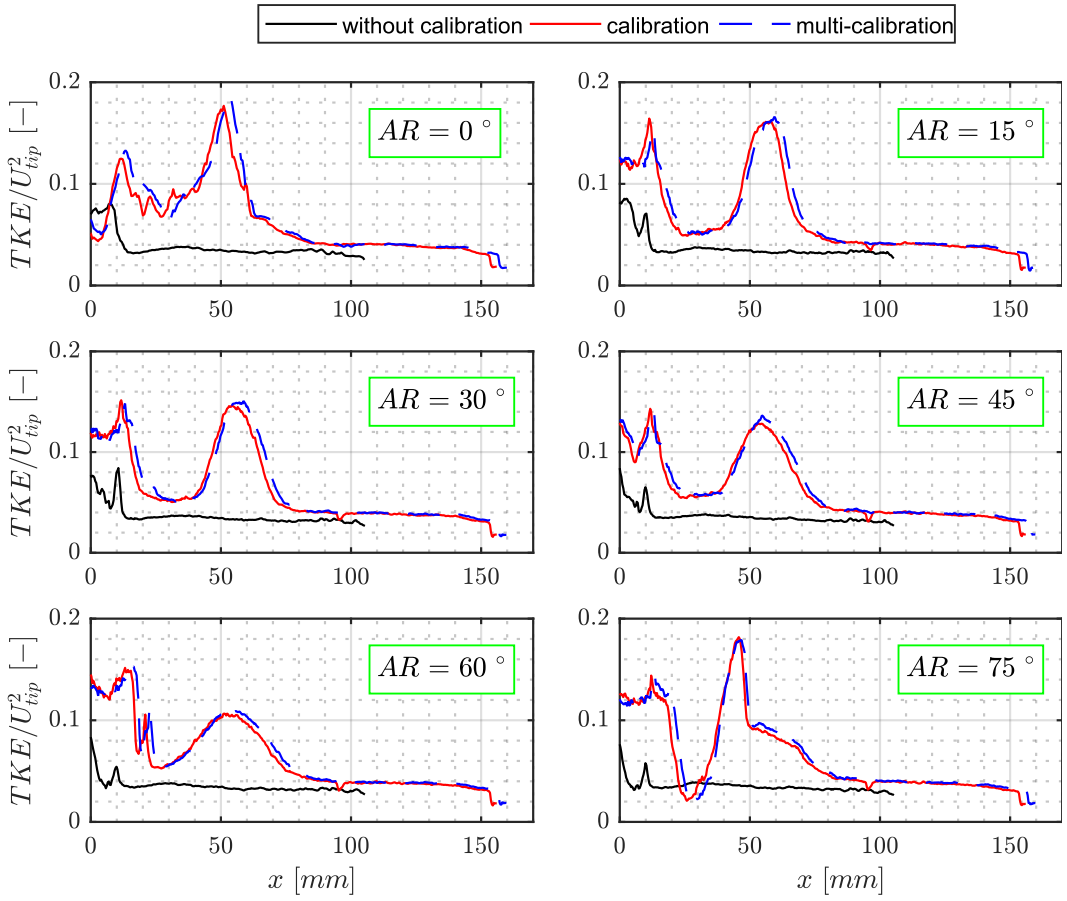

Figure 3.9. Radial profiles of normalized turbulent kinetic energy for images without calibration, with calibration (Soloff et al., 1997) and with the proposed multicalibration.

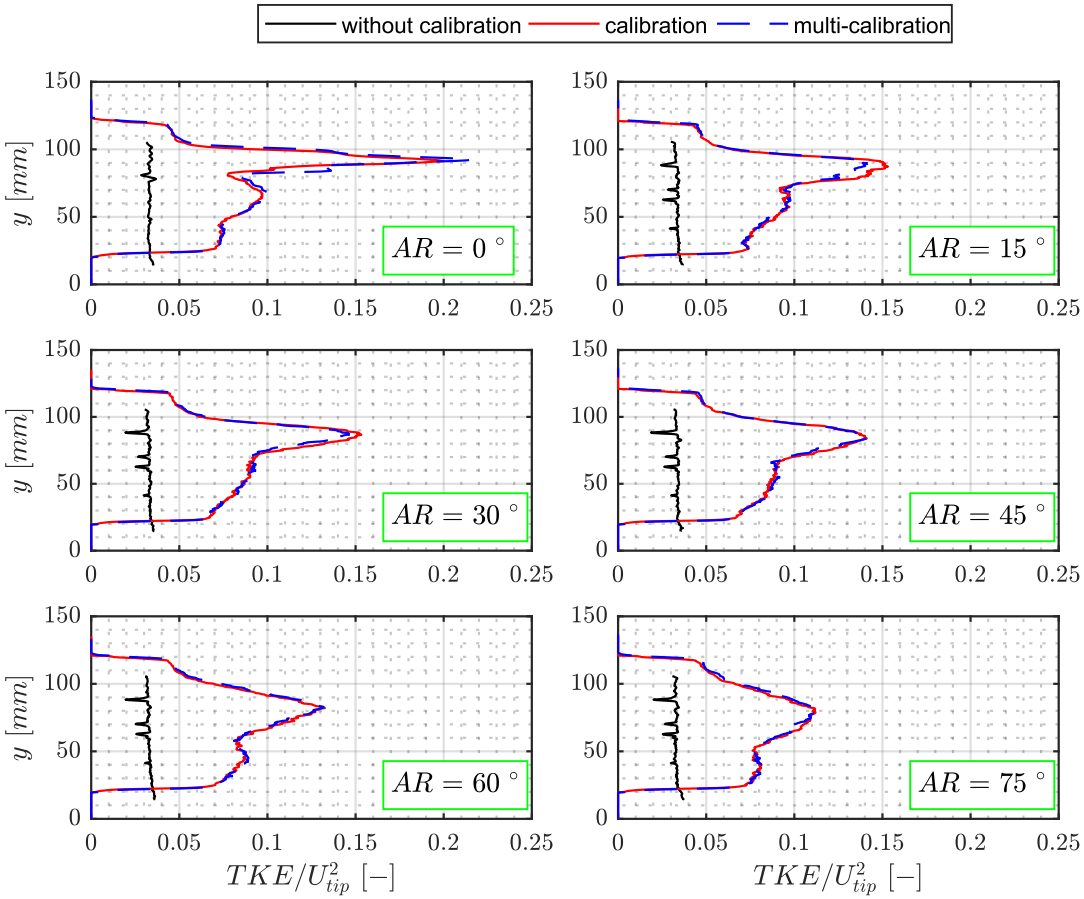

Figure 3.10. Axial profiles of normalized turbulent kinetic energy for images without calibration, with calibration (Soloff et al., 1997) and with the proposed multicalibration.

4. CONCLUSION

This work investigated and compare the performance of two calibration approaches to compensate image distortions of PIV measurements in a stirred tank without using solutions in the physical space, such as correction boxes: the first one developed by Soloff et al. (1997) and a proposed new multicabration strategy In the proposed calibration, images were investigated from two cameras positioned in different perspectives but focusing on the same plane of the object, where a mapping function for each camera was estimated through a calibration target. For both methods the Camera 2, positioned closer to the normal axis of the calibration target, showed higher adjustment error of the mapping function than Camera 1. For the camera positioned with the smallest angular displacement in relation to the object plane, the error of adjustment of the mapping function and the qualitative analysis of the grid overlap obtained using the approach developed by Soloff et al. (1997) showed good results to reduce image distortions. However, only the regions close

to the impeller shaft and the impeller tip were adequately compensated. Then, the multicalibration strategy was used to optimize these regions, and this method showed a better adjustment of the mapping function in the region close to the wall. In contrast, the region close to the impeller shaft was distorted. The distributions of turbulent kinetic energy (TKE) from dewarped images obtained by the different approaches of calibration and without calibration were also evaluated. For this analysis, only the images from Camera 1 were used, which showed smaller adjustment error. The results showed that the calibration and the multicalibration did not present significant differences in the estimation of TKE. Consequently, for this purpose, both were considered adequate in the analysis of the stirred tanks.

5. ACKNOWLEDGEMENTS

This study was financed by Petrobras S/A (process number 2017/00376-1) and National Council for Scientific and Technological Development (CNPq; process numbers 168390/2018-3, 142604/2019-4, and 140997/2019-9).

6. REFERENCES

Adrian, R. J. and Westerweel, J., 2011. *Particle Image Velocimetry*. Cambridge University Press, New York, 1st edition.

Alberini, F., Liu, L., Stitt, E. H. and Simmons, M. J. H., 2017. Comparison between 3-D-PTV and 2-D-PIV for determination of hydrodynamics of complex fluids in a stirred vessel. *Chemical Engineering Science*, Vol. 171, p. 189–203.

Alonzo-Garcia, A., Mendoza-Escamilla, V. X., Martinez-Delgadillo, S. A., Gonzalez-Neria, I., Del C Gutiérrez-Torres, C. and Jiménez-Bernal, J. A., 2019. On the performance of different rans based models to describe the turbulent flow in an agitated vessel using non-structured grids and PIV validation. *Brazilian Journal of Chemical Engineering*, Vol. 36(1), p. 361–382.

Barbutti, A. D., de Lima Amaral, R., de Moura, H. L., Júnior, F. D. A. O., Nunhez, J. R., & de Castilho, G. J., 2021. A new field correction method for PIV measurements based on mutual information: Case study on a stirred tank flow. *Measurement*, 186, 110130.

Chung, K. H.K., Barigou, M. and Simmons, M. J. H., 2007. Reconstruction of 3-D flow field inside miniature stirred vessels using a 2-D PIV technique. *Chemical Engineering Research and Design*, Vol. 85(5A), 560–567.

Chung, Kenneth H.K., Simmons, M. J. H. and Barigou, M., 2009. Angle-resolved particle image velocimetry measurements of flow and turbulence fields in small-scale stirred vessels of different mixer configurations. *Industrial and Engineering Chemistry Research*, Vol. 48(2), p. 1008–1018.

de Lamotte, A., Delafosse, A., Calvo, S., Delvigne, F. and Toye, D., 2017. Investigating the effects of hydrodynamics and mixing on mass transfer through the free-surface in stirred tank bioreactors. *Chemical Engineering Science*, Vol. 172, p. 125–142.

Elsinga, G. E., Van Oudheusden, B. W. and Scarano, F., 2005. Evaluation of aero-optical distortion effects in PIV. *Experiments in Fluids*, Vol. 39(2), p. 246–256.

Escudié, R. and Liné, A., 2003. Experimental analysis of hydrodynamics in a radially agitated tank. *AIChE Journal*, Vol. 49(3), p. 585–603.

Fang, J., Ling, X. and Sang, Z. F., 2011. Experimental and Numerical Studies of the Flow Field in a Stirred Tank Equipped with Multiple Side-Entering Agitators. *Chemical Engineering and Technology*, Vol. 34(10), p. 1619–1629.

Fritsch, F. N., and Carlson, R. E., 1980. Monotone Piecewise Cubic Interpolation. *SIAM Journal on Numerical Analysis*, Vol 17(2), p. 238–246.

Gómez, C., Bennington, C. P. J. and Taghipour, F., 2010. Investigation of the flow field in a rectangular vessel equipped with a side-entering agitator. *Journal of Fluids Engineering, Transactions of the ASME*, Vol 132(5), p. 0511061–13.

Huber, P. J., 2004. Scale Estimates. In *Robust Statistics* (p. 107–126). John Wiley and Sons, Inc, Hoboken, 1st edition.

Khan, F. R., Rielly, C. D., and Brown, D. A. R., 2006. Angle-resolved stereo-PIV measurements close to a down-pumping pitched-blade turbine. *Chemical Engineering Science*, Vol. 61(9), p. 2799–2806.

Kilander, J., and Rasmuson, A., 2005. Energy dissipation and macro instabilities in a stirred square tank investigated using an le PIV approach and LDA measurements. *Chemical Engineering Science*, *60*(24), 6844–6856.

Kim, B. J. and Sung, H. J., 2006. A further assessment of interpolation schemes for window deformation in PIV. *Experiments in Fluids*, Vol. 41(3), p. 499–511.

Kresta, S. M. and Wood, P. E., 1991. Prediction of the three-dimensional turbulent flow in stirred tanks. *AIChE Journal*, Vol. 37(3), p. 448–460.

Li, Z., Bao, Y. and Gao, Z., 2011. PIV experiments and large eddy simulations of single-loop flow fields in Rushton turbine stirred tanks. *Chemical Engineering Science*, Vol. 66(6), p. 1219–1231.

Micheletti, M., Baldi, S., Yeoh, S. L., Ducci, A., Papadakis, G., Lee, K. C., and Yianneskis, M., 2004. On spatial and temporal variations and estimates of energy dissipation in stirred reactors. *Chemical Engineering Research and Design*, Vol. 82(9 - special issue), p. 1188–1198.

Prasad, A. K., 2000. Stereoscopic particle image velocimetry. *Experiments in Fluids*, Vol. 29(2), p. 103–116.

Prasad, Ajay K., and Jensen, K., 1995. Scheimpflug stereocamera for particle image velocimetry in liquid flows. *Applied Optics*, p. 34(30), p. 7092-7099.

Raffel, M., Willert, C. E., Scarano, F., Kähler, C. J., Wereley, S. T. and Kompenhans, J., 2018. *Particle Image Velocimetry*. Springer International Publishing, Cham, 3rd edition.

Rottier, C., Godard, G., Corbin, F., Boukhalfa, A. M., & Honoré, D., 2010. An endoscopic

particle image velocimetry system for high-temperature furnaces. *Measurement Science and Technology*, 21(11), 115404. https://doi.org/10.1088/0957-0233/21/11/115404

Scarano, F., 2002. Iterative image deformation methods in PIV. *Measurement Science and Technol*, Vol. 13(13), p. 1–19.

Sharp, K. V. and Adrian, R. J., 2001. PIV Study of small-scale flow structure around a Rushton turbine. *AIChE Journal*, Vol. 47(4), p. 766–778.

Soloff, S. M., Adrian, R. J. and Liu, Z. C., 1997. Distortion compensation for generalized stereoscopic particle image velocimetry. *Measurement Science and Technology*, Vol. 8(12), p. 1441–1454.

Stelmach, J., Musoski, R., Kuncewicz, C. and Głogowski, M., 2019. Turbulent energy dissipation rate and turbulence scales in the blade region of a self-aspirating disk impeller. *Journal of Applied Fluid Mechanics*, Vol. 12(3), p. 715–728.

Tsai, R., 1987. A versatile camera calibration technique for high-accuracy 3D machine vision metrology using off-the-shelf TV cameras and lenses. *IEEE Journal on Robotics and Automation*, 3(4), 323-344.

Westerweel, J. and Scarano, F., 2005. Universal outlier detection for PIV data. *Experiments in Fluids*, Vol. 39(6), p 1096–1100.

Wieneke, B., 2005. Stereo-PIV using self-calibration on particle images. *Experiments in Fluids*, Vol. 39(2), p. 267–280.

Wieneke, B., 2017. *PIV Uncertainty Quantification and Beyond*. Ph.D thesis. Delft University of Technology, Delft.

Zhang, M., Xu, M., & Hung, D. L., 2014. Simultaneous two-phase flow measurement of spray mixing process by means of high-speed two-color PIV. *Measurement Science and Technology*, 25(9), 095204.

CHAPTER 4

A NEW FIELD CORRECTION METHOD FOR PIV MEASUREMENTS BASED ON MUTUAL INFORMATION: CASE STUDY ON A STIRRED TANK FLOW

In this chapter, the results and discussions are presented in an article format. This second article was published in the journal "Measurement" in September of 2021.

A NEW FIELD CORRECTION METHOD FOR PIV MEASUREMENTS BASED ON MUTUAL INFORMATION: CASE STUDY ON A STIRRED TANK FLOW

Aliandra Duarte Barbutti[1], Rodrigo de L. Amaral[2], Helder L. de Moura[1], Francisco de A. Oliveira Júnior[1,] José R. Nunhez[1], Guilherme J. de Castilho[1].

[1]University of Campinas, School of Chemical Engineering, Process Engineering Department.

[2]POLI, University of São Paulo, POLI, Department of Mechanical Engineering, NDF.

Published manuscript in *Measurement*

PII: S0263224121010496
DOI: https://doi.org/10.1016/j.measurement.2021.110130
To appear in: *Measurement*
Received date: 28 March 2021
Revised date: 11 August 2021
Accepted date: 30 August 2021
Final version published online: 11 September 2021

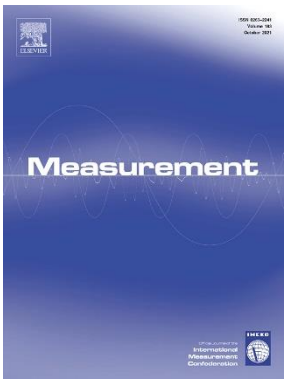

ABSTRACT - Particle image velocimetry (PIV) is an experimental approach widely used to investigate the flow inside stirred tanks. PIV noise sources deteriorate the velocity fields and compromise the measurements, mainly in the estimation of the turbulent parameters. PIV correction approaches based on the primary peak ratio (PPR), namely the ratio between the primary correlation peak to the second highest peak, are used when identifying outliers in the velocity field becomes difficult. However, in some cases, PPR is not sensitive to noise sources and may fail to identify outliers. Therefore, this work proposes a new method of field correction based on mutual information, which is estimated by dividing the height of the cross-correlation peak by the magnitude of the autocorrelation. Analysis were performed using PIV data measured in a 50 liters stirred tank. Results show that the proposed methodology can be a valuable tool for the correction of noisy fields.

Keywords: PIV, Field Correction, Mutual Information, Stirred Tank.

1. INTRODUCTION

Stirred tanks are widely used for engineering applications in several types of industries, such as chemical, petrochemical, pharmaceutical, food and wastewater treatment. The flow patterns generated by the impellers have transient and spatial scales that are functions of the geometry, number of blades, angle, diameter and position of the impeller(s) inside the tank. In addition, flow parameters, such as the distribution of turbulent kinetic energy (TKE), are often used to optimize tank design in order to maximize the mixing quality at the lowest energy cost (Baldi and Yianneskis, 2004; Gabriele et al., 2009).

Particle image velocimetry (PIV) is an experimental technique widely used to determine the velocity flow fields in stirred tanks. In this case, the region of interest is divided into small areas, known as interrogation windows, where the velocity of a particle population is determined through a correlation between two instants of time. The accuracy of the estimation of the turbulent parameters is directly related to the size of this window, i.e., the spatial resolution. The greater the precision of the estimative, the smaller is the interrogation window and, consequently, the higher is the spatial resolution. However, controlling the PIV noise level at a high spatial resolution is challenging. Despite the growing number of studies using PIV experiments, there are few regarding noise sources and optimization of image processing in stirred tanks to ensure the quality of measurements (Saarenrinne et al., 2001; Escudié and Liné, 2003; Svensson and Rasmuson, 2006; Gabriele et al., 2009; Guida et al., 2010; Delafosse et al., 2011; Unadkat et al., 2011; Liu et al., 2016; Hu et al., 2018; Alonzo-Garcia et al., 2019).

The PIV performance is subject to interferences caused by noisy sources that generate uncertainties in the measurements directly affecting the quality of the data. In a field without noise, the velocity vectors in the interrogation window vary smoothly in relation to their neighborhood. Despite the efforts in many studies to minimize noise sources in the physical and image space, it is difficult to avoid the presence of false vectors completely (Dabiri, 2006; Adrian and Westerweel, 2011; Sciacchitano and Scarano, 2014). According to Wieneke (2017), the error sources in PIV can be related to systematic and random errors. Systematic errors follow a trend that makes them predictable, such as calibration errors and errors due to the failure to adjust the correlation peak that depend on the diameter of the particle image. On the other hand, random errors are different for each measurement and are associated with the recording noise, the density and the homogeneity

of the tracer particles, the velocity gradients, the shadow effects, and the laser light reflection. Outliers, which are also called false vectors or spurious vectors - are generated by random noise sources and are very different from the rest of the data, so they are easily observed. Despite of numerous PIV advances to improve the PIV accuracy and the reducing of noise levels, there are still gaps in terms of flow field correction that need to be investigated. There is a limitation in the solving for the flow structures smaller than the interrogation window. Some methods have been developed and adapted to support noise sources, such as large velocity gradients, different densities of the tracer particles and high dispersion in the particle brightness (Nogueira et al., 1999; Adrian and Westerweel, 2011; Raffel et al., 2018), but there is still a need to develop new method which will help understanding these small structures.

The noise effects must be compensated in the physical (or image) space to minimize their influence on the quality of the PIV measurements. In the physical space, for example, the curvature effects of the stirred tank wall can be compensated using a second rectangular tank filled with the same fluid inside the tank. (Khan et al., 2004; Gabriele et al., 2009; Guida et al., 2010; Escudié and Liné, 2003; Liu et al., 2016; Hu et al., 2018). In addition, the noise generated by the reflection of the laser light on the impeller and deflectors can be reduced by painting them black (Svensson and Rasmunson, 2006; Roy et al., 2010). The noise effects that cannot be minimized by adjustments in the physical space must be treated in the image space. The treatment is conducted in the pre-processing, processing, and post-processing stages of the PIV measurements. For example, the use of space and time filters in the pre-processing reduces the background noise of the images and the laser light reflection of the tank wall and of the impeller. In the PIV processing these effects can be eliminated or minimized using phase filters in the correlation plane. The accuracy of the PIV measurements can be improved using a series of spectral filters based on the particle image diameter optimized for cross-correlation combined with advanced windowing techniques. In addition, smoothing filters can be applied in the processing step to reduce noise sensitivity (Eckstein and Vlachos, 2009). In the post-processing stage, it is possible to identify, remove and correct spurious vectors using temporal and spatial filters based on the connectivity of the neighborhood. In addition, filling the interrogation windows with valid velocity vectors becomes necessary in the PIV post-processing after the application of these filters (Foucaut et al., 2000; Nogueira et al., 2001; Adrian and Westerweel, 2011; Raffel et al., 2018).

The identification and correction of outliers are directly related to the quality indicators in the velocity field or in the correlation plane. Quality indicators can be parameters or variables directly related to the presence of outliers in the measurements. In the velocity field, these indicators can be associated to the prior knowledge of the flow patterns, such as an experimental condition. In stirred tanks, for example, the velocity of the impeller tip (U_{tip}) can be used as a threshold for identifying outliers. In the PIV technique, quality indicators can be useful for adjusting the experimental setup and for the reconstructing of the data, defining which are the best processing parameters (Martins et al., 2015). In this case, false vectors can be established as those that exceed U_{tip} (Gabriele et al., 2009; Guida et al., 2010). Unadkat (2010) adopted that false vectors are those greater than 1.5 x U_{tip} and these were approximated by linear interpolation of the surrounding vectors. Another commonly used approach for detecting PIV outliers is comparing the velocity of an interrogation window with its neighborhood (n x n). In a field without noise, the velocity vectors in the interrogation window vary smoothly in relation to their neighborhood, showing good spatial coherence. Based on that, the Median Absolute Deviation (MAD) method and the Universal Outliers Detection (UOD) method developed by Westerweel and Scarano (2005) can be used (Mosteller and Tukey, 1977; Sachs, 1984). However, these approaches can fail in the presence of clusters of outliers. The group of outliers or clusters of outliers, as they are mentioned in this paper, refers to a group of false velocity vectors concentrated in a region with a different order of magnitude for the velocity vectors which are present in the field of view. Moreover, in one ideal situation, approaches based on spatial coherence should use the smallest neighborhood size to prevent intrinsic flow variations from deteriorating (Adrian and Westerweel, 2011; Raffel et al., 2018).

In the correlation plane, signal-to-noise ratio (SNR) metrics can be used as a threshold to identify outliers similar to U_{tip} in the velocity field. The ratio between the first and second highest peak in the correlation, known as the Primary Peak Ratio (PPR), is the most widely used SNR metric (Xue et al., 2014). The combination of MAD, UOD, PPR and other approaches are also used to correct the velocity fields with noise. Roy et al. (2010) used a combination of three methods to validate the velocity vectors. According to the authors, the vectors whose PPR was greater than 1.2 were considered to be valid in a first velocity field correction. In a second correction, vectors with a magnitude greater than 1.15 x U_{tip} were removed. Afterwards, vectors with a horizontal magnitude greater than

half of the U_{tip} were also removed. Finally, vectors that were in great disagreement with their spatial neighborhood (7x7) were removed using a sliding average validation method.

Numerical investigations have shown that false vectors are avoided when PPR > 2. However, the effect of the presence of noise in the correlation plane is felt mainly in the shape of the peak and not in its height. This behavior can restrict the application of the PPR as an indicator of outliers (Kähler and Kompenhans, 2000; Pereira et al., 2004; Hain and Kahler, 2007; Wieneke, 2017). Xue et al. (2015) introduced a new metric, known as mutual information (MI), in order to better represent the signal related to the correlation of particles in the window. MI computes the apparent amount of common information contained in the particle patterns of two consecutive images without prior knowledge of the particle field. MI is calculated using the information from the recorded particle images as well as the autocorrelation and the cross-correlation of the two consecutive particle images. Although MI has been later used as an estimator of PIV uncertainty quantification, there are no references in the literature for the identification of outliers and field correction based on this approach. The present work aims to propose and investigate the performance of a field correction method based on MI as a post-processing filter for the identification and elimination of outliers of velocity fields measured with PIV in a stirred tank.

2. MUTUAL INFORMATION AS OUTLIER IDENTIFIER

Keane and Adrian (1992) defined the valid detection probability (VDP) parameter as the probability that the highest correlation peak corresponds to the true mean displacement of the particle image in the interrogation window. In the correlation plane, the quality of the PIV measurements is directly associated with the calculation of the highest displacement correlation peak, and in valid measurements of vector movement, the displacement peak is greater than the secondary peak. If two correlation peaks have the same height, a spurious displacement vector can be calculated. Based on Monte Carlo simulations of particle images, Keane and Adrian (1992) analyzed that the VDP is adequate when the number of particle images (N_I) within the interrogation window is equal or greater than 6. If this number is less than 6, the probability of a random peak being greater than the peak corresponding to the displacement particle image increases considerably in the correlation function (Keane and Adrian, 1992; Scharnowski et al., 2019). Considering the need to achieve high values for the VDP parameter to calculate velocity fields which are both valid and accurate. Keane and Adrian (1990) determined a relationship, called the

effective number of particle images (Equation 4.1), that guarantees 95% reliability in the obtaining of a valid measurement. In Equation (4.1) F_I and F_O are the loss of correlation due to the movements in and out of the plane, respectively. Other losses of correlation such as those related to the displacement gradients (FΔ) and image noises (Fσ) should be considered in PIV experiments (Scharnowski et al., 2019).

$$N_I F_I F_O \geq 6 \qquad \text{Equation 4.1}$$

The shape of the correlation peak (Sciacchitano et al., 2013; Wieneke, 2015) and the signal-to-noise ratio (SNR) metrics can be used as indicators of PIV quality or to estimate measurement uncertainty (Charonko and Vlachos, 2013; Xue et al., 2015). Besides the Primary Peak Ratio (PPR), others SNR metrics related to peak correlation detectability were used to estimate PIV measurement uncertainties. Kumar and Hassebrook (1990) quantified the SNR through the peak root mean square ratio (PRMSR) and the peak of correlation energy (PCE). Xue et al. (2014) calculated SNR metrics and developed models for estimating uncertainties using PPR, PRMSR, PCE and cross-correlation entropy. Xue et al. (2015) established analytically that $N_I F_I F_O$= 0.971 MI. The estimation of MI consists in dividing the magnitude of highest peak in the cross correlation by the height of the autocorrelation of the 'mean' particle with a diameter determined from the image autocorrelation. The metric MI proved to be robust in estimating the PIV uncertainty in real experiments (Xue et al., 2015). However, this metric has not yet been used as a parameter for the identifying of outliers in PIV post-processing.

Considering the standard Gaussian distribution as a reference, the particle image can be obtained by Equation 4.2, where J_0 is the mean value of the maximum intensity of the particle images, d0 is the diameter, $X' = X + dX$, $Y' = Y = dY'$, and x_p and y_p are the coordinates of the center of the particle. In practice, d0 is the average value of the diameter of the particle images in the two correlated interrogation windows. It is possible to obtain d_0 through the three-point Gaussian fit of the peak obtained in the autocorrelation of two interrogation windows, as presented in Equation 4.3. In this equation, s and t are the offsets in the X and Y directions, respectively. The height of the autocorrelation peak (A_0) can be obtained by Equation 4.4.

$$P(X,Y) = \iint J_0 e^{\left(-8\left(\frac{(X-X')^2}{d_0^2}+\frac{(Y-Y')^2}{d_0^2}\right)\right)} \otimes \delta(X' - x_p, Y' - y_p)\, dX'dY' \quad \text{Equation 4.2}$$

$$A(s,t) = \iint P(X,Y) \times P(X+s, Y+t)\, dXdY \quad \text{Equation 4.3}$$

$$A_0 = \frac{1}{16} J_0^2 d_0^2 \pi \quad \text{Equation 4.4}$$

The analytical form of images 1 and 2 is given by Equation 4.5, in order to obtain the highest peak of the cross-correlation plane (R). In Equation 4.5, I_1 and I_2 are the intensity distributions of the two correlated interrogation regions, which are defined by Equations Equation 4.6 and Equation 4.7. Considering the background image noise after PIV pre-processing as negligible, the intensity distributions of the images 1 and 2 can be considered as the sum of all particle images within the interrogation window. It is assumed that the laser pulse-to-pulse variation is negligible and that the correlated particles in frames 1 and 2 are identical after the PIV pre-processing, that is, $J_{i1} = J_{i2}$ and $d_{i1} = d_{i2}$. The primary peak height of the cross-correlation plane can be expressed by Equation 4.8.

$$R(s,t) = \iint I_1(X,Y) \times I_2(X+s, Y+t)\, dXdY \quad \text{Equation 4.5}$$

$$I_1 = \iint \sum_{p_1} J_{i1}\, e^{\left(-8\left(\frac{(X-X')^2}{d_{i1}^2}+\frac{(Y-Y')^2}{d_{i1}^2}\right)\right)} \otimes \delta(X' - x_{p_i}, Y' - y_{p_i})\, dX'dY' \quad \text{Equation 4.6}$$

$$I_2 = \iint \sum_{p_2} J_{i2}\, e^{\left(-8\left(\frac{(X-X')^2}{d_{i2}^2}+\frac{(Y-Y')^2}{d_{i2}^2}\right)\right)} \otimes \delta\left(X' - \left(x_{p_i} + \Delta x_i\right), Y' - \left(y_{p_i} + \Delta y_i\right)\right) dX'dY' \quad \text{Equation 4.7}$$

$$C_{max} = max\left(\sum_{p_c}\iint J_i^2 e^{-8\left[\frac{(X-x_{p,i})^2}{d_i^2}+\frac{(Y-y_{p,i})^2}{d_i^2}\right]} \times e^{-8\left[\frac{(X-x_{p,i})^2}{d_i^2}+\frac{(Y-y_{p,i})^2}{d_i^2}\right]} dXdY\right) = \sum_{p_c}\frac{1}{16}J_i^2 d_i^2\pi \quad \text{Equation 4.8}$$

In Equation 4.8, the value of C_{max} is the sum of the magnitudes of the autocorrelation of all pairs of particles correlated within the interrogation window. The mutual information (MI) is defined by the division of the height of the cross-correlation peak by the magnitude of the autocorrelation by Equation 4.9.

$$MI = \frac{C_{max}}{A_0} = \frac{\sum_{p_c}\frac{1}{16}J_i^2 d_i^2\pi}{\frac{1}{16}J_0^2 d_0^2\pi} \quad \text{Equation 4.9}$$

Figure 4.1 shows the time-averaged u and the RMS of the u fluctuation (u') fields in a section of a channel with periodic hills. This example was taken using raw images from the 4th PIV Challenge (Kähler et al., 2016) and processed by the authors of this work. All the PIV processing details are presented in Table 4.1. The final size of the chosen interrogation window was 24 px with 50% overlap, which produced a 12 px grid. The reasons of that choice were based on the difficulty of guaranteeing the quality of the velocity fields in those conditions. Although the time-averaged velocity field u showed a good spatial coherence, a high number of outliers was observed in the RMS of u' field. The presence of these outliers was mainly related to the low tracer density per pixel in the right region of the image frame, as shown in Figure 4.2. PIV post-processing methods based on neighborhood connectivity, such as MAD or UOD, fails mainly in the presence of a high number of outliers grouped, that is, a cluster of outliers. Figure 4.3 presents the raw instantaneous velocity field and its correction based on the MAD post-processing method of the same turbulent flow in a section of a channel with periodic hills. The spatial neighborhood used in the MAD correction was 3x3 interrogation windows, which can remove outliers that appear isolated in the field but fails in the presence of clusters of outliers. Analyzing the distribution of the time-averaged SNR metrics in Figure 4.4, it can

be observed that low MI values are directly related to the behavior of the low density of particle images and, consequently, to the high number of outliers in RMS of the u' field. In this case, the separation of noise using MI presents a higher performance than that observed by PPR.

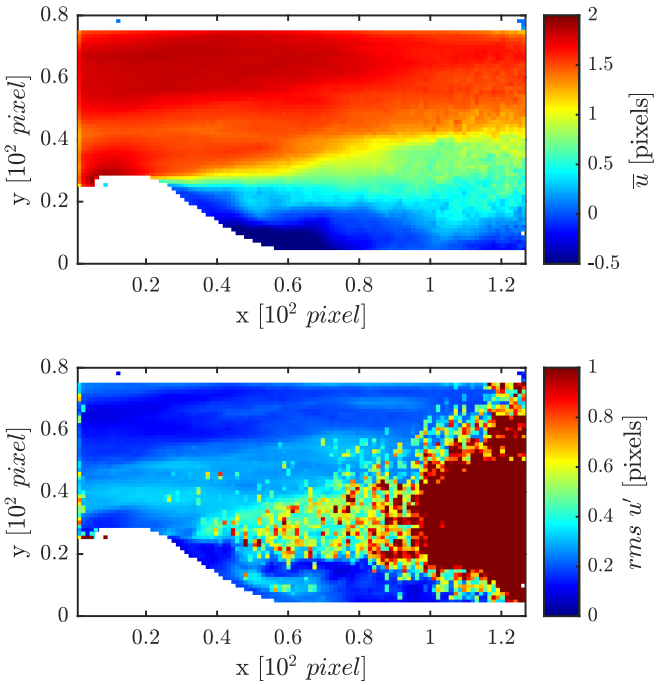

Figure 4.1. Time-averaged u and RMS of the u fluctuation (u') fields of a turbulent flow in a section of a channel with periodic hills.

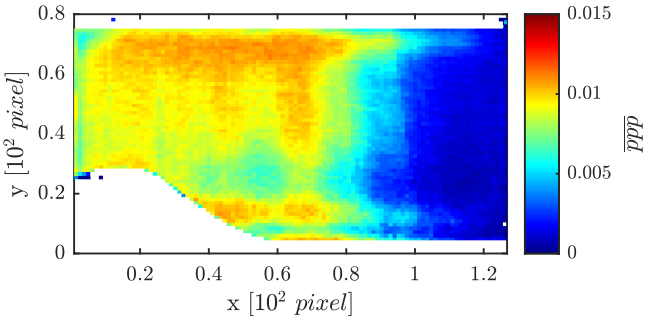

Figure 4.2. Distribution of the time-averaged of particle per pixel (*ppp*) of a turbulent flow in a section of a channel with periodic hills.

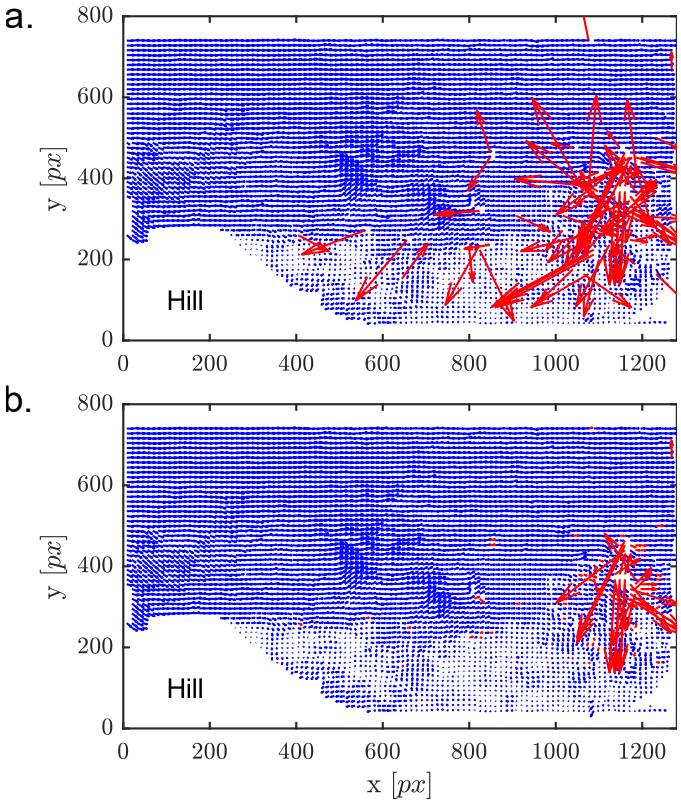

Figure 4.3. (a) Raw instantaneous velocity field and (b) its correction based on MAD of a turbulent flow in a section of a channel with periodic hills.

Table 4.1. PIV evaluation parameters used in this work for the case study of a turbulent flow in a channel with periodic hills.

Preprocessing	**Interrogation**	**Correlation**
- Gaussian filter (3 px, standard deviation of 0.3); - Mean sliding subtraction filter (7 x 7 px); - Intensity capping (Shavit *et al*. 2007); - Mean sliding subtraction filter (10 x 10 px); - Gaussian filter (3 px, standard deviation of de 0.6)	- A multigrid analysis with discrete window offset (Scarano, 2001; Kim and Sung, 2006) was applied in which the size of the interrogation window is progressively decreased. - Four steps were used: the first three steps gradually decreased from interrogation windows of 64 px with 25% overlap to 32 px with 25% overlap. The last step was 32 px with 50% of overlap.	- Standard Cross-Correlation. - 3 point Gaussian fit

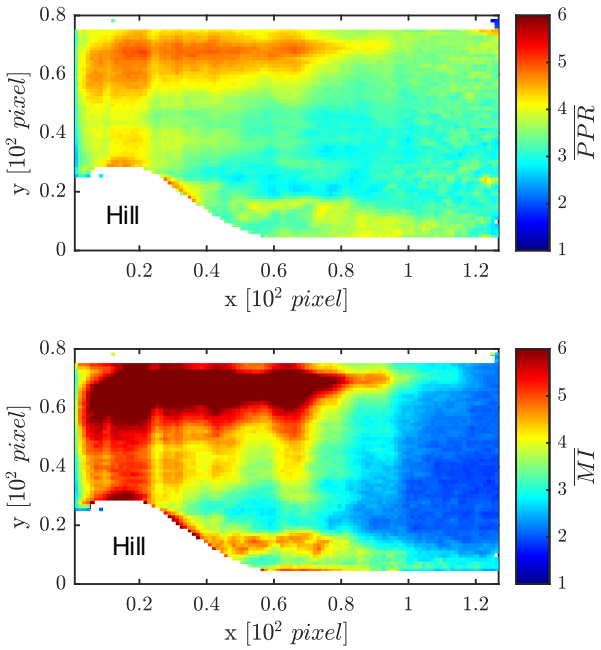

Figure 4.4. Distribution of the time-averaged PPR and MI of a turbulent flow in a section of a channel with periodic hills.

Figure 4.5 shows the instantaneous velocity field of the same turbulent flow in a section of a channel with periodic hills after applying a SNR threshold equal to 2 before using MAD in the PIV post-processing. The number of outliers removed by the MI approach (MI-MAD) was greater than those by PPR approach (PPR-MAD). This can also be seen in Figure 4.6, where RMS of u' field after the application of (a) PPR-MAD and (b) MI-MAD is presented. The spatial neighborhood used in the MAD approach was 3x3 interrogation windows.

For comparison, RMS of u' field obtained by the multi-frame pyramid correlation of the time-resolved measurements is presented in Figure 4.6c as reference. The multi-frame pyramid approach is based on the combination of correlation maps that are obtained at different temporal separations. This correlation approach eliminates more PIV errors than the standard cross-correlation, for example. However, this approach is limited to time-resolved measurements and requires a high computational cost. In our case, the level of the pyramid chosen was at most equal to two, that is, an instantaneous field was determined by optimizing three correlation maps (for example, based on the correlation of frames 1-2, frames 2-3 and frames 1-3). The details of this approach are presented by Sciacchitano et al. (2012). Besides eliminating more outliers, the MI approach resulted in less information loss than PPR for a SNR threshold equal to 2, as shown in Figure 4.7. The differences between the field with correction based on the MI approach and the one obtained by the multi-frame pyramid correlation (reference field) can also be explained by the presence of some outliers and data loss. It is possible to eliminate more outliers by increasing the SNR threshold, however the amount of lost data would also be increased. While removing noise, data can be lost because there is no spatial information to reconstruct the field. This occurs because we used a small neighborhood (3x3 interrogation windows) in order to avoid masking the high velocity gradients. Although the noise in Figure 4.5b was completely removed, the data was not reconstructed due to the clusters of outliers. Larger interrogation windows (5x5 or 7x7) could reconstruct the field, but they would mask the high velocity gradients. Unfortunately, it is not possible to analyze the effect of the SNR threshold in the channel, since only 1044 images were provided in the challenge in order to estimate the turbulent parameters and higher-order moments of the velocity fluctuations of a unsteady flow . However, in this work, the effect of the SNR threshold will be presented in detail for a case study of a stirred tank steady flow.

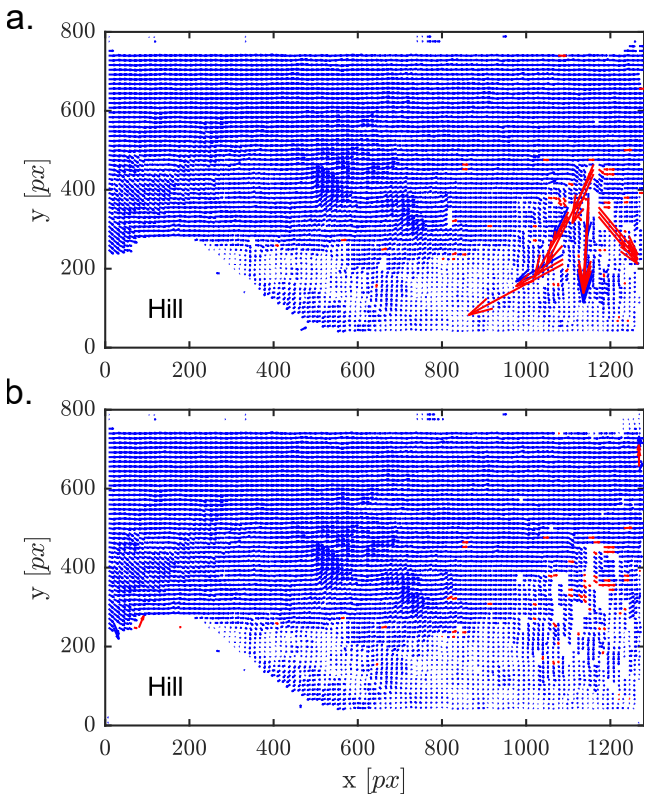

Figure 4.5. Instantaneous field corrected by (a) PPR-MAD and (b) MI-MAD methods for a SNR threshold equal to 2 of a turbulent flow in a section of a channel with periodic hills.

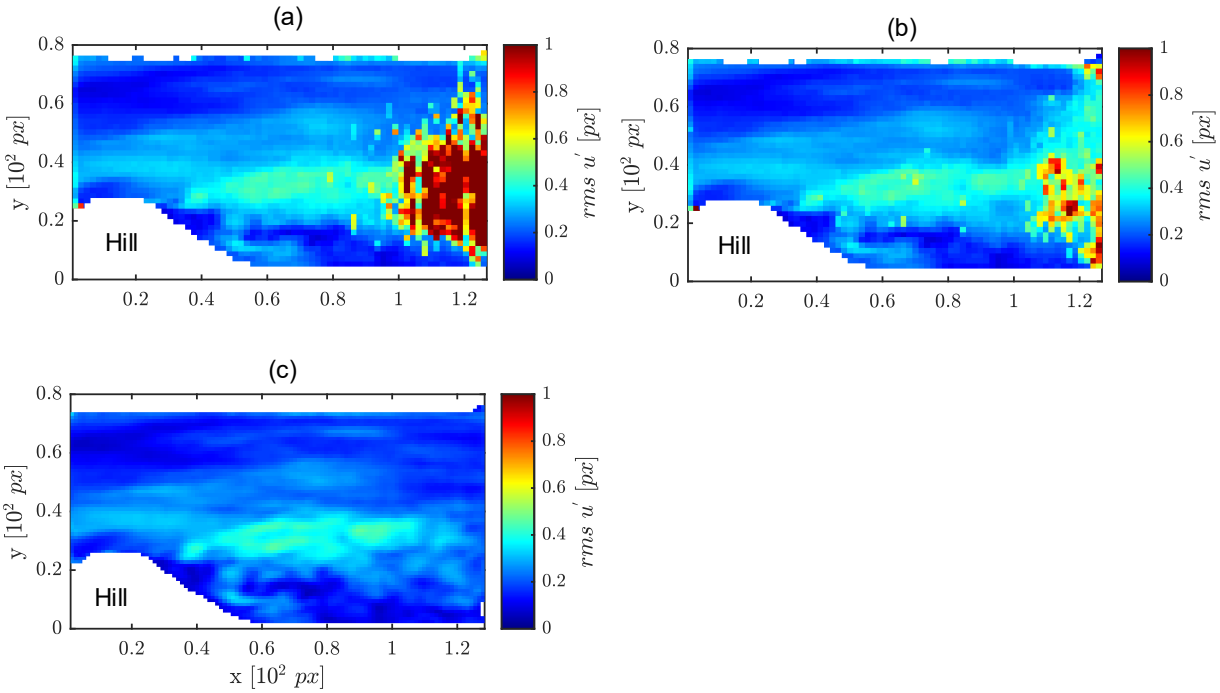

Figure 4.6. RMS of u' field after the application of (a) PPR- MAD and (b) MI-MAD methods in the PIV measurements of a turbulent flow in a section of a channel with periodic hills, and (c) reference of the RMS of u' field obtained by the pyramid correlation.

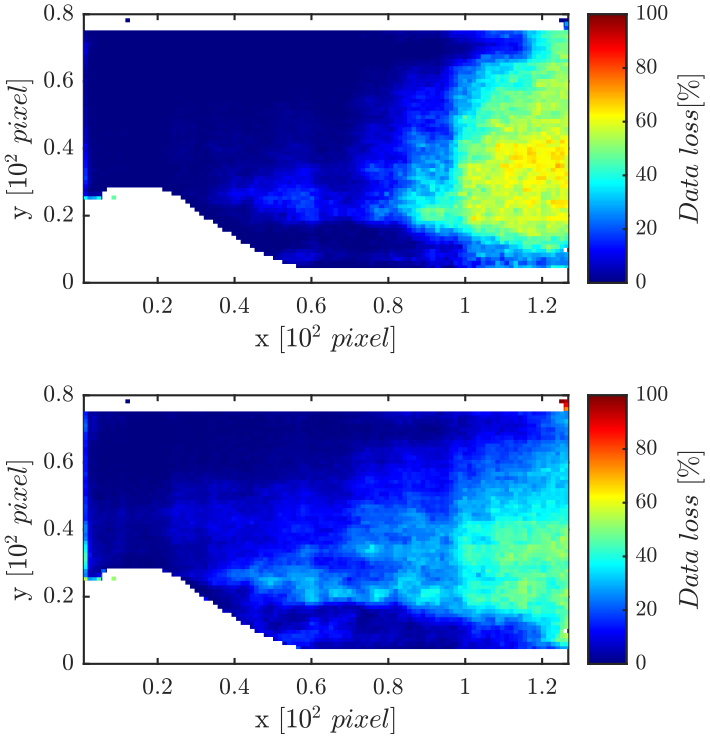

Figure 4.7. Data loss after the application of (a) PPR- MAD and (b) MI-MAD methods in the PIV measurements of a turbulent flow in a section of a channel with periodic hills.

3. CASE STUDY ON A STIRRED TANK FLOW

To evaluate the performance of the post-processing using MI thresholds and compare it with the standard PPR method, a case study was carried out in a stirred tank for different values of SNR limits and different spatial resolutions. The latter was obtained by reducing the size of the interrogation windows. Spatial resolution is an important parameter that characterizes the overall performance of the PIV measurement. Likewise, at high spatial resolution of the data field it is necessary to resolve large and small scales structures in the flow (Raffel et al., 2018). As stated earlier, optimizing noise levels in stirred tanks with high spatial resolution is a challenging task due to high number of outliers and consequent loss of flow information.

3.1. EXPERIMENTAL SYSTEM AND DATA ACQUISITION

Figure 4.8a shows the agitation system used to acquire the experimental data. The mixing system consists of a 50 L cylindrical tank made of acrylic with a 10% torispherical bottom head made of stainless-steel 316-L. The tank structure is made of stainless-steel

304. The dimensions of the tank are T = 380 mm inner diameter and H = 760 mm height, and it is equipped with four equally spaced vertical baffles. A down-pumping PBT 45° impeller was used to agitate the system and the impeller shaft was centrally located in the tank. This impeller has four 45° pitched blades (D = T/3, C = T/3) and four equally spaced baffles (B = 0.12T), as shown in Figure 4.8b. The fluid used was water at room temperature (20 °C ± 1) and the tracer particles were made of polyamide with a diameter of 20 μm. The stirred tank was filled to a height of 380 mm, that is, H = T (square batch). The velocity applied to the system was 660 rpm in a turbulent flow ($Re = \rho N D^2/\mu \cong 172000$). The impeller tip velocity, $U_{tip} = \pi DN$, was calculated to be 4.32 m/s.

The PIV acquisition used a classic system (PIV 2C-2D) from Dantec Dynamics. The laser system Nd: YAG laser, 200 mJ, 532 nm, was applied with a light sheet thickness of 2 mm. The *DynamicStudio* software was used for all the data acquisition. The camera used for recording the images was the FlowSense EO 8M-21 model (3312 x 2488 pixels). The resolution of the imaging system was 23.81 px/mm.

The flow information was obtained using the azimuthal position of the 0° light plane (Figure 4.8c). The camera was positioned at σ = 10º to the normal of the light sheet (object plane) as presented in Figure 4.8 d. This position was used to decrease the image distortion caused by the curvature of the tank mainly in the wall region. In addition, a 2D calibration based on the method developed by Soloff et al. (1997) was used for distortion compensation through a third-order polynomial function. This 2D calibration approach is similar to those used by Rottier et al. (2010), who compensated the distortion effect of endoscopic images, and Zang et al. (2014), who performed measurements on spray mixing process. We chose not to use the conventional method that applies a liquid-filled box for distortion compensation because other experiments in which measurements were performed at different azimuthal positions were carried out for further analysis to be presented in a future work. For these measurements, the use of the box would be less practical. The 2D calibration was performed using a 270 mm x 190 mm plate in ABS polymer with a pattern of 0.5 mm diameter points and 1.5 mm spacing printed on the plate as shown in Figure 4.9. For the adjustment of the polynomial function, more than nine thousand points were used. In Figure 4.9, the calibration error in the center of the tank was less than 1 pixel (R1 and R2) and less than 2 pixels in the region near the wall (R3). The alignment of the grid over the target points indicates a perfect calibration. Based on the distortion analysis performed by Elsinga et al. (2005), there was no enlargement of the

correlation peak or sudden change in the SNR metrics in the wall region, represented by R3 in Figure 4.9, for the interrogation windows used in this work.

The image recording was performed in a double-frame mode. To obtain statistically consistent PIV results, 1,000 pairs of images were recorded for the analyzed area. The adjustment of the time between consecutive frames is also important for the quality of the PIV measurements. The interframe time used was 100 μs, which was chosen based on a previous analysis of the PPR in the correlation plane for an interrogation window equal to 48 px. This time was also chosen to guarantee that the mean and maximum displacement of the particle image within the interrogation window was 5 px and 20 px, respectively. This strategy is important to avoid subpixel displacement and peak-locking effect, which impairs the determination of the velocity field (Adrian and Westerweel, 2011; Raffel et al., 2018).

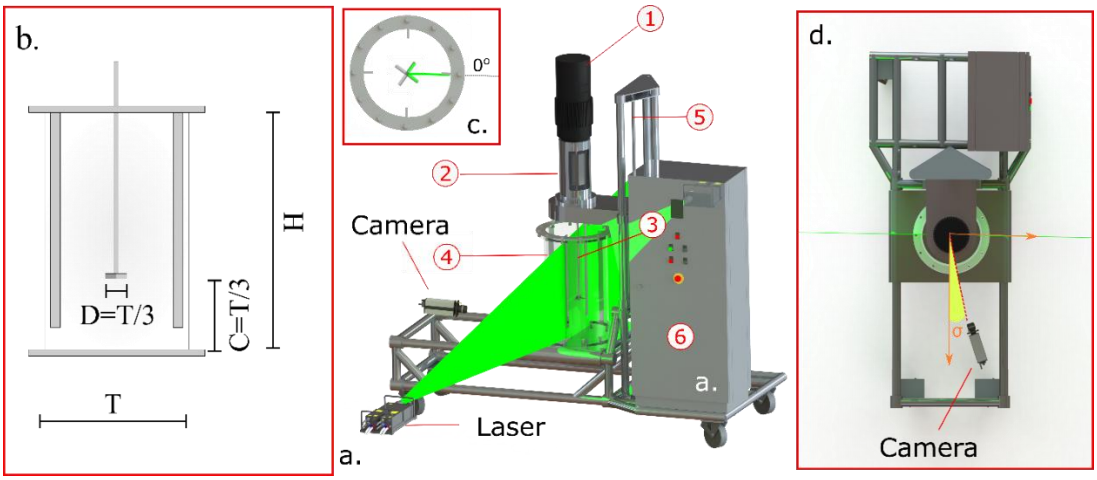

Figure 4.8. (a) Experimental stirred tank and PIV: (1) engine; (2) torque meter; (3) impeller shaft; (4) tank; (5) impeller height adjustment system; (6) frequency inverter electrical control panel. (b) Tank and impeller dimension details. (c) Position of the azimuthal plane of the PIV measurements. (d) Camera position from the laser sheet.

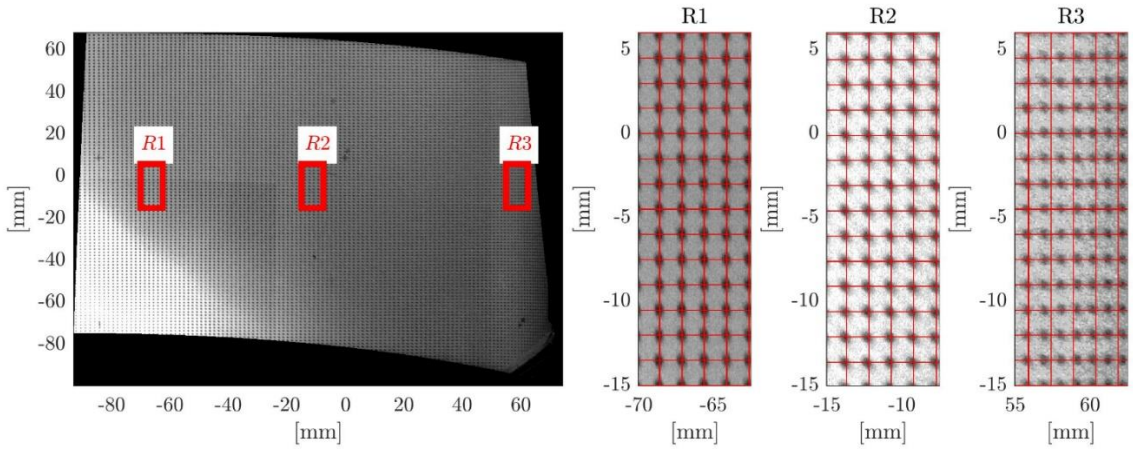

Figure 4.9. Dewarped image of the target after 2D calibration procedure.

3.2. DATA PROCESSING

All data processing was carried out using in-house Matlab codes developed by this research group. The recorded images were preprocessed with the main objective of removing backlight and reflections caused by the tank structure. Moreover, the individual images were smoothed, and their contrasts increased. The following sequence of filters were applied to the raw image: a Gaussian filter (3x3 pixels), local minimum intensity subtraction (7x7 pixels), Intensity Capping (Shavit et al, 2007) histogram elongation, three times the local average subtraction and a Gaussian filter (3x3 pixels) again. The PIV processing was performed using the PRANA toolbox inside Matlab (Eckstein and Vlachos, 2009). A multigrid analysis with a discrete window offset (Scarano, 2001; Kim and Sung, 2006) was applied in which the size of the interrogation window (IW) is decreased progressively in order to analyze the effect of spatial resolution. In this work, five passes were used: the first three passes gradually decreased from interrogation windows of 48 px with 25% overlap to 27 px with 25.9 % overlap. The last two passes were with interrogation windows of 27 px with 44.4% of overlap to 27 px with 62.9% of overlap. The final interrogation window (IWf) for each pass was of 36, 27, 20, 15 and 10 px. Details of the multigrid interrogation procedure are presented in Table 4.2. The interrogation window size for Pass 1 was chosen based on the one-quarter rule and on the interframe time as detailed in Section 3.1. In the case of Pass 1 of the multigrid procedure, the maximum displacement of the particle image population should be one quarter of IW (Keane and Adrian, 1990). The choice of the final interrogation window size for the other passes depends on the particle image concentration (Scarano, 2001; Kim and Sung, 2006).

Moreover, the choice of three first and three last passes aims to investigate the dominant effect of the initial interrogation window and overlap (Over) in the fields, respectively. The correlation used was the Standard Cross-Correlation. The post-processing filter developed by Westerweel and Scarano (2005) was used at the end of each step to eliminate outliers, avoiding instabilities and noise propagation in the multigrid approach. In this case, a removal threshold of 2 was used. Despite the use of this filter, the results generated in this step will be referred to as raw fields.

Table 4.2. Details of the multigrid interrogation procedure

Pass	**IW [px]**	**Over [%]**	**IW_f**	
			[px]	**[mm]**
1	48	25.0	36	1.512
2	36	25.0	27	1.134
3	27	25.9	20	0.84
4	27	44.4	15	0.63
5	27	63.0	10	0.42

3.3. PERFORMANCE OF THE POST-PROCESSING BASED ON MI THRESHOLDING

Three strategies presented in Figure 4.10 were applied to compare and to investigate the performance of the PIV post-processing based on mutual information thresholding. In the first strategy (Post-processing 1), the Median Absolute Deviation (MAD) followed by an interpolation was applied to the data. In the second and third post-processing strategies, a PPR and MI thresholds were applied before Post-Processing 1. In this work, Post-processing 1, 2 and 3 will be referred to as MAD, PPR-based and MI-based corrections. MAD is a post-processing method widely used to identify noise in PIV measurements. The MAD scale is calculated according to Equation 4.10 (Huber, 1981), where b = 1,4826, x_j is the number of original observations and M_i is the median of the local neighborhood. According to Miller (1991), if the estimated velocity value in the interrogation window is more than three times the MAD value, the vector is considered as an outlier and it is excluded. The identification and removal of false vectors was followed by an interpolation

on a 3x3 interrogation window (IW). If it fails and does not generate a valid vector, that is, a vector with a spatial coherence preserved, a new interpolation on a 5x5 interrogation window needs to be performed. The MAD and the interpolation procedures are performed twice in a sequence for an effective reconstruction of the velocity field without noise. It is important to notice that the use of large windows can cause the removal of high velocity gradients and velocity fluctuations. Moreover, a large neighborhood, or being more specific, a large kernel, can interpret real flow signals as noise. However, the use of automatic correction filters can also exclude vectors that are correct, deteriorating the quality of the measurement.

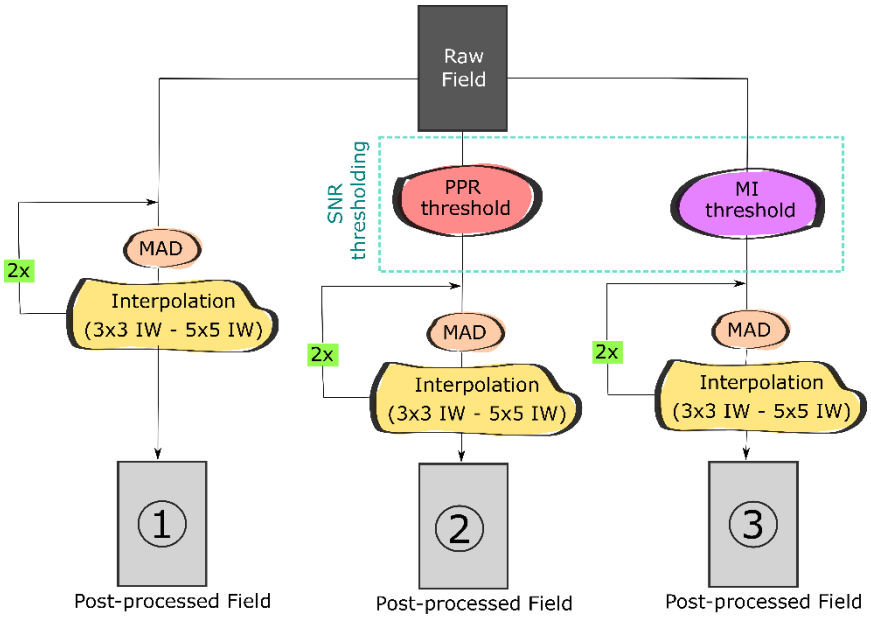

Figure 4.10. Three different PIV post-processing strategies investigated in this work: MAD correction (Post-processing 1), PPR-based correction (Post-processing 2) and MI-based correction (Post-processing 3)

$$MAD = bM_i(|x_i - M_j(x_j)|) \qquad \text{Equation 4.10}$$

In the presence of clusters of outliers, the MAD performance decreases considerably and is not effective. In that case, Post-processing 2 and Post-processing 3 propose the use of PPR and MI thresholds to eliminate false vectors, which are related to low SNR values, before applying the MAD correction. Essentially, the PPR and MI thresholds act based on the exclusion of the velocity vectors that have values of SNR lower than an established limit (SNRL). In these strategies, MAD and interpolation procedures

play a fundamental role in the reconstruction of the velocity field, since the amount of data lost is greater than that observed for the MAD correction. In this work, different SNRL values (from 1.25 up to 2.75) were investigated to determine the most suitable setup for the field correction. The analyses of the three strategies were done for all the five steps of the multigrid analysis, that is, for five different sizes of interrogation windows. Due to the flow restriction within the stirred tank, the amount of noise in all fields analyzed was estimated by the U_{tip} threshold. In addition, the information loss as a result of PPR-based and MI-based correction was also investigated, hence it influences the determination of mean and turbulent flow parameters.

3.4. RESULTS AND DISCUSSION

Figure 4.11 presents the instantaneous velocity field before and after Post-processing 1 (MAD correction) for final interrogation windows (IWf) of 36 and 10 px. It can be noticed that for the IWf of 36 px there were no velocity values with magnitude above $U_{tip} = 4.32\ m/s$. However, for the IWf of 10 px, clusters of outliers are observed at the bottom of the tank, at the impeller tip and below the impeller. It should be noticed that the MAD correction was not capable of eliminating the outliers. Figure 4.12 presents the percentage of noise for an instantaneous raw velocity field and after the MAD correction for five different final interrogation windows (IWf). This figure shows that the noise level in the instantaneous raw images increased with the decreasing of the final interrogation window or, in other words, with the increasing of the spatial resolution. This effect is even more noticeable for the case of the MAD correction. In the instantaneous velocity field, the noisy source is directly related to the light reflections on the impeller and to the laser pulse oscillation and/or shadows formed by the structure of the tank below the impeller. The irregular lighting generated by these problems was only observed in some pair of frames. Figure 4.13 shows the distribution of particle per pixel (ppp) for the pair of frames used for the calculation of the instantaneous velocity field presented in Figure 4.11. The non-homogeneous distribution is a problem that directly interferes on the number of particle image (N_I), which may compromise the quality of the measurement (see Equation 4.1). In addition to the light reflection, the high velocity gradients and the out-of-plane particle motion help to explain the outliers found at the tip of the impeller.

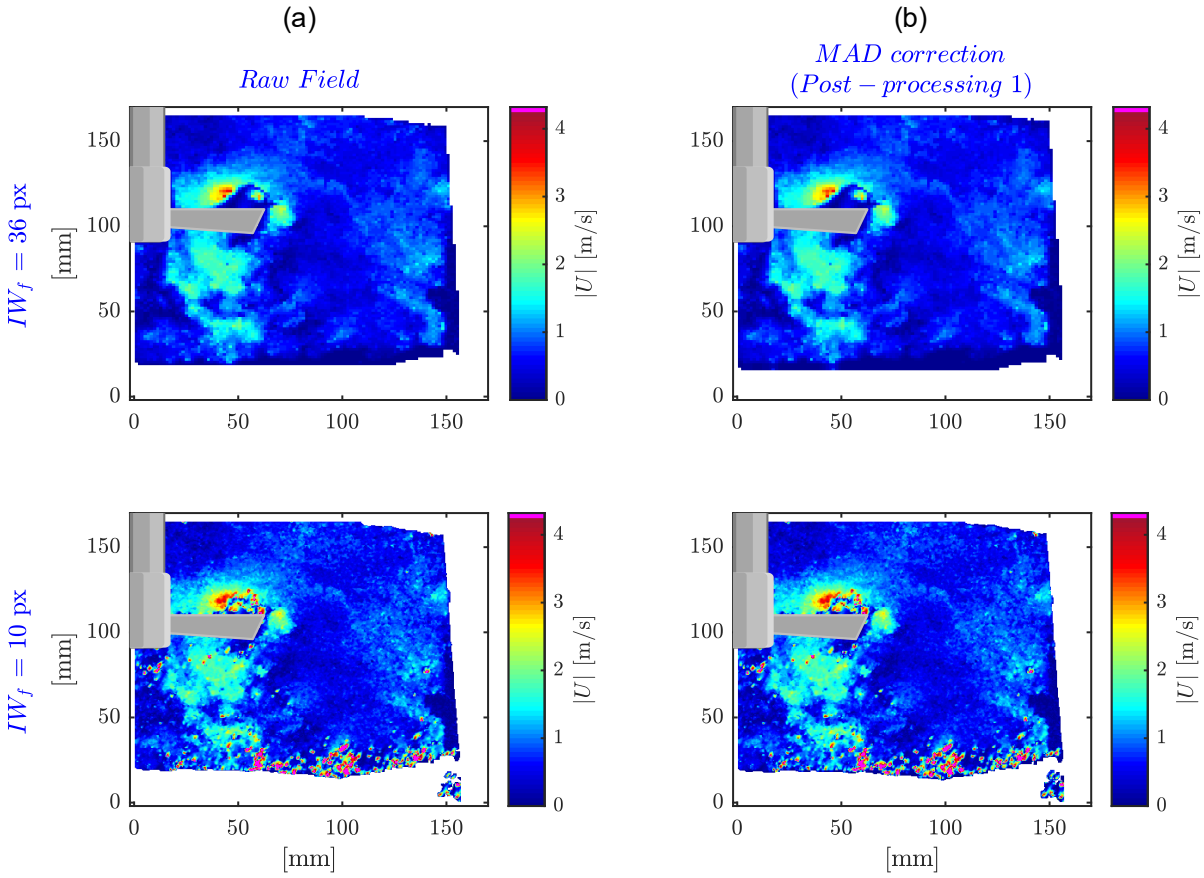

Figure 4.11. Instantaneous velocity field (a) raw and (b) after MAD correction (Post-processing 1) for final interrogation windows (IW_f) of 36 and 10 px.

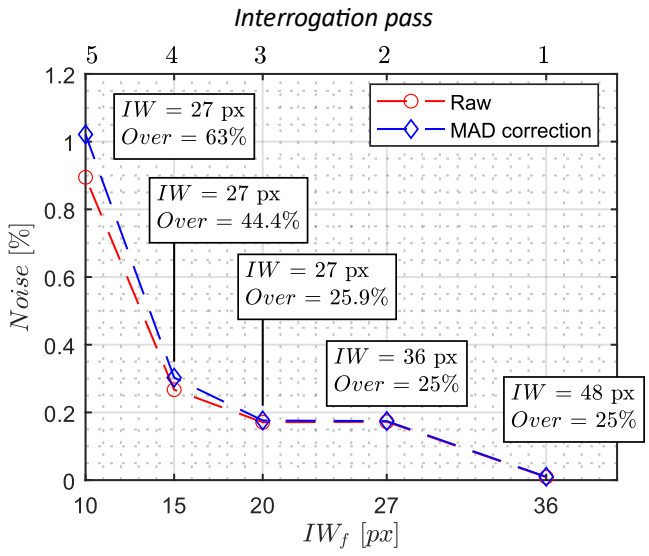

Figure 4.12. Percentage of noise for five different final interrogation windows (IW_f) for an instantaneous raw velocity field and after MAD correction (Post-processing 1).

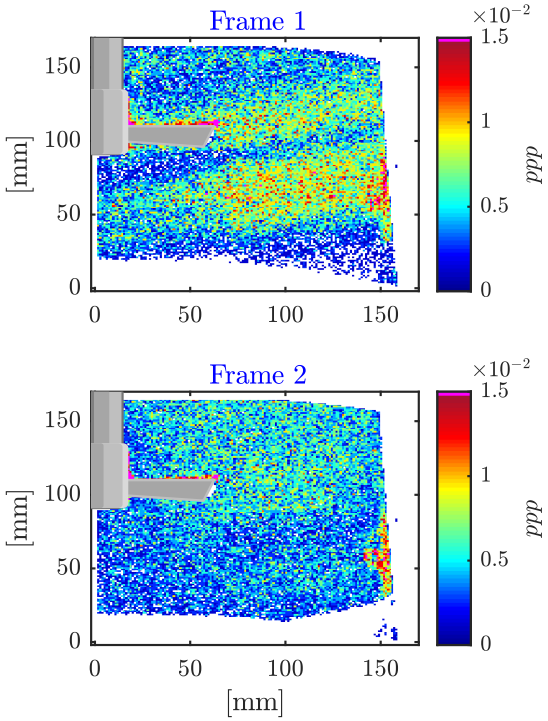

Figure 4.13. Distributions of the *particle per pixel* (*ppp*) in Frames 1 and 2 used for the calculation of the instantaneous velocity field presented in Figure 4.11.

The SNR fields obtained from the PPR and MI methods for the instantaneous velocity field shown in Figure 4.11 are presented in Figure 4.14. The SNR values calculated by the MI method were higher than those calculated by the PPR. This result was similar to the case of the turbulent flow in a channel with periodic hills, as shown in the Section 2 of this work. The SNR fields also show that the lower SNR values were found at the bottom of the tank, at the impeller tip and at the impeller bottom regions. The lower the SNR, the greater the presence of outliers. Therefore, these results are in agreement when compared with the velocity field presented in Figure 4.11, especially for the case of the higher resolutions. Figure 4.15 presents the probability density function (pdf) of the SNR fields for the five final interrogation windows used. It can be noticed that the SNR values decrease considerably with the decreasing of the interrogation windows (IW). However, the SNR does not vary with the increasing of the overlap (final interrogation windows of 20, 15 and 10 px).

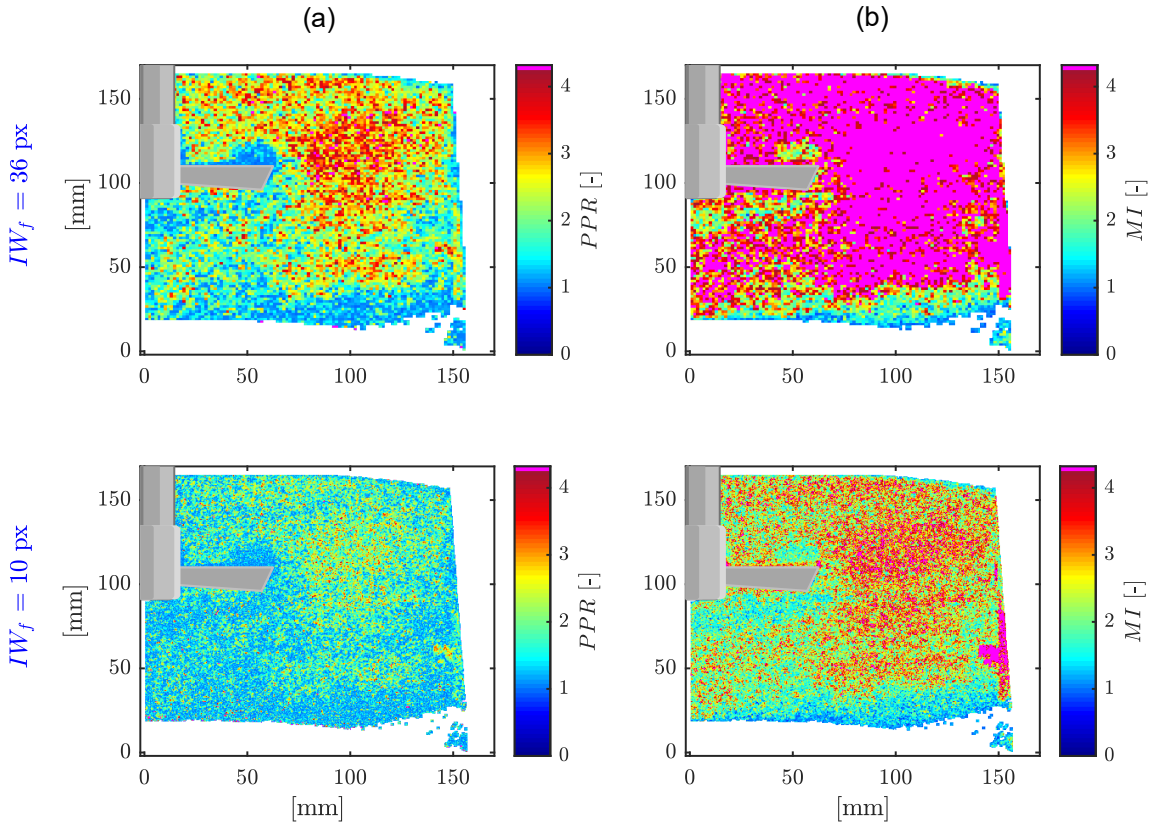

Figure 4.14. Signal-to-noise ratio (SNR) fields obtained from the (a) PPR and (b) MI methods for the instantaneous velocity field presented in Figure 4.11 with final interrogation windows (IW_f) of 36 and 10 px.

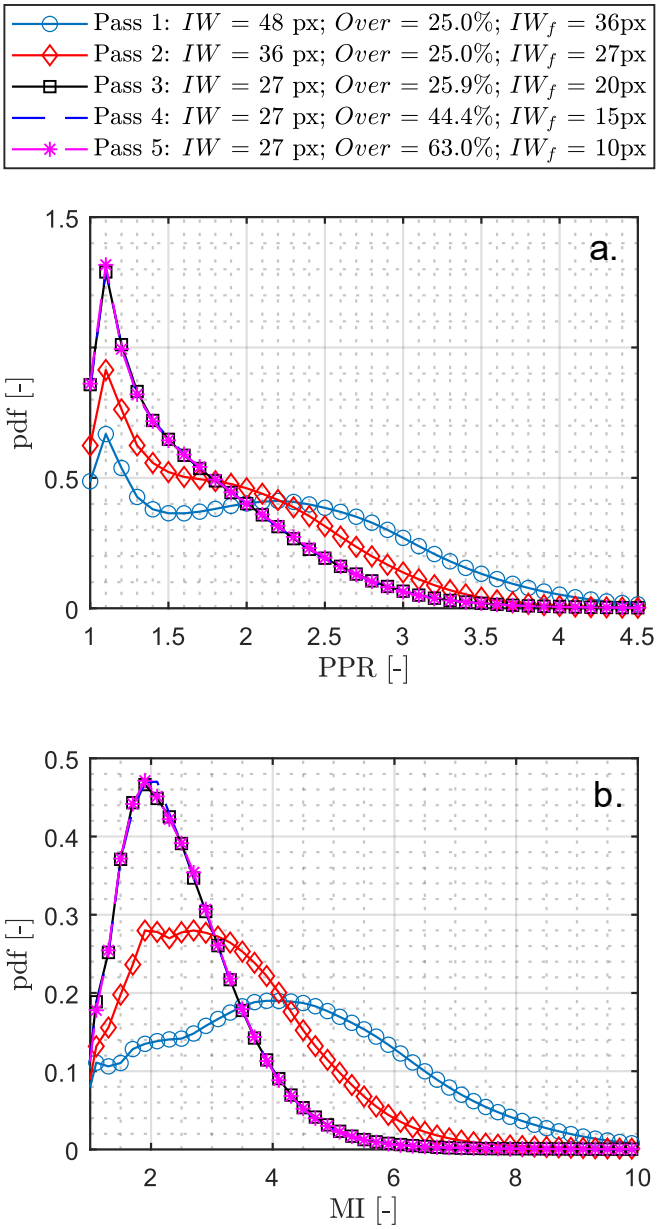

Figure 4.15. Probability density function (pdf) of the SNR fields obtained from (a) the PPR and (b) MI methods for the instantaneous velocity fields presented in Figure 4.11 varying the interrogation passes.

Figure 4.16 shows the instantaneous velocity field obtained by the application of the SNR threshold (SNRL) in order to verify the difference in terms of performance of both the PPR-based and MI-based corrections. Only the final interrogation window of 10 px (0.42 mm) was used, since the presence of outliers is higher for this processing condition. The values of SNRL varied from 1.75 to 2.75 and, for each case, all the velocities with values lower than the SNRL were considered outliers and consequently were removed. From Figure 4.16a and Figure 4.16b, which show the PPR and MI thresholding,

respectively, it can be observed that as the SNRL value increases, more vectors are eliminated. Consequently, among these removals, valid vectors may be lost. This result is mainly observed for the PPR thresholding (Figure 4.16a). The full effect of the PIV corrections based on the PPR and MI can be seen in Figure 4.16c and Figure 4.16d, respectively. The MI-based correction showed a better performance for the elimination of outliers by thresholding, followed by the reconstruction of lost data through the MAD and Interpolation procedures. Distributions of the percentage of noise and data loss as function of the SNR threshold are presented in Figure 4.17 for both the PPR-based and MI-based corrections. The percentage of noise in the field was estimated as the ratio of the number of interrogation windows with velocity greater than U_{tip} by the number of interrogation windows with velocity. For both corrections, the noise in the instantaneous velocity field was below 0.5% for values of SNRL between 1.75 and 2.5. For the PPR-based correction, the noise percentage increased significantly for SNRL > 2.5 due to a greater elimination of valid velocity vectors in relation to false velocity vectors. It can be observed that the data loss is greater for the PPR-based correction for all values of SNRL considered. Therefore, the MI-based correction has advantages over the PPR-based correction due to a lesser data loss.

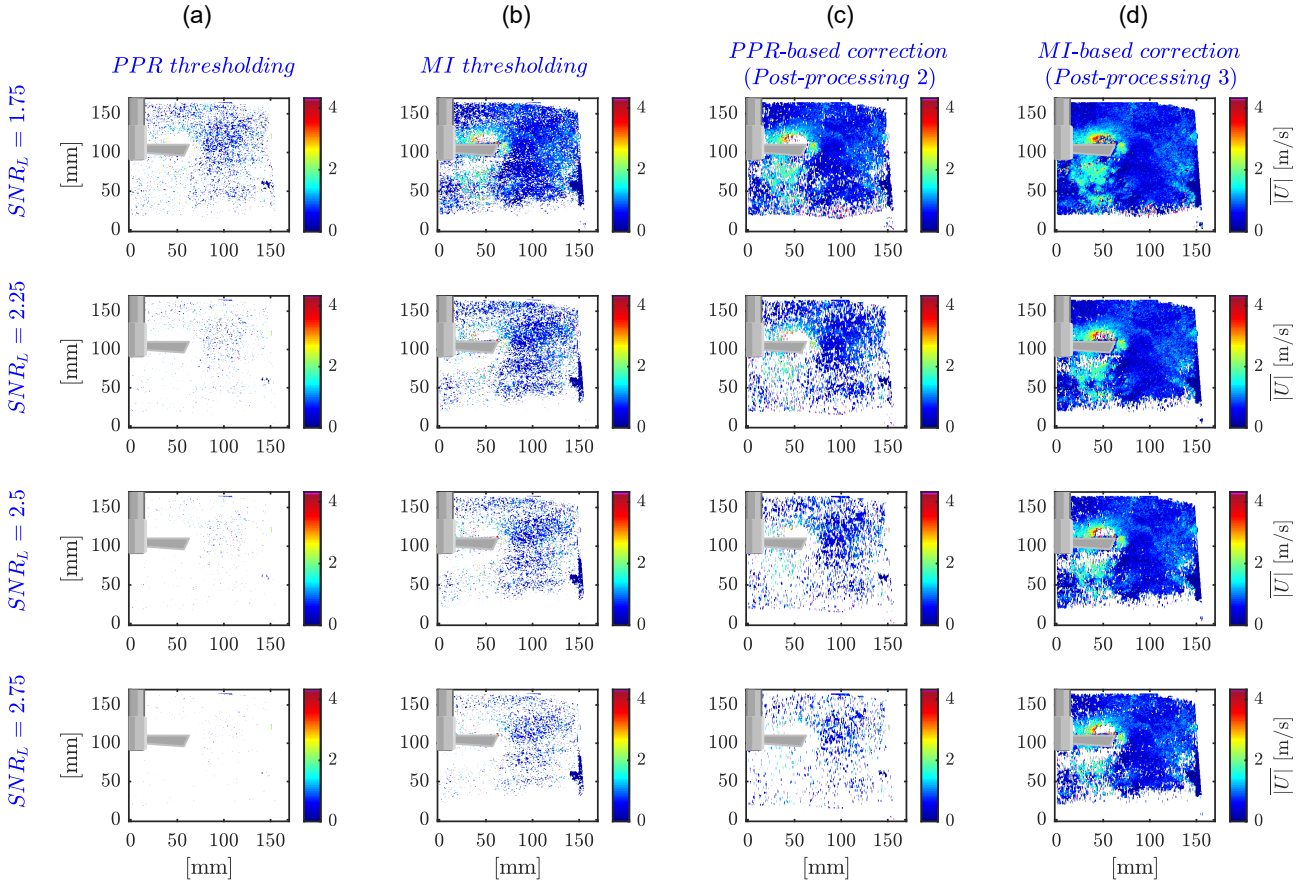

Figure 4.16. Instantaneous velocity field after applying: (a) PPR threshold, (b) MI threshold, (c) PPR-based correction (Post-processing 2) and (d) MI-based correction (Post-processing 3) for different SNR thresholds and IW_f = 10 px (0.42 mm).

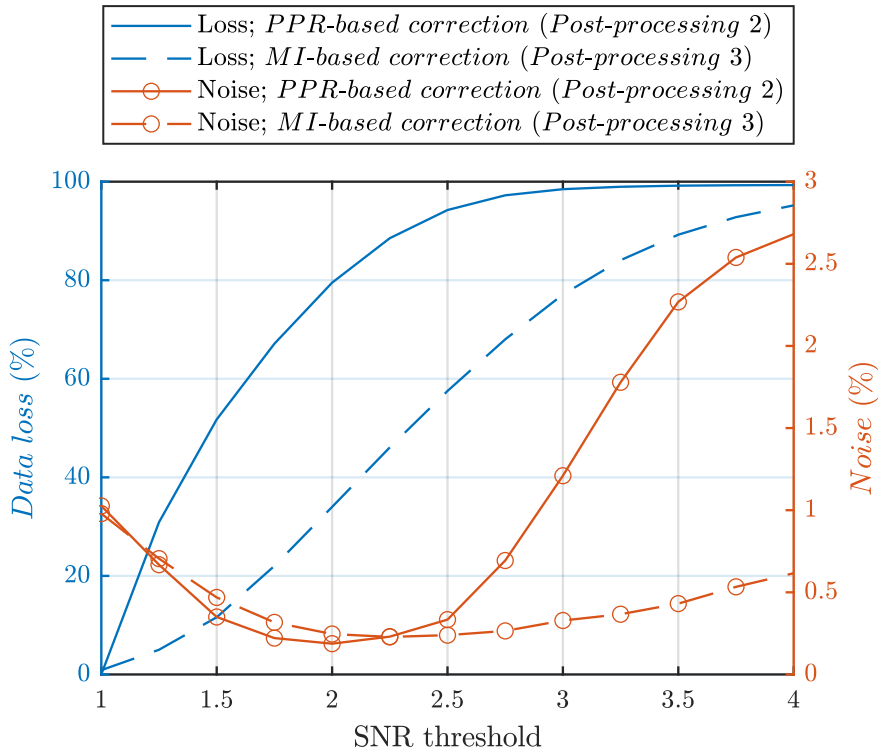

Figure 4.17. Percentage of data loss and noise after applying the PPR-based correction (Post-processing 2) and the MI-based correction (Post-processing 3) for the instantaneous velocity field with IW_f = 10 px (0.42 mm).

Distributions of the percentage of noise and data loss over time for 1,000 velocity fields obtained after the PPR-based and the MI-based correction for IWf = 10 px are presented in Figure 4.18. In this case, the percentage of noise and data loss was calculated by using the time series of each interrogation window. Over time, the percentage of noise decreased considerably with the increasing of the SNRL for the MI-based correction. Similar to the behavior observed in the instantaneous field of Figure 4.16 and Figure 4.17, the number of data loss was greater for the PPR-based correction as the value of SNRL was increased. For SNRL > 2.5, a large part of the region below the impeller showed data loss of more than 50%, after the PPR-based correction. At the bottom edge of the field, a large amount of data was also lost for the MI-based correction due to the presence of outliers caused mainly by the low values of particle per pixel (ppp). The data lost for the PPR-based correction occurred in almost all the region below the impeller for SNRL ≥1.75. On the other hand, after applying the MI-based correction, this behavior was observed only for SNRL = 2.5. The distribution of the time-averaged and of the standard deviation of particle

per pixel (*ppp*) for the 1,000 velocity fields are presented in Figure 4.19. The results show that the time-averaged *ppp* fields are more homogeneous than those observed for the instantaneous noisy pair of frames in Figure 4.13, which indicates that the instability of the laser light occurred only in a few images. In addition, this can also be observed by the uniform distribution of the standard deviation of *ppp*.

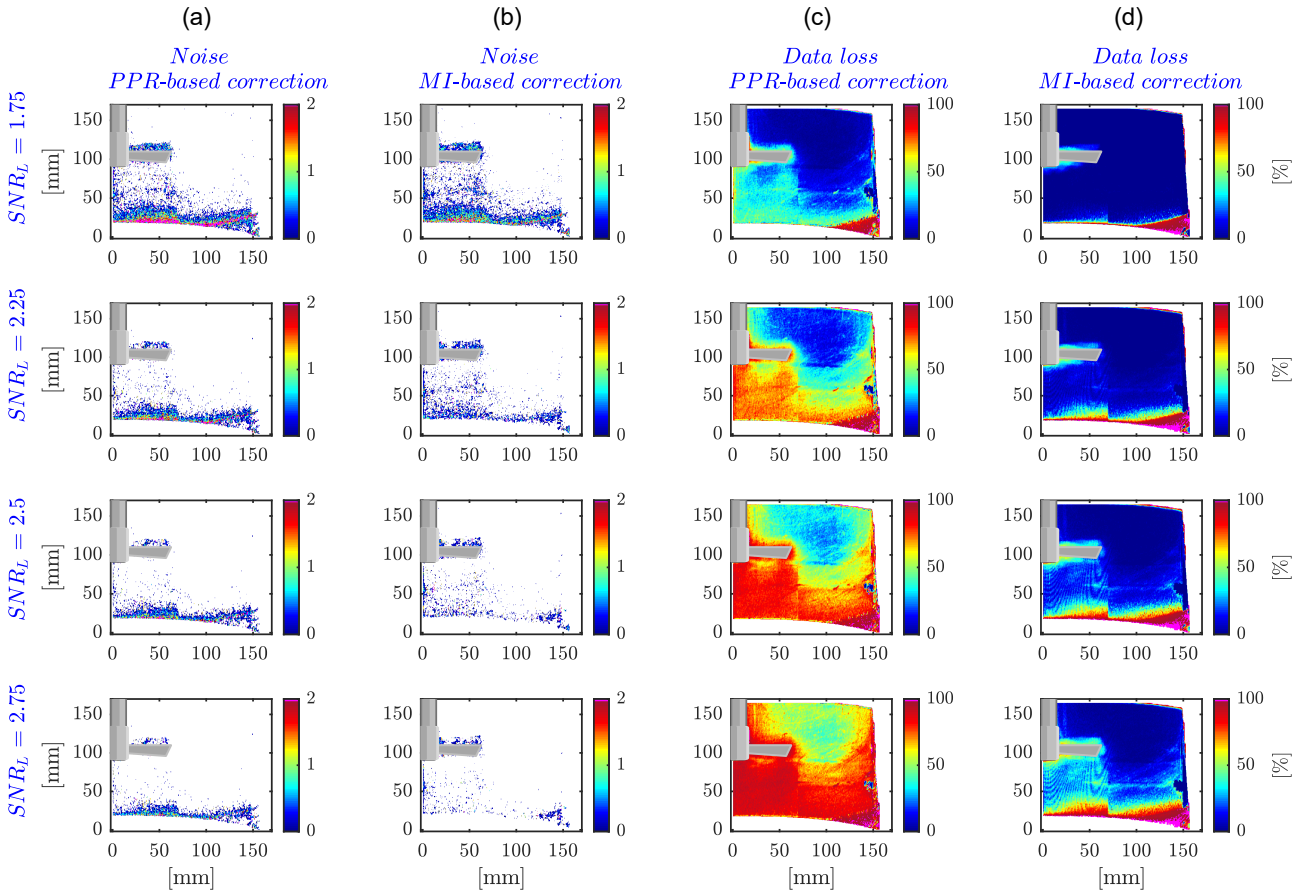

Figure 4.18. Distributions of the percentage of (a-b) noise and (c-d) data loss over time for 1,000 velocity fields after PPR-based and MI-based correction for IW_f = 10 px (0.42 mm).

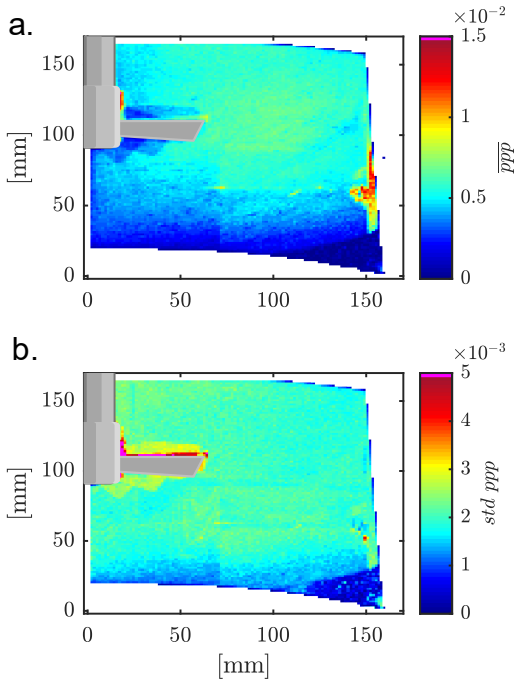

Figure 4.19. Distributions of (a) time-averaged and (b) standard deviation of *particle per pixel* (ppp) for 1,000 velocity fields.

The number of valid vectors can interfere in the convergence of the measurements and, consequently, in the calculation of the time-averaged and the turbulent flow parameters. This interference can be evaluated by analyzing the time-averaged velocity $|\overline{U}|$ fields and the turbulent kinetic energy (TKE) fields, after applying either the PPR-based or else the MI-based corrections for different SNRL values and a final interrogation window, IWf =10 pixels (0.42 mm), as presented in Figure 4.20 and Figure *4.21*. The isotropy condition was used to calculate the TKE (Equation 4.11), where u' and v' are the fluctuations of the horizontal and vertical velocity components, respectively. By applying the Helland spectrum theory, Saarenrinne et al. (2001) reported that it is possible to obtain a 95% accuracy in the TKE estimation when the size of the final interrogation window is approximately 20 times the length of the Kolmogorov scale, η. Furthermore, the accuracy of TKE is approximately 65% when IWf $\approx 90\eta$. The Kolmogorov scale can be determined by Equation 4.12, where $\boldsymbol{\nu}$ is the kinematic fluid viscosity and $\boldsymbol{\varepsilon}$ is the energy dissipation rate. According to Liu et al. (2016), it is possible to determine ε using Equation 4.13 by assuming the uniform rate distribution in the tank, where P represents the power and V the volume of the tank. The tank power was obtained through the experimental curve shown in Figure 4.22 as $P \approx 68.5W$. In this work, $\eta = 0.0293\ mm$, IWf = 0.42 mm and IWf$/\eta$ = 14.48, which represents an accuracy greater than 96% on the estimation of TKE.

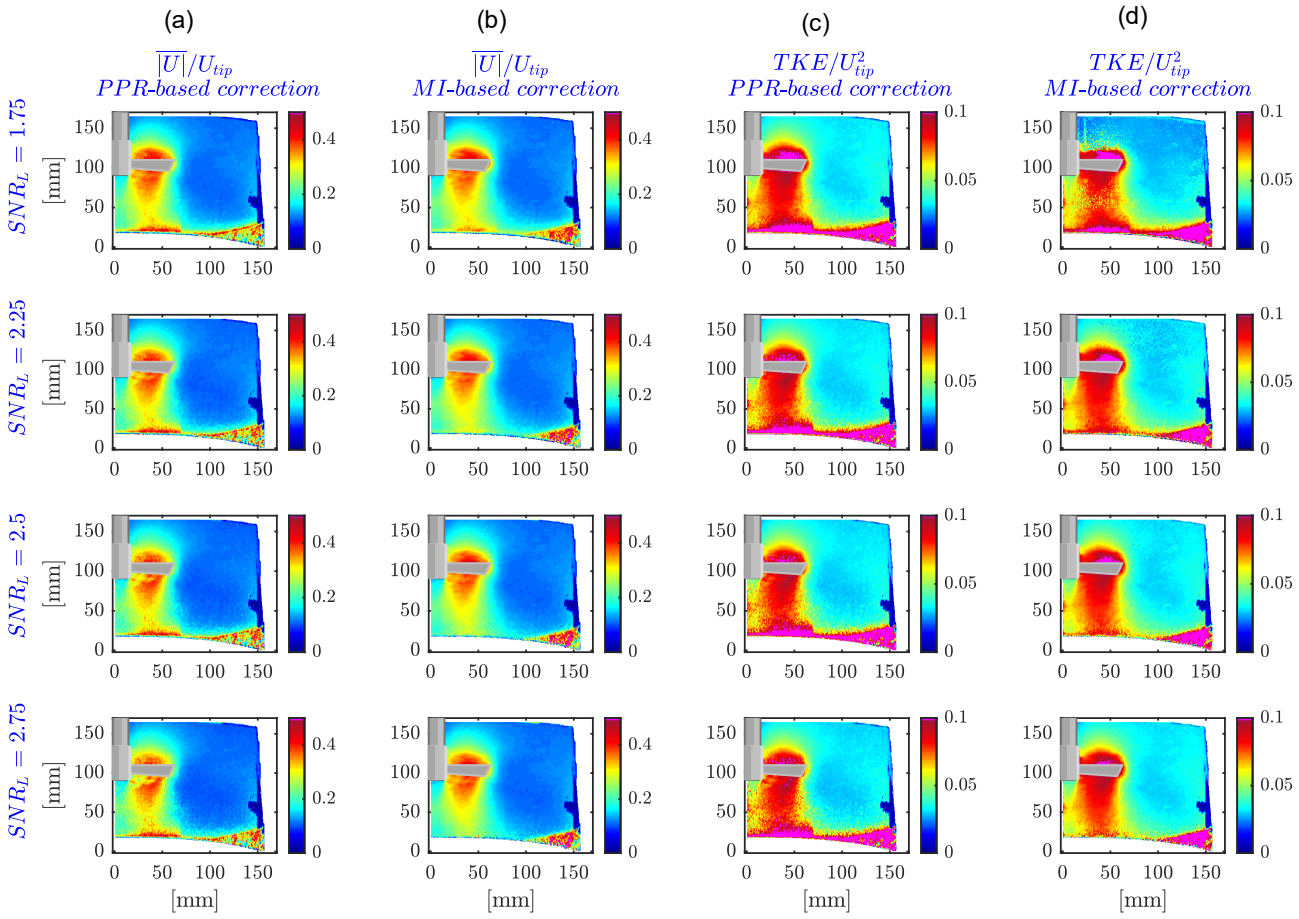

Figure 4.20. (a-b) Time-averaged velocity and (c-d) turbulent kinetic energy (TKE) normalized fields after the application of the PPR-based and the MI-based correction for different values of SNR_L and IW_f =10 pixels (0.42 mm).

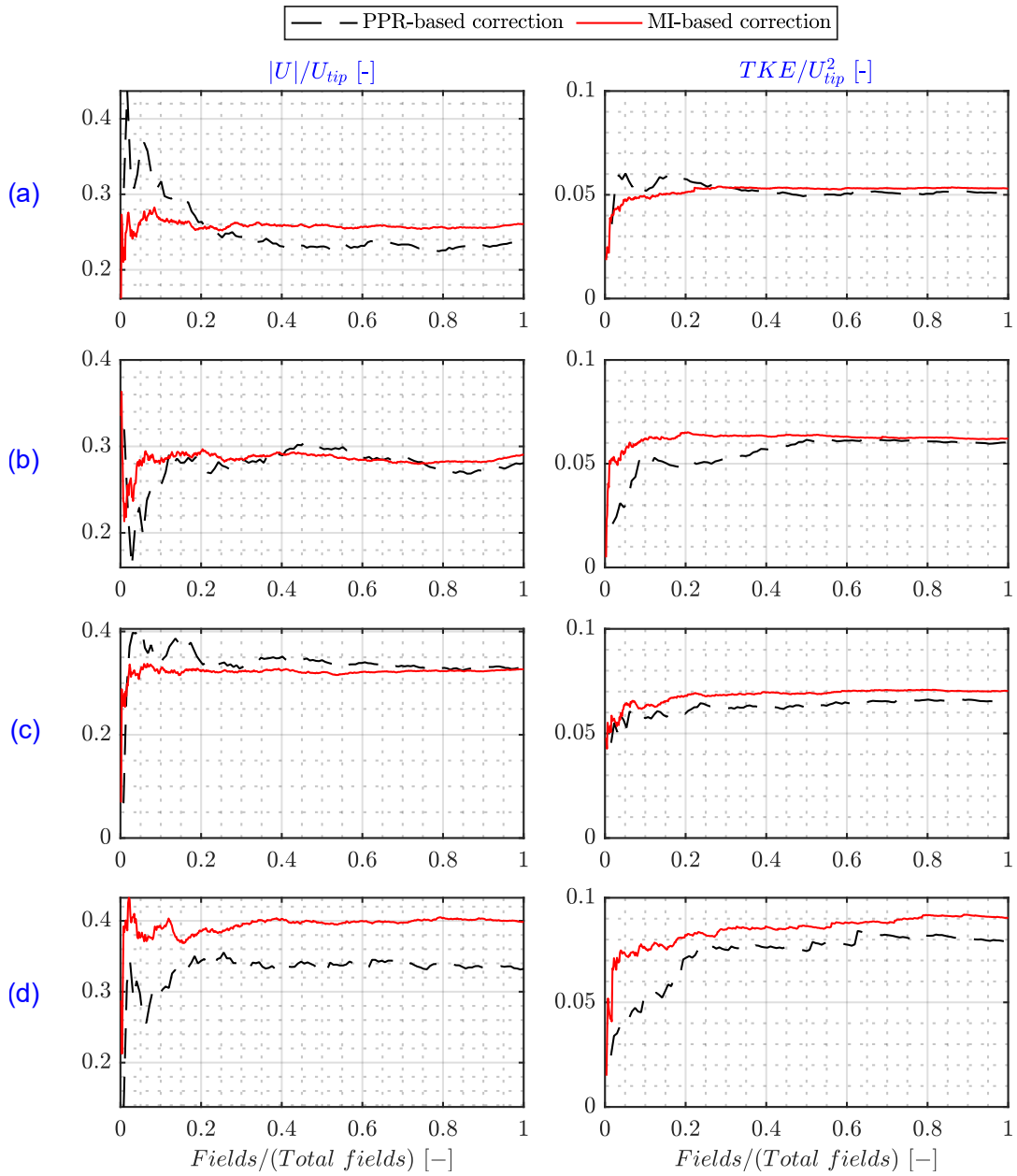

Figure 4.21. Evolution of normalized velocity and TKE with the number of fields after the application of the PPR-based and MI-based correction for SNR_L =2.75 at x = 50 mm and (a) y = 50, (b) 75, (c) 90, and (d) 100 mm.

$$TKE = \frac{3}{4}(rms\ u' + rms\ v')$$ Equation 4.11

$$\eta = \left(\frac{v^3}{\varepsilon}\right)^{1/4}$$ Equation 4.12

$$\varepsilon = \bar{\varepsilon}_T = \frac{P}{\rho V} \qquad \text{Equation 4.13}$$

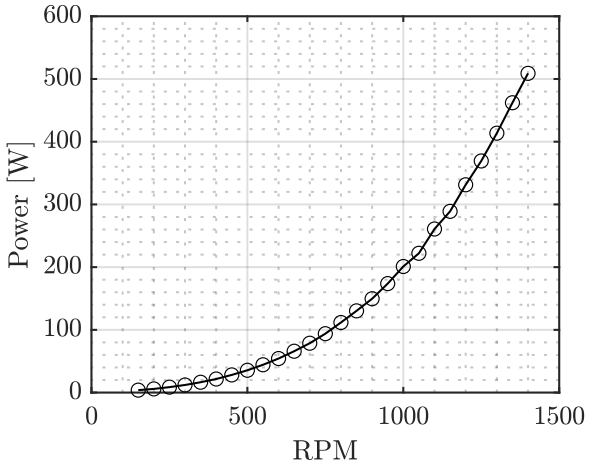

Figure 4.22. Experimental curve of tank power by RPM.

There were practically no differences between the PPR-based and MI-based corrections on the time-averaged velocity, $|\bar{U}|$, except near the bottom edge of the fields and in the region close to the impeller, as shown in Figure 4.20. However, as the value of SNRL increases, the effect of the data loss in the TKE fields is clearly seen in the region below the impeller for the PPR-based correction. This can be easily seen in Figure 4.21d, where the $\overline{|U|}/U_{tip}$ and TKE/U_{tip}^2 values for the two correction approaches were different. The results after applying the MI-based correction converged more easily than for the PPR-based correction in Figure 4.22. Analysis of the statistical convergence of the second moment of u, $\overline{u'u'}$, and v, $\overline{v'v'}$, are presented in Figure 4.23. The convergence envelope based on 95% reliability margin is described in detail by Benedict and Gould (1996). For the MI-based correction, the number of valid fields is adequate and there is no sampling error. However, for the PPR-based correction, there was no statistical convergence in the cases presented in Figure 4.23a and Figure 4.23b. This can be attributed to the data loss or to the remaining noise, which can also be seen in Figure 4.18.

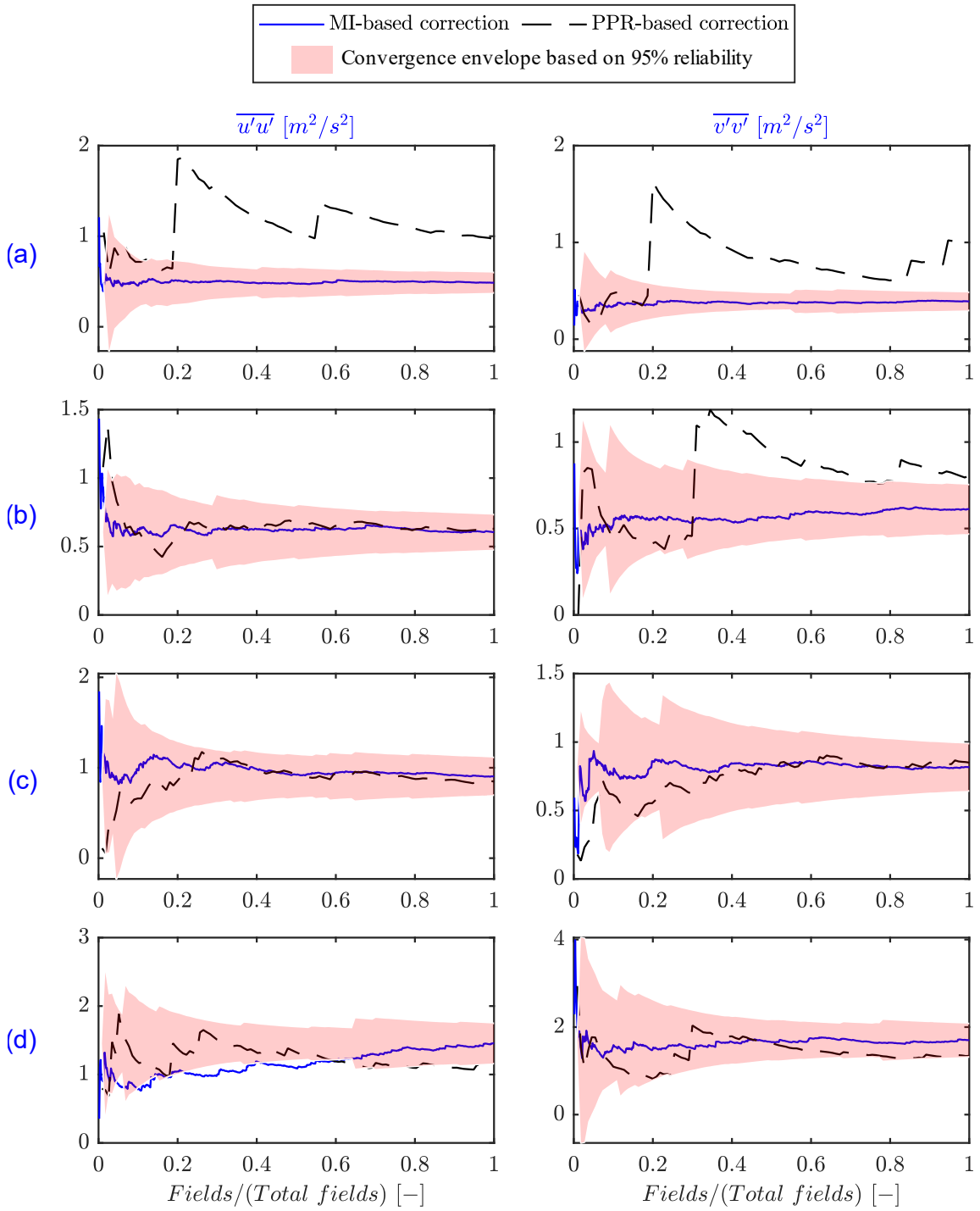

Figure 4.23. Analysis of the statistical convergence of the second moment of u, $\overline{u'u'}$, and v, $\overline{v'v'}$, after the application of the PPR-based and MI-based correction for SNR_L =2.75 at x = 50 mm and (a) y = 50, (b) 75, (c) 90, and (d) 100 mm.

Figure 4.24 presents the time-averaged velocity field obtained by Silva (2020) through numerical simulation under the same experimental conditions of this work. Silva (2020) used four different RANS based turbulence models (Standard k-ε, RNG k-ε,

Realizable k-ε and k-ω SST) and OpenFOAM to obtain the simulated time-averaged velocity field. The values for the PPR-based correction are lower than those presented by Silva (2020) in the region close to the impeller (Figure 4.21d). The MI-based correction presents more reliable results especially for higher values of SNR limits. Although the time-average field presented by Silva (2020) has experimental coherence, the results obtained by applying the four different RANS based turbulence models underestimated the TKE values. The values of TKE obtained in this work are consistent and have the same order of magnitude with the results presented by Guida et al. (2010), who evaluated the influence of the azimuthal position of PIV measurements in a turbulent stirred tank flow (Re = 40000) using a six-blade PBT impeller .

The deterioration of the time-averaged velocity and the TKE fields caused by the PPR-based correction can be resolved by increasing the number of recorded images. However, this can increase the acquisition time and make the laser light pulse in an unstable manner, decreasing the quality of the PIV images. After applying the MI-based correction, the outliers were treated with a minimum of data loss, showing a better spatial coherence with the TKE neighborhood without compromising the flow structure. According to the PIV experiments conducted by Kotek et al. (2017), who evaluated the flow in a stirred tank, the velocity profiles demonstrated the influence of the spatial resolution on the vortexes. Large interrogation windows are more favorable to omit turbulent fluctuations while small windows have higher local velocities and smaller turbulent eddies. In addition, the increase in the number of the velocity vectors is more likely to improve TKE (Liu et at., 2016). On the other hand, the increment in the spatial resolution must always be accompanied by noise analysis and field correction to avoid data loss. In this criterion, the results presented show that the MI-based correction can be a valuable tool for the treatment of noise.

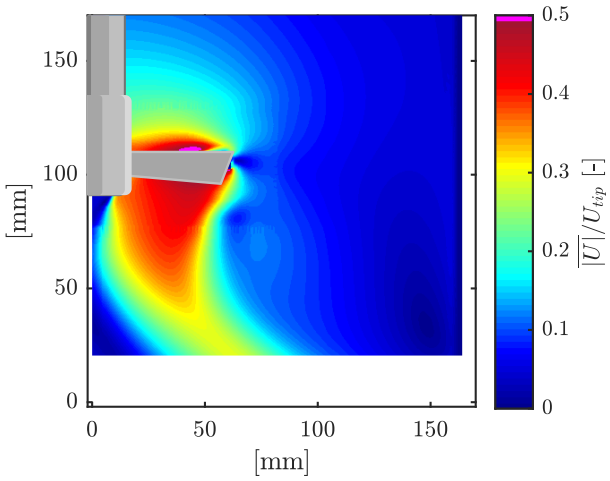

Figure 4.24. Time-averaged velocity field obtained by Silva (2020) through numerical simulation under the same experimental conditions of this work.

4. CONCLUSION

A new field correction for PIV measurements based on mutual information was developed, applied and had its effectiveness verified for the PIV data measured in 50 liters stirred tank. Results indicate that the performance and the identification and the elimination of noisy values of the proposed field correction was better than the already known approaches based on the Median Absolute Deviation (MAD) and the Primary Peak Ratio (PPR). By analyzing the measurements with high spatial resolutions, the correction based on mutual information eliminated more outliers and, at the same time, preserved the averaged velocity and the turbulent kinetic energy fields. The correction based on the PPR thresholding and MAD filtering did not identify the major part of the false vectors. Further, the correction based on the PPR deteriorated the velocity fields by reducing the number of valid vectors and increasing noise, especially for higher SNR thresholds. Therefore, the results presented show that the proposed methodology can be a valuable tool for the correction of noisy fields in measurements with high spatial resolution.

5. ACKNOWLEDGEMENTS

The authors would like to express their gratitude to Petrobras S/A – Brazil (Grant No. 2017/00376-1), to CNPQ (nº 168390/2018-3 and 134445/2019-8) and to CAPES (nº 33003017034P8) for the financial support provided. The authors would also like to thank the PIVbr group (www.piv.eng.br) for all their collaboration.

6. REFERENCES

Adrian, L., Adrian, R. J., & Westerweel, J., 2011. *Particle image velocimetry* (No. 30). Cambridge university press.

Alonzo-Garcia, A., Mendoza-Escamilla, V. X., Martinez-Delgadillo, S. A., Gonzalez-Neria, I., Del C Gutiérrez-Torres, C., & Jiménez-Bernal, J. A., 2019. On the performance of different rans-based models to describe the turbulent flow in an agitated vessel using non-structured grids and PIV validation. *Brazilian Journal of Chemical Engineering*, 36(1), 361–382. doi.org/10.1590/0104-6632.20190361s20180091

Baldi, S., Yianneskis, M., 2004. On the quantification of energy dissipation in the impeller stream of a stirred vessel from fluctuating velocity gradient measurements. *Chemical Engineering Science*, [S.L.], v. 59, n. 13, p. 2659-2671. Elsevier BV. dx.doi.org/10.1016/j.ces.2004.03.021.

Benedict, L. H.; Gould, R. D., 1996. Towards better uncertainty estimates for turbulence statistics. Experiments in Fluids. 22. 129 -136

Charonko, J. J., & Vlachos, P. P., 2013. Estimation of uncertainty bounds for individual particle image velocimetry measurements from cross-correlation peak ratio. *Measurement Science and Technology*, 24(6), 065301.

Dabiri, D., 2006. "Cross-correlation digital particle image velocimetry—a review." Turbul. ABCM Curitiba, p. 155-199.

Delafosse, A., Collignon, M. L., Crine, M., & Toye, D., 2011. Estimation of the turbulent kinetic energy dissipation rate from 2D-PIV measurements in a vessel stirred by an axial Mixel TTP impeller. *Chemical Engineering Science*, 66(8), 1728-1737. doi.org/10.1016/j.ces.2011.01.011

Eckstein, A., & Vlachos, P. P., 2009. Digital particle image velocimetry (DPIV) robust phase correlation. *Measurement Science and Technology*, 20(5), 055401. doi.org/10.1088/0957-0233/20/5/055401

Elsinga, G. E.; van Oudheusden, B. W.; Scarano, F., 2005. Challenges in particle imaging through compressible flows. II International Workshop on the Application of PIV in Compressible Flows. 6-8 June. Delft, The Netherlands.

Escudié, R., & Liné, A., 2003. Experimental analysis of hydrodynamics in a radially agitated tank. *AIChE journal*, 49(3), 585-603. https://doi.org/10.1002/aic.690490306

Foucaut J. M., Carlier J. e Stanislas M., 2000. Post-processing of PIV records to allow derivative computation. *10th Int. Symp. on Appl. of Laser Tech. to Fluid Mech.* Lisbon.

Gabriele, A.; Nienow, A.w.; Simmons, M.j.h., 2009. Use of angle resolved PIV to estimate local specific energy dissipation rates for up- and down-pumping pitched blade agitators in a stirred tank. *Chemical Engineering Science*, [s.l.], v. 64, n. 1, p.126-143. Elsevier BV. dx.doi.org/10.1016/j.ces.2008.09.018.

Guida, A., Nienow, A. W., & Barigou, M., 2010. The effects of the azimuthal position of the measurement plane on the flow parameters determined by PIV within a stirred vessel. *Chemical Engineering Science*, 65(8), 2454-2463. doi.org/10.1016/j.ces.2009.12.012

Hain, R., Kähler, C.J., 2007. Fundamentals of multiframe particle image velocimetry (PIV). Exp. Fluids 42, 575–587. doi:10.1007/s00348-007-0266-6.

Hu, Y., Wu, J., Poncin, S., Cao, Z., Li, Z., & Li, H. Z., 2018. Flow field investigation of high solid anaerobic digestion by Particle Image Velocimetry (PIV). *Science of The Total Environment*, 626, 592-602. dx.doi.org/10.1016/j.scitotenv.2018.01.111.

Huber, P. J., 1981. *Robust statistics*. New York: John Wiley

Kähler, C. J., Astarita, T., Vlachos, P. P., Sakakibara, J., Hain, R., Discetti, S., ... & Cierpka, C., 2016. Main results of the 4th International PIV Challenge. Experiments in Fluids, 57(6), 97. doi.org/10.1007/s00348-016-2173-1

Kähler, C.J., Kompenhans, J., 2000. Fundamentals of multiple plane stereo particle image velocimetry. Exp. Fluids 29, S070–S077. doi:10.1007/s003480070009

Keane, R. D., & Adrian, R. J., 1990. Optimization of particle image velocimeters. I. Double pulsed systems. *Measurement science and technology*, 1(11), 1202. doi.org/10.1088/0957-0233/1/11/013

Keane, R. D., & Adrian, R. J., 1992. Theory of cross-correlation analysis of PIV images. *Applied scientific research*, 49(3), 191-215. doi.org/10.1007/978-94-011-2690-8_1

Khan, F. R., Rielly, C. D., & Hargrave, G. K., 2004. A Multi-Block Approach to Obtain Angle-Resolved PIV Measurements of the Mean Flow and Turbulence Fields in a Stirred Vessel. *Chemical Engineering & Technology: Industrial Chemistry-Plant Equipment-Process Engineering-Biotechnology*, 27(3), 264-269. doi.org/10.1002/ceat.200401998

Kim, B. J., & Sung, H. J., 2006. A further assessment of interpolation schemes for window deformation in PIV. *Experiments in fluids*, 41(3), 499-511. doi.org/10.1007/s00348-006-0177-y

Kotek, M., Jasikova, D., Kysela, B., Sulc, R., & Kopecky, V., 2017. PIV study of flow field in Rushton turbine stirred vessel influenced by spatial resolution. *International Journal of Theoretical and Applied Mechanics*, 2.

Kumar, B. V., & Hassebrook, L., 1990. Performance measures for correlation filters. *Applied optics*, 29(20), 2997-3006. doi.org/10.1364/AO.29.002997

Liu, N., Wang, W., Han, J., Zhang, M., Angeli, P., Wu, C., & Gong, J., 2016. A PIV investigation of the effect of disperse phase fraction on the turbulence characteristics of liquid–liquid mixing in a stirred tank. *Chemical Engineering Science*, 152, 528-546. doi.org/10.1016/j.ces.2016.06.040

Martins, F. J., Foucaut, J. M., Thomas, L., Azevedo, L. F., & Stanislas, M., 2015. Volume reconstruction optimization for tomo-PIV algorithms applied to experimental data. *Measurement Science and Technology*, 26(8), 085202. doi.org/10.1088/0957-0233/26/8/085202

Miller, J., 1991. “Reaction time analysis with outlier exclusion: Bias varies with sample size”. *The Quarterly Journal of Experimental Psychology*, 43(4), 907–912. doi:10.1080/14640749108400962.

Mosteller, F., & Tukey, J. W., 1977. *Data analysis and regression: a second course in statistics*.

Nogueira, J., Lecuona, A., & Rodriguez, P. A., 1999. Local field correction PIV: on the increase of accuracy of digital PIV systems. *Experiments in fluids*, 27(2), 107-116. doi.org/10.1007/s003480050335

Nogueira, J., Lecuona, A., & Rodriguez, P. A., 2001. Local field correction PIV, implemented by means of simple algorithms, and multigrid versions. *Measurement Science and Technology*, 12(11), 1911. doi.org/10.1088/0957-0233/12/11/321

Pereira, F., Ciarravano, A., Romano, G.P., Di Felice, F., 2004. Adaptive multi-frame PIV, in: 12th International Symposium on Applications of Laser Techniques to Fluid Mechanics. Portugal.

Raffel, M., Willert, C., and Kompenhans, J., 2018. *Particle image velocimetry: a practical guide*. Berlin: Springer. doi.org/10.1007/978-3-540-72308-0

Rottier, C; Godard, G; Corbin, F; Boukhalfa, A. M.; Honoré, D., 2010. An endoscopic particle image velocimetry system for high-temperature furnaces. Meas. Sci. Technol. 21 115404 (9pp)

Roy, S., Acharya, S., & Cloeter, M. D., 2010. Flow structure and the effect of macro-instabilities in a pitched-blade stirred tank. *Chemical Engineering Science*, 65(10), 3009-3024. doi.org/10.1016/j.ces.2010.01.025

Saarenrinne, P., Piirto, M., & Eloranta, H., 2001. Experiences of turbulence measurement with PIV. *Measurement Science and Technology*, 12(11), 1904. doi.org/10.1088/0957-0233/12/11/320

Sachs, L., 1984. Applied statistics: a handbook of techniques. Springer Science & Business Media.

Scarano, F., 2001. Iterative image deformation methods in PIV. *Measurement science and technology*, 13(1), R1. doi.org/10.1088/0957-0233/13/1/201

Scharnowski, S., Sciacchitano, A., & Kähler, C. J., 2019. On the universality of Keane & Adrian's valid detection probability in PIV. *Measurement Science and Technology*, 30(3), 035203. doi.org/10.1088/1361-6501/aafe9d

Sciacchitano, A., & Scarano, F., 2014. Elimination of PIV light reflections via a temporal high pass filter. *Measurement Science and Technology*, 25(8), 084009. doi.org/10.1088/0957-0233/25/8/084009

Sciacchitano, A., Wieneke, B., & Scarano, F., 2013. PIV uncertainty quantification by image matching. *Measurement Science and Technology*, 24(4), 045302. doi.org/10.1088/0957-0233/24/4/045302

Sciacchitano, A.; Scarano, F.; Wieneke, B., 2012. Multi-frame pyramid correlation for time-resolved PIV. Exp Fluids. 53:1087–1105.

Shavit, U., Lowe, R.J., Steinbuck, J. V., 2007. Intensity Capping: a simple method to improve cross-correlation PIV results. Exp. Fluids 42, 225–240. doi:10.1007/s00348-006-0233-7.

Silva, P. T. D., 2020. Estudo do escoamento em tanque agitado por PIV e CFD. Master's in chemical engineering, University of Campinas. http://repositorio.unicamp.br/jspui/handle/REPOSIP/359434

Soloff, S. M.; Adrian, R. J.; Liu Z-C., 1997. Distortion compensation for generalized stereoscopic particle image velocimetry. Meas. Sci. Technol. 8. 1441–1454.

Svensson, F. J., & Rasmuson, A., 2006. PIV measurements in a liquid–liquid system at volume percentages up to 10% dispersed phase. *Experiments in fluids*, 41(6), 917-931. dx.doi.org/10.1007/s00348-006-0211-0.

Unadkat, H., 2010. *Investigation of turbulence modulation in solid-liquid suspensions using FPIV and micromixing experiments* (Doctoral dissertation, Loughborough University).

Unadkat, H., Rielly, C. D., & Nagy, Z. K., 2011. PIV study of the flow field generated by a sawtooth impeller. *Chemical engineering science*, 66(21), 5374-5387. dx.doi.org/10.1016/j.ces.2011.07.046.

Westerweel, J., & Scarano, F, 2005. Universal outlier detection for PIV data. *Experiments in fluids*, 39(6), 1096-1100. doi.org/10.1007/s00348-005-0016-6

Wieneke, B. F. A., 2017. PIV uncertainty quantification and beyond (Doctoral dissertation, Delft University of Technology). doi.org/10.4233/uuid:4ca8c0b8-0835-47c3-8523-12fc356768f3

Wieneke, B., 2015. PIV uncertainty quantification from correlation statistics. *Measurement Science and Technology*, 26(7), 074002. doi.org/10.1088/0957-0233/26/7/074002

Xue, Z., Charonko, J. J., & Vlachos, P. P., 2014. Particle image velocimetry correlation signal-to-noise ratio metrics and measurement uncertainty quantification. *Measurement Science and Technology*, 25(11), 115301. doi.org/10.1088/0957-0233/25/11/115301

Xue, Z., Charonko, J. J., & Vlachos, P. P., 2015. Particle image pattern mutual information and uncertainty estimation for particle image velocimetry. *Measurement Science and Technology*, 26(7), 074001. doi.org/10.1088/0957-0233/26/7/074001

Zhang, M.; Xu, M.; Hung, D. L. S., 2014. Simultaneous two-phase flow measurement of spray mixing process by means of high-speed two-color PIV. Meas. Sci. Technol. 25. 095204 (9pp)

CHAPTER 5

FINAL CONSIDERATIONS

This chapter presents the final conclusions regarding the general and specific objectives outlined in this Dissertation. Finally, suggestions for future work are highlighted with a view to the continuity of the theme of the Dissertation.

5.1. CONCLUSION

Works applying PIV technique for the study of the flow in stirred tanks have been very relevant to understand the turbulent flow in these systems and to optimize the efficiency of the mixing processes. Nevertheless, PIV measurements are subject to the effects of noise sources, such as laser light reflection, difference in refractive index, tank curvature, among others. As a result, there is a distortion of the field and generation of incorrect data, deteriorating the quality of the measurements. In particular, the development of optimization methods of PIV processing steps has shown to be essential to reduce the effects of noise sources and image distortion. These optimizations allow to increase the quality of PIV measurements and to quantify turbulent parameters with greater accuracy.

Many studies focus on minimizing the effects of noise sources in the physical space; however, these techniques are often not feasible (high cost and limited space). Few works detail the PIV optimization methods in image space, which justifies the central theme of this dissertation. In this context, the study of turbulent water flow in a stirred tank using the PIV technique was proposed to evaluate the performance of different optimization strategies, and the main conclusions found in this work are presented as follows:

- The multicalibration strategy presented promising results, especially for cameras positioned with the smallest angular displacement in relation to the object plane.
- The multicalibration method showed better adjustment of the mapping function in the region close to the wall comparing to the usual methods.

- The commonly used calibration method proposed by Sollof et al. (1997) and the multicalibration proposed in this study did not present significant differences in the estimation of TKE. Consequently, both were considered adequate in the analysis of the flow in stirred tanks similarly to the one used in this work.
- The results of the TKE measurements after field correction using the mutual information (MI) technique showed better spatial coherence with its neighborhood without compromising the flow structure.
- The MI correction method showed lower noise and data loss over time for velocity fields than the standard PPR technique for the same SNR values.
- The field correction based on mutual information eliminated more outliers and, at the same time, preserved the averaged velocity and the turbulent kinetic energy fields than already known approaches (MAD and PPR).
- The proposed methodology based on Mutual Information can be a valuable tool for the correction of noisy fields in measurements with high spatial resolution.

5.2. SUGGESTIONS FOR FUTURE WORK

Based on the conclusions obtained in this study, some suggestions to follow up this Dissertation are proposed:

- Application of the proposed optimization methods in different types of impellers and tank sizes.
- More detailed investigation concerning the error and uncertainty associated with the PIV technique (2C-2D).
- Application of post-processing methods for field correction in tanks stirred with non-Newtonian fluids.
- Study the use of PIV technique and optimization to estimate TKE and EDR from velocity fields obtained with Stereo-PIV (3C-2D) measurements using different operating parameters with different Reynolds numbers and impeller configurations.
- Development of new spatial and temporal filters for identification of false vectors and field correction for time-resolved measurements.

REFERENCES

Adatrao, S. & Sciacchitano, A., 2019. Elimination of unsteady background reflections in PIV images by anisotropic diffusion. *Measurement Science and Technology*, 30(3), p. 035204.

Adrian, R. J., 1997. Dynamic ranges of velocity and spatial resolution of particle image velocimetry. *Measurement Science and Technology*, 8(12), p. 1393.

Adrian, R. J. & Westerweel, J., 2011. *Particple Image Velocimetry*. New York: Cambridge University Press.

Alberini, F., Liu, L., Stitt, E. H. & Simmons, M. J. H., 2017. Comparison between 3-D-PTV and 2-D-PIV for determination of hydrodynamics of complex fluids in a stirred vessel. *Chemical Engineering Science*, Volume 171, pp. 189-203.

Alonzo-Garcia, A. et al., 2019. On the performance of different rans based models to describe the turbulent flow in an agitated vessel using non-structured grids and PIV validation. *Brazilian Journal of Chemical Engineering*, 36(1), pp. 361-382.

Amaral, R. d. L., 2017. *Quality analysis of 2D-2C and 2D-3C F-PIV measurements of the liquid phase velocity in a bubble column.* Campinas: Thesis (PhD degree) – Universidade Estadual de Campinas.

Aubin, J. et al., 2004. PIV measurements of flow in an aerated tank stirred by a down-and an up-pumping axial flow impeller. *Experimental Thermal and Fluid Science*, 28(5), pp. 447-456.

Bakker, A., Myers, K. J., Ward, R. W. & Lee, C. K., 1996. The laminar and turbulent flow pattern of a pitched blade turbine. *Transactions of IChemE*, Volume 74, pp. 485-491.

Baldi, S. & Yianneskis, M., 2004. On the quantification of energy dissipation in the impeller stream of a stirred vessel from fluctuating velocity gradient measurements. *Chemical Engineering Science*, 07, 59(13), pp. 2659-2671.

Charonko, J. J. & Vlachos, P. P., 2013. Estimation of uncertainty bounds for individual particle image velocimetry measurements from cross-correlation peak ratio. *Measurement Science and Technology*, 24(6), p. 065301.

Chung, K. H. K., Barigou, M. & Simmons, M. J. H., 2007. Reconstruction of 3-D Flow Field Inside Miniature Stirred Vessels Using a 2-D PIV Technique. *Chemical Engineering Research and Design*, 85(5), pp. 560-567.

Chung, K. H., Simmons, M. J. & Barigou, M., 2009. Angle-Resolved Particle Image Velocimetry Measurements of Flow and Turbulence Fields in Small-Scale Stirred Vessels of Different Mixer Configurations. *ndustrial & Engineering Chemistry Research*, 48(2), pp. 1008-1018.

Cressall, R. & Smith, B. L., 2006. *Correlated Bias Uncertainty in PIV Data due to Interrogation Window Overlap.* Washington, DC, USA, Fluids Engineering Division Summer Meeting.

Cutter, L. A., 1966. Flow and turbulence in a stirred tank. *AIChE Journal*, 12(1), pp. 35-45.

Dabiri, D., 2006. *Cross-correlation digital particle image velocimetry-a review.* s.l., s.n.

de Lamotte, A. et al., 2017. Investigating the effects of hydrodynamics and mixing on mass transfer through the free-surface in stirred tank bioreactors. *Chemical Engineering Science*, 11, 172(23), pp. 125-142.

Delafosse, A., Collignon, M. L., Crine, M. & Toye, D., 2011. Estimation of the turbulent kinetic energy dissipation rate from 2D-PIV measurements in a vessel stirred by an axial Mixel TTP impeller. *Chemical Engineering Science*, 66(8), pp. 1728-1737.

Depardon, S. et al., 2005. Skin friction pattern analysis using near-wall PIV. *Experiments in Fluids*, 39(5), pp. 805-818.

Driss, Z. et al., 2014. Measurements to Study the Effect of the Reynolds Number on the Hydrodynamic Structure in a Baffled Vessel Stirred by a Rushton Turbine. *American Journal of Energy Research*, 2(3), pp. 67-73.

Duncan, J., Dabiri, D., Hove, J. & Gharib, M., 2010. Universal outlier detection for particle image velocimetry (PIV) and particle tracking velocimetry (PTV) data. *Measurement Science and Technology*, 21(5), p. 057002.

Elsinga, G. E., Van Oudheusden, B. W. & Scarano, F., 2005a. Evaluation of aero-optical distortion effects in PIV. *Experiments in Fluids*, 39(2), p. 246–256.

Elsinga, G. E., van Oudheusden, B. W. & Scarano, F., 2005b. Modeling of particle imaging through shock waves. *Optical Modeling and Performance Predictions II*, Volume 5867.

Elsinga, G. E., van Oudheusden, B. W. & Scarano, F., 2005c. The effect of particle image blur on the correlation map and velocity measurement in PIV. *In: Optical Diagnostics. International Society for Optics and Photonics*, Volume 5880, p. 588010.

Escudié, R. & Liné, A., 2003. Experimental analysis of hydrodynamics in a radially agitated tank. *AIChE journal*, 49(3), pp. 585-603.

Fang, J., Ling, X. & Sang, Z.-F., 2011. "Experimental and numerical studies of the flow field in a stirred tank equipped with multiple side-entering agitators. *Chemical engineering & technology*, 34(10), pp. 1619-1629.

Ferguson, J. & Kemblowski, Z., 1991. *Applied fluid rheology.* London: Elsevier.

Foucaut, J. M., Carlier, J. & Stanislas, M., 2000. *Post-processing of PIV records to allow derivative computation.* Lisbon, Portugal, s.n.

Fritsch, F. N. & Carlson, R. E., 1980. Monotone piecewise cubic interpolation. *SIAM Journal on Numerical Analysis*, 17(2), pp. 238-246.

Gabriele, A., Nienow, A. W. & Simmons, M. J. H., 2009. Use of angle resolved PIV to estimate local specific energy dissipation rates for up-and down-pumping pitched blade agitators in a stirred tank. *Chemical Engineering Science*, 64(1), pp. 126-143.

Gómez, C., Bennington, C. P. J. & Taghipour, F., 2010. Investigation of the flow field in a rectangular vessel equipped with a side-entering agitator.. *Journal of Fluids Engineering*, 132(5).

Guida, A., Nienow, A. W. & Barigou, M., 2010. The effects of the azimuthal position of the measurement plane on the flow parameters determined by PIV within a stirred vessel. *Chemical Engineering Science*, 65(8), pp. 2454-2463.

Guida, A., Nienow, A. W. & Barigou, M., 2010. The effects of the azimuthal position of the measurement plane on the flow parameters determined by PIV within a stirred vessel.. *Chemical Engineering Science*, 65(8), pp. 2454-2463.

Gui, L., Longo, J. & Stern, F., 2001. Towing tank PIV measurement system, data and uncertainty assessment for DTMB Model 5512. *Experiments in Fluids*, 31(3), pp. 336-346.

Hain, R. & Kähler, C. J., 2007. Fundamentals of multiframe particle image velocimetry (PIV). *Experiments in fluids*, 42(3), pp. 575-587.

Hart, D. P., 2000. PIV error correction. *Experiments in fluids,*, 29(1), pp. 13-22.

Honkanen, M. & Nobach, H., 2005. Background extraction from double-frame PIV images. *Experiments in fluids*, 38(3), pp. 348-362.

Howell, J. A., 2018. *Distribution of Particle Image Velocimetry (PIV) Errors in a Planar Jet.* s.l.:s.n.

Huang, H. T., Fiedler, H. E. & Wang, J. J., 1993. Limitation and improvement of PIV, Part I: Limitation of conventional techniques due to deformation of particle image patterns. *Experiments in fluids*, 15(3), pp. 168-174.

Huber, P. J., 2004. Scale Estimates. Em: *Robust Statistics.* 1 ed. Hoboken: John Wiley and Sons, Inc., p. 107–126.

Hu, Y. et al., 2018. Flow field investigation of high solid anaerobic digestion by Particle Image Velocimetry (PIV). *Science of The Total Environment*, Volume 626, pp. 592-602.

Jaszczur, M. & Młynarczykowska, A., 2020. A general review of the current development of mechanically agitated vessels. *Processes*, 8(8), p. 982.

Kähler, C. J., 2009. High resolution measurements by long-range. *Proceedings of VKI Lecture Series on Recent Advances in Particle Image Velocimetry*, pp. 26-30.

Kähler, C. J., Scholz, U. & Ortmanns, J., 2006. Wall-shear-stress and near-wall turbulence measurements up to single pixel resolution by means of long-distance micro-PIV. *Experiments in fluids*, 41(2), pp. 327-341.

Keane, R. D. & Adrian, R. J., 1990. Optimization of particle image velocimeters. I. Double pulsed systems. *Measurement science and technology*, 1(11), p. 1202.

Keane, R. D. & Adrian, R. J., 1992. Theory of cross-correlation analysis of PIV images. *Applied scientific research*, 49(3), pp. 191-215.

Keane, R. D., Adrian, R. & Zhang, Y., 1995. Super-resolution particle imaging velocimetry. *Measurement Science and Technology*, 6(6), p. 754.

Khan, F. R., Rielly, C. D. & Brown, D. A. R., 2006. Angle-resolved stereo-PIV measurements close to a down-pumping pitched-blade turbine. *Chemical Engineering Science*, 05, 61(9), pp. 2799-2806.

Kilander, J. & Rasmuson, A., 2005. Energy dissipation and macro instabilities in a stirred square tank investigated using an LE PIV approach and LDA measurements. *Chemical Engineering Science*, 60(24), pp. 6844-6856.

Kim, B. J. & Sung, H. J., 2006. A further assessment of interpolation schemes for window deformation in PIV. *Experiments in fluids*, 41(3), pp. 499-511.

Kotek, M. et al., 2017. PIV study of flow field in Rushton turbine stirred vessel influenced by spatial resolution.. *International Journal of Theoretical and Applied Mechanics*, Volume 2, pp. 79-84.

Kresta, S. M. & Wood, P. E., 1991. Prediction of the three-dimensional turbulent flow in stirred tanks. *AIChE journal*, 03, 37(3), pp. 448-460.

Kumar, B. V. & Hassebrook, L., 1990. Performance measures for correlation filters. *Applied optics*, 29(20), pp. 2997-3006.

Kumaresan, T. & Joshi, J. B., 2006. Effect of impeller design on the flow pattern and mixing in stirred tanks.. *Chemical engineering journal*, 115(3), pp. 173-193.

Kumaresan, T., Nere, N. K. & Joshi, J. B., 2005. Effect of internals on the flow pattern and mixing in stirred tanks. *Industrial & engineering chemistry research*, 44(26), pp. 9951-9961.

La Vision, 2017. *FlowMaster Product-Manual for DaVis 8.4.* s.l.:s.n.

Lavoie, P. et al., 2007. Spatial resolution of PIV for the measurement of turbulence. *Experiments in Fluids*, 43(1), pp. 39-51..

Li, G. et al., 2018. Particle image velocimetry experiments and direct numerical simulations of solids suspension in transitional stirred tank flow. *Chemical Engineering Science*, Volume 191, pp. 288-299.

Liu, N. et al., 2016. A PIV investigation of the effect of disperse phase fraction on the turbulence characteristics of liquid–liquid mixing in a stirred tank. *Chemical Engineering Science*, Volume 152, pp. 528-546.

Liu, Z., Zheng, Y., Jia, L. & Zhang, Q., 2007. An experimental method of examining three-dimensional swirling flows in gas cyclones by 2D-PIV. *Chemical Engineering Journal*, 133(1-3), pp. 247-256.

Li, Z., Bao, Y. & Gao, Z., 2011. PIV experiments and large eddy simulations of single-loop flow fields in Rushton turbine stirred tanks. *Chemical Engineering Science*, 66(6), pp. 1219-1231.

Li, Z., Song, G., Bao, Y. & Gao, Z., 2013. Stereo-PIV experiments and large eddy simulations of flow fields in stirred tanks with Rushton and curved-Blade turbines. *AIChE Journal*, 59(10), pp. 3986-4003.

Masullo, A. & Theunissen, R., 2016. Adaptive vector validation in image velocimetry to minimise the influence of outlier clusters. *Experiments in Fluids*, 57(3), p. 33.

Micheletti, M. et al., 2004. On spatial and temporal variations and estimates of energy dissipation in stirred reactors. *Chemical Engineering Research and Design*, 82(9), pp. 1188-1198.

Moura, H. L. d., 2017. *Análise da qualidade de medidas F-PIV e da fluidodinâmica em coluna de bolhas utilizando invariantes caóticos.*. Faculdade de Engenharia Química, Universidade Estadual de Campinas: Thesis (PhD degree).

Nogueira, J., Lecuona, A. & Rodriguez, P. A., 1997. Data validation, false vectors correction and derived magnitudes calculation on PIV data. *Measurement Science and Technology*, 8(12), p. 1493.

Nogueira, J., Lecuona, A. & Rodriguez, P. A., 2001. Local field correction PIV, implemented by means of simple algorithms, and multigrid versions. *Measurement Science and Technology*, 12(11), p. 1911.

Nogueira, J., Lecuona, A. & Rodriguez, P. A., 2005. Limits on the resolution of correlation PIV iterative methods. *Experiments in fluids*, 39(2), pp. 305-313.

Patwardhan, A. W. & Joshi, J. B., 1999. Relation between flow pattern and blending in stirred tanks. *Industrial & engineering chemistry research*, 38(8), pp. 3131-3143.

Perrard, M., Le Sauze, N., Xuereb, C. & Bertrand, J., 2000. *Characterisation of the Turbulence in a Stirred Tank Using Particle Image Velocimetry*. s.l., Elsevier Science, pp. 345-352.

Prasad, A. K., 2000. Stereoscopic particle image velocimetry. *Experiments in Fluids*, 29(2), p. 103–116.

Prasad, A. K. & Jensen, K., 1995. Scheimpflug stereocamera for particle image velocimetry in liquid flows. *Applied Optics*, 34(30), pp. 7092-7099.

Raffel, M. et al., 2018. *Particle image velocimetry: a practical guide.* s.l.:Springer.

Reynolds, W. C. & Hussain, A. K. M. F., 1972. . The mechanics of an organized wave in turbulent shear flow. Part 3. Theoretical models and comparisons with experiments.. *Journal of Fluid Mechanics*, 54(2), pp. 263-288.

Roth, G. I. & Katz, J., 2001. Five techniques for increasing the speed and accuracy of PIV interrogation. *Measurement Science and Technology*, 12(3), p. 238.

Saarenrinne, P., Piirto, M. & & Eloranta, H., 2001. Experiences of turbulence measurement with PIV. *Measurement Science and Technology*, 12(11), p. 1904.

Scarano, F., 2001. Iterative image deformation methods in PIV. *Measurement science and technology*, 13(1).

Scharnowski, S., Sciacchitano, A. & Kähler, C. J., 2019. On the universality of Keane & Adrian's valid detection probability in PIV. *Measurement Science and Technology*, 30(3), p. 035203.

Sciacchitano, A. et al., 2015. Collaborative framework for PIV uncertainty quantification: comparative assessment of methods. *Measurement Science and Technology*, 26(7), p. 074004.

Sciacchitano, A. & Scarano, F., 2014. Elimination of PIV light reflections via a temporal high pass filter. *Measurement Science and Technology*, 25(8).

Sciacchitano, A., Wieneke, B. & Scarano, F., 2013. PIV uncertainty quantification by image matching. *Measurement Science and Technology*, 24(4), p. 045302.

Sharp, K. V. & Adrian, R. J., 2001. PIV Study of small-scale flow structure around a Rushton turbine. *AIChE Journal*, 47(4), pp. 766-778.

Shinneeb, A. M., Bugg, J. D. & Balachandar, R., 2004. Variable threshold outlier identification in PIV data. *Measurement Science and Technology*, 15(9), p. 1722.

Soloff, S. M., Adrian, R. J. & Liu, Z. C., 1997. Distortion compensation for generalized stereoscopic particle image velocimetry. *Measurement Science and Technology*, 8(12), pp. 1441-1454.

Sophia, L. V., 2010. *Análise comparativa das laternativas para simulação CFD de tanque de mistura operando em regime turbulento.* s.l.:Dissertação (Mestrado em Engenharia Mecânica) - Centro Universitário da FEI, São Bernardo do Campo.

Stanislas, M., Okamoto, K., Kähler, C. J. & Westerweel, J., 2005. Main results of the second international PIV challenge. *Experiments in fluids*, 39(2), pp. 170-191.

Stelmach, J., Musoski, R., Kuncewicz, C. & Głogowski, M., 2019. Turbulent Energy dissipation rate and turbulence scales in the blade region of a self-aspirating disk impeller. *J. Appl. Fluid Mech,* 12(3), pp. 715-728.

Story, A., Jaworski, Z., Simmons, M. J. & Nowak, E., 2018. Comparative PIV and LDA studies of Newtonian and non-Newtonian flows in an agitated tank.. *Chemical Papers*, Volume 72, pp. 593-602.

Svensson, F. J. & Rasmuson, A., 2006. PIV measurements in a liquid–liquid system at volume percentages up to 10% dispersed phase. *Experiments in fluids*, 41(6), pp. 917-931.

Tatterson, G. B., 1994. *Scaleup and design of industrial mixing processes.* New York: McGraw Hill.

Tatterson, G. B., 1994. *Scaleup and design of industrial mixing processes.* New York: McGraw-Hill.

Theunissen, R., Scarano, F. & Riethmuller, M. L., 2006. An adaptive sampling and windowing interrogation method in PIV. *Measurement Science and Technology*, 18(1), p. 275.

Timmins, B. H., Wilson, B. W., Smith, B. L. & Vlachos, P. P., 2012. A method for automatic estimation of instantaneous local uncertainty in particle image velocimetry measurements. *Experiments in fluids,*, 53(4), pp. 1133-1147.

Uhl, V. & Gray, J. B., 1966. *Mixing - theory and practive.* New York: Academic Press.

Unadkat, H., Rielly, C. D. & Nagy, Z. K., 2011. PIV study of the flow field generated by a sawtooth impeller. *Chemical Engineering Science*, 66(21), pp. 5374-5387.

Vergel, J. L. G., 2013. Estudo da influência da malha computacional, modelos de turbulência e aspectos numéricos da modelagem CFD em impelidores PBT usando malhas não-estruturadas. *Dissertação (mestrado) - Universidade Estadual de Campinas, Faculdade de Engenharia Química, Campinas, SP*, p. 121.

Wang, H. et al., 2015. Proper orthogonal decomposition based outlier correction for PIV data. *Experiments in Fluids*, 56(2), pp. 1-15.

Wang, Y., Rao, Q., Fan, J. & Fei, W., 2006. PIV measurements and CFD simulation of viscous fluid flow in a stirred tank agitated by a Rushton turbine. *In Proceedings of the 5th International Conference on CFD in the Process Industries.*

Westerweel, J., 1993. Digital particle image velocimetry: theory and application. *PhD thesis, TU Delft, Delft University of Technology*.

Westerweel, J., 1994. Efficient detection of spurious vectors in particle image velocimetry data. *Experiments in Fluids*, 16(3), pp. 236-247.

Westerweel, J. & Scarano, F., 2005. Universal outlier detection for PIV data. *Experiments in fluids*, 39(6), pp. 1096-1100.

Wieneke, B., 2005. Stereo-PIV using self-calibration on particle images. *Experiments in fluids*, 39(2), pp. 267-280.

Wieneke, B. F. A., 2017. *PIV uncertainty quantification and beyond.* s.l.:Doctoral Thesis. Delft University of Technology.

Wieneke, B. & Pfeiffer, K., 2010. Adaptive PIV with variable interrogation window size and shape. *15th Int Symp on Applications of Laser Techniques to Fluid Mechanics*.

Wilcox, D. C., 1998. *Turbulence modeling for CFD.* La Canada, CA: DCW industries, Inc.

Willert, C., 1997. Stereoscopic digital particle image velocimetry for application in wind tunnel flows. *Measurement science and technology*, 8(12), p. 1465.

Willert, C. E. & Gharib, M., 1991. Digital particle image velocimetry. *Experiments in fluids*, 10(4), pp. 181-193.

Xue, Z., 2014. Particle Image Velocimetry Correlation Signal-to-noise Metrics, Particle Image Pattern Mutual Information and Measurement uncertainty Quantification. *Doctoral dissertation, Virginia Tech*.

Xue, Z., Charonko, J. J. & Vlachos, P. P., 2014. Particle image velocimetry correlation signal-to-noise ratio metrics and measurement uncertainty quantification. *Measurement Science and Technology*, 25(11), p. 115301.

Yianneskis, M., Popiolek, Z. & Whitelaw, J. H., 1987. An experimental study of the steady and unsteady flow characteristics of stirred reactors. *Journal of Fluid Mechanics*, Volume 175, pp. 537-55.

Zhang, P., Chen, G., Duan, J. & Wang, W., 2018. Mixing characteristics in a vessel equipped with cylindrical stirrer. *Results in Physics*, pp. 699-705.

Zhou, G. & Kresta, S. M., 1996. Impact of tank geometry on the maximum turbulence energy dissipation rate for impellers. *AIChE journal*, 42(9), pp. 2476-2490.